

NASA Contractor Report 174841

NASA-CR-174841  
19850013010

Effect of Reduction of Strategic Columbium Addition in 718 Alloy  
on the Structure and Properties

Karl R. Ziegler and John F. Wallace

Case Western Reserve University  
Cleveland, Ohio

January 1985

LIBRARY COPY

NOV 27 1990

LANGLEY RESEARCH CENTER  
LIBRARY NASA  
HAMPTON, VIRGINIA

Prepared for

NATIONAL AERONAUTICS AND SPACE ADMINISTRATION  
Lewis Research Center  
Under Grant NAG 3-268



EFFECT OF REDUCTION OF STRATEGIC COLUMBIUM ADDITION IN 718 ALLOY  
ON THE STRUCTURE AND PROPERTIES

ABSTRACT

by

KARL R. ZIEGLER & JOHN F. WALLACE

Inconel Alloy 718 is a Nickel-Iron-base superalloy strengthened by the precipitation of the metastable  $\text{Ni}_3\text{Cb}-\gamma''$  phase. Large coherency strains between  $\gamma''$  and the matrix result in a slow precipitation rate and an intermediate maximum use temperature. The combination of slow precipitation rate and the relative formability and machinability of Alloy 718 make it a popular material for the fabrication of superalloy components. The dependence on foreign sources of Cb has pointed out the desirability of reducing the Cb content of Alloy 718 while maintaining the tensile and stress-rupture properties of the original alloy. The purpose of this investigation was to determine the effects of reduced Cb, and substitutions for Cb, on the properties of Alloy 718.

A series of alloys was developed having a base composition similar to Alloy 718, with reduced Cb levels of 3.00 and 1.10 wt % Cb.

N85 - 21320H

Substitutions of 3.0% W, 3.0W + 0.9V or Mo increased from 3.0 to 5.8% were made for the Cb in these alloys. Two additional alloys, one containing 3.49% Cb and 1.10% Ti and another containing 3.89% Cb and 1.27% Ti were also studied. Solution and age heat treatments were optimized for each alloy to develop a proper microstructure. Some alloys were also processed by direct aging for substitution in the high strength applications of the standard alloy. Tensile properties at room and elevated temperatures, stress-rupture tests and an analysis of extracted phases were carried out for each of the alloys.

The reduction in Cb content required the substitution of other elements to maintain the properties of the original alloy. Additions of solid solution elements to a reduced Cb alloy had no significant effect on the properties of the alloys under either process condition. The solution and age alloys with substitutions of 1.27% Ti at 3.89% Cb had tensile properties similar to those of the original alloy and stress-rupture properties superior to the original alloy. The improved stress-rupture properties were the result of significant precipitation of  $\text{Ni}_3\text{Ti}-\gamma'$  in the alloy, which is more stable than  $\gamma''$  at the elevated temperatures. At lower temperatures the new alloy benefits from the  $\gamma''$  strengthening. With more precise control and proper processing, the reduced Cb direct-age alloy could substitute for Alloy 718 in high strength applications.

## TABLE OF CONTENTS

	<u>Page No.</u>
ABSTRACT . . . . .	i
INTRODUCTION . . . . .	1
LITERATURE REVIEW . . . . .	1
PROCEDURE . . . . .	31
RESULTS . . . . .	37
DISCUSSION . . . . .	59
CONCLUSIONS . . . . .	80
REFERENCES . . . . .	82
TABLES . . . . .	93
FIGURES . . . . .	120



## INTRODUCTION

This investigation was undertaken to determine the structure and property aspects of chemistry variation in a Ni-Fe-base superalloy. Following is a review of the metallurgy of superalloys in general and of Inconel Alloy 718 specifically. A description of the purpose of the investigation follows the review.

## LITERATURE REVIEW

### Superalloy History

Alloys for high temperature applications have been in use since the 1930's. The advances in superturbocharged piston engines, and then jet engines, have increased the demands on component materials (Figure 1). The so called "superalloys" were developed from the precipitation hardening stainless steels. The major advance was the increase in Ni to stabilize the austenite matrix at high temperatures. The base elements of superalloys are from Group VIIIA of the periodic table. The elements Ni, Fe and Co, together or separately, form the matrix. These elements lack a single d-band electron, making them tolerant of large alloying additions. When a binary alloying element is added this band is filled, forming a stable solution. The solubility of other metals in Ni, Fe and Co are high (1). These base elements always form an FCC matrix, which is also tolerant of additions.

Three groups of superalloys are based upon the dominant matrix element. The groups are: Co-base, Ni-base and Ni-Fe-base superalloys. This review will concentrate on Ni- and Ni-Fe-base superalloys. These alloys could be further separated according to their use condition - cast or wrought. The addition of Fe to Ni-base alloys promotes precipitation in wrought superalloys and promotes formability (2). Ni-base alloys contain at least 25 wt. % Ni to ensure an FCC matrix (austenitic), subsequently referred to as  $\gamma$  (gamma) phase. Limited Co additions are possible to reduce the Ni requirement and raise the use temperature. Some Ni-Fe-base alloys contain more Fe than Ni (Table I).

#### Strengthening of Superalloys

In Ni and Ni-Fe base super alloys, strength is provided by two mechanisms. Each mechanism is enhanced through the addition of specific elements, yet each element has an effect on both mechanisms. Solid solution strengthening elements such as Cr, Mo, Al and W have atomic volumes much different than the matrix elements and expand the matrix lattice. The most likely candidate elements for solid solution strengthening have atomic sizes 1 to 13% larger than the matrix elements. Larger atomic sizes are not tolerated within the matrix lattice (4,5,6). The ability of an element to be accepted as a solute also depends on the solute-solvent valencies. Solid solution strengtheners increase the flow stress of a material by imposing strains on the matrix lattice. These strains increase the energy required to move dislocations through the matrix (4). This

energy is provided by a stress or by temperature. Solute elements can alter the stacking fault energy (SFE) of the material, increasing the flow stress. Solute atoms can develop short range order, increasing the entropy of the system. This increases the energy input required to disrupt the order, increasing the flow stress (5,7). Short range order decreases with temperature, so this contribution to strengthening is sensitive to the thermal history of the material. The mechanical properties of the solute elements will influence the flow stress. Elements with a high modulus, strength, flow stress, ductility, etc. will inhibit dislocation movement, increasing the flow stress of the material. The quantitative effects of the more potent superalloy solid solution strengtheners are shown in Figures 2 and 3. The elements that exert the greatest influence on the matrix lattice (as a binary addition to Ni) are W and Mo. They also change the room temperature flow stress more than other elements. Al provides substantial solid solution effects but is more potent as a precipitation hardening element in Ni-base superalloys. Elements such as C, B and N can provide solid solution effects by their tendency to occupy interstitial sites in a lattice (4,8). While C and B influence material properties more through the formation of carbides and borides, respectively, interstitial N can be a significant solid solution strengthener in superalloys.

The greatest contribution to Ni- and Ni-Fe-base superalloy strength is the precipitation of an ordered, coherent FCC and/or BCT phase. The stable or metastable FCC phase has an  $A_3B$  chemistry

and an  $L1_2$  structure (9,10). In Ni- and Ni-Fe-base superalloys, this phase is  $Ni_3Ti$  and/or  $Ni_3Al$ , referred to as  $\gamma'$  (gamma prime). The BCT precipitate, based on  $Ni_3V$ , has a  $DO_{22}$  structure (11,12,13,14). This precipitate is called  $\gamma''$  (gamma double prime) (Figure 4). The chemistry of the precipitate is subject to some controversy. Some investigators report a  $Ni_xCb$  ( $x = 2.5-2.8$ ) composition while others propose  $Ni_3Cb$  (16). Disagreement also exists over the elements contained in the BCT structure. There are indications that only Cb is present (17) while others show that Al and Ti can substitute for some Cb in the same manner as for  $\gamma'$  (6). It has been determined that, in Ni-Fe-base superalloys,  $Ni_3Al - \gamma'$  does not precipitate alone (2). Al can substitute into the structure of  $Ni_3Ti$ , but the major contribution of Al may be as a solid solution strengthener and for oxidation resistance (2).

It has been shown that the presence of Fe is required to permit the precipitation of  $\gamma''$  in Ni-base superalloys (18). The addition of up to 10 at. % Cb in a Ni matrix produced virtually no  $\gamma''$  precipitation. When Fe was present, no lattice matching between the FCC-Ni and BCT- $\gamma''$  occurs (2,6,15). At low Fe additions  $\gamma''$  precipitation is inhibited by the BCC structure of Fe. Above a certain Fe level the electronic configuration changes such that an FCC structure is promoted (15). In joining with Ni it forms a matrix that matches the BCT-  $\gamma''$  lattice closely enough to permit precipitation. The Fe and additions of Cr also distort the Ni lattice, increasing the lattice parameter (2,6,19). This reduces

lattice parameter differences between the  $\gamma$  and  $\gamma''$ , making precipitation more favorable. The presence of Al inhibits  $\gamma''$  precipitation by altering the lattice structure, again increasing the  $\gamma - \gamma''$  mismatch.

In  $\gamma'$  strengthened superalloys the precipitate is spherical to cuboidal in shape (9,20,21). The distortion from spherical is caused by lattice strains between the matrix and precipitate. These strains depend on the chemistry of the matrix and the precipitate. The  $\gamma''$  precipitates have a disc morphology (2,7,11,12,22,23,24). This morphology is the result of anisotropic coherency strains between the matrix and precipitate. The BCT lattice of  $\gamma''$  is, in effect, two FCC lattices stacked together (Figure 4). A change in atom position on the shared center plane occurs because the Ni atoms shift to edge positions and Cb must occupy the face position (6,7,15,25,26). The matching between the precipitate and the matrix becomes anisotropic. This enhances growth in the longitudinal direction and inhibits growth in the transverse direction.

The growth of  $\gamma'$  and  $\gamma''$  precipitates is described by the theory of Lifshitz, Slyozov and Wagner (LSW) (27). The theory describes growth as diffusion controlled with the size of the particle changing linearly with (time)<sup>1/3</sup>. The aging temperature will change the slope of this behavior but the growth is linear over time. The growth is described by the equation (for disc particles):

$$\bar{d}^3 - d_0^3 = K t$$

where  $\bar{d}$  is the mean disc diameter,  $\bar{d}_0$  is the original mean disc diameter and  $t$  is the time.  $K$  is a constant described by:

$$K = \frac{128}{9} \frac{Pq D C_e V_m^2}{RT}$$

where  $P$  is the particle peripheral interface energy,  $q$  is the particle aspect ratio,  $D$  is the solute diffusion coefficient,  $C_e$  is the equilibrium solute concentration and  $V_m$  is the molar volume of the precipitate. The activation energy of the growth process can be determined from the slope of the plot of particle size vs time, the temperature, the aspect ratio and the equilibrium solute concentration. The activation energy, in the LSW Theory, is equal to the solute diffusion through the matrix. The size distribution of particles in Alloy 718 is skewed to particles larger than predicted by the LSW Theory. This was found to be the result of the large strain field surrounding the  $\gamma''$  precipitate. The strain field, the result of  $\gamma - \gamma''$  mismatch enhances the coarsening of  $\gamma''$  particles. Diffusion rate changes occur when particles encounter one another.

The mechanisms of precipitation hardening in superalloys are numerous and varied. The relative contribution of each mechanism also varies with the superalloy system. The strengthening effect of  $\gamma'$  in Ni-base superalloys will depend on (4,28): (1)  $\gamma'$  volume fraction, (2)  $\gamma'$  radius, (3) solid solution strength of  $\gamma'$  (and  $\gamma$ ), and (4) presence of hyperfine  $\gamma'$ . The  $\gamma'$  phase strengthens through

the following mechanisms (4): (1) coherency strains between  $\gamma'$  and  $\gamma$ , (2) modulus mismatch between  $\gamma$  and  $\gamma'$ , (3) ordering of  $\gamma'$ , (4) stacking fault energy (SFE) differences between  $\gamma$  and  $\gamma'$ , (5) interfacial energy creation, (6) temperature dependence of lattice strength. The predominant  $\gamma'$  strengthening mechanisms are ordering of  $\gamma'$  and the formation of anti-phase boundaries, which is due to differences in the stacking fault energy in  $\gamma$  and  $\gamma'$  (4,10,28,29,30,31,32). Both mechanisms inhibit dislocation motion as the result of a higher energy region or boundary. Dislocations travelling in pairs, with a stacking fault between, encounter  $\gamma'$  particles. The first dislocation will move into the particle more easily in alloys with low SFE  $\gamma'$ . The anti phase boundary within the particle is more difficult for the dislocation to penetrate (10,29). The dislocation motion is inhibited by the differences in SFE between  $\gamma$  and  $\gamma'$ . Ordered particles are a region of higher entropy. To lower this energy through the displacement of precipitate particles and increased disorder requires an increased energy input. Coherency strains are also a potential contributor to precipitate strength. These strains are the fitting together of two FCC lattices with different lattice parameters. The required continuity between the two lattices creates a strain on each lattice (29). These higher energy boundaries must be overcome for dislocations to move. Similar reasoning is used to describe the interfacial energy creation. In this case the creation of a new surface requires more energy than maintaining the  $\gamma - \gamma'$  interface.

Coherency strains, degree of ordering, modulus mismatch and SFE differences can increase with temperature. The interfacial energy will decrease with an increase in temperature (4).

The strengthening mechanisms in Ni-Fe-base superalloys are the same as those for Ni-base superalloys. In Ni-Fe-base superalloys strengthened by  $\gamma''$  the relative contribution of each mechanism to overall strength is different than in  $\gamma'$  strengthened alloys. The  $\gamma''$  strengthened alloys rely primarily on coherency strains between  $\gamma''$  and  $\gamma$  for strength (25,33,34). In superalloys that are used at high temperatures, coherency strains between the matrix and precipitate are not relied upon for strength (6). The potent effect of these strains on strength is sacrificed to insure a stable precipitate at these temperatures.

An optimum amount of a strengthening phase exists for a superalloy. In  $\gamma'$  strengthened superalloys a  $\gamma'$  volume fraction of 0.60 provides the best properties (1). Alloys strengthened by  $\gamma''$  precipitation have an optimum volume fraction of 0.20. Coherency strains extend a significant distance away from the  $\gamma - \gamma'$  interface (35,36). Lattice distortions make the nucleation of precipitates impossible near other precipitate particles. The interaction of the distortions result in a balance between particle size and distribution.

The precipitation of  $\gamma'$  and  $\gamma''$  phases are the result of classical solution and age heat treatment. The first stage, solution heat treatment, required an anneal at temperatures high

enough to drive all solute atoms into solution and to homogenize the alloy structure. Typically this is near the melting point of the alloy. To retain this homogenized structure, the alloy is quenched to room temperature. The quench rate depends on the atoms in the alloy, but a water quench or air cooling is usually sufficient in superalloys. Heating the alloying to lower elevated temperatures will allow the supersaturated solution to precipitate phases that are stable at that temperature and solute content. All the characteristics of age hardened metal alloys with respect to time and temperature are obeyed in superalloys.

At sufficiently high temperatures or long enough times at a particular temperature Ni-Fe-base superalloys hardened by metastable precipitates will overage. Overaging is first manifest in particle coarsening. Coarsening is the result of growth overtaking the nucleation of new particles and competition between existing particles, resulting in the dominance of a few precipitate particles. At higher age temperatures  $\gamma'$  ripening is overcome by the precipitation of the stable  $\eta$  (eta) phase (1). The  $\eta$  phase also has the  $\text{Ni}_3\text{Ti}$  composition. This phase has an HCP structure, is incoherent and precipitates initially at grain boundaries. The  $\eta$  phase can precipitate in a cellular morphology similar to pearlite, with alternating  $\gamma$  and  $\eta$  plates. It can also form a Widmanstätten morphology, starting at grain boundaries and growing outward, through  $\gamma'$  particles. Superalloys precipitating the  $\gamma''$  phase also initially overage by coarsening of the precipitates (36). At higher

temperatures the stable phase,  $\delta$  (delta) predominates (25,37,38,39, 40). The  $\delta$  phase has an orthorhombic structure, initially precipitated at grain boundaries in a cellular or Widmenstätten morphology. The  $\delta$  phase has composition of  $\text{Ni}_3\text{Cb}$ , a slight variation on the metastable  $\gamma''$  composition of  $\text{Ni}_x\text{Cb}$  ( $x = 2.5-2.8$ ).

Since  $\eta$  and  $\delta$  are incoherent with the matrix, they provide no strengthening and only occupy volume. These phases consume Ti and Cb which are needed for  $\gamma'$  and  $\gamma''$  precipitation, reducing the potential volume fraction of strengthening phase. It is also likely that the Widmenstätten forms of  $\eta$  and  $\delta$  serve as crack initiation sites. Some evidence suggests that grain boundary  $\eta$  and  $\delta$  improves ductility and stress rupture strength. While some  $\delta$  may be desirable to reduce grain boundary sliding, the service temperature of  $\gamma'$  and  $\gamma''$  strengthened superalloys is limited by the precipitation of this  $\eta$  and/or  $\delta$ .

#### Oxidation Resistance

Superalloys are used in high temperature applications because of their high temperature strength and creep resistance. Resistance to internal oxidation and corrosion is also essential at these temperatures (41,42). Alloys used in applications where an aggressive environment is present contain significant amounts of Cr and Al (43,44,45). These elements form very stable oxides and provide protective oxide coatings at high temperatures to prevent further attack of the base metal. Superalloys can contain 10 to 30 wt % Cr for oxidation resistance. In Ni-Fe-base superalloys, some

of the Al present is available to resist oxidation, the balance is found in  $\text{Ni}_3(\text{Ti},\text{Al})$ .

### Secondary Phases

Several elements are present in superalloys beyond the main constituents mentioned above. Some of these elements, such as B, C and Zr are added for a specific purpose. Other elements are undesirable and promote phases that are deleterious to physical and/or mechanical properties. Examples of the latter include Si, Mn, P and S. The relative effects of some elements in superalloys are shown in Table I.

The presence of only a trace amount of C will cause the formation of carbides. The presence of other elements and the heat treatment have some effects on the type of carbide present. The most prevalent and most stable carbide in Ni- and Ni-Fe-base superalloys is the MC carbide, where M is the metal atom. The possible metal atoms, in decreasing stability are (1,46): Ta, Cb, Ti, V. The formation of  $\text{M}_{23}\text{C}_6$  and  $\text{M}_6\text{C}$  is influenced by the relative amounts of Cr, Mo and W (1,47). The heat treatment also exerts a strong influence on these two carbides. At low age temperatures  $\text{M}_{23}\text{C}_6$  is more stable (1). This carbide forms with Cr, Mo, Fe and W. At higher aging temperatures  $\text{M}_6\text{C}$  is more stable. At these temperatures  $\eta$  and  $\delta$  precipitate at grain boundaries, occupying the preferred  $\text{M}_{23}\text{C}_6$  site (48).  $\text{M}_6\text{C}$  is also promoted over  $\text{M}_{23}\text{C}_6$  when Mo and W are present in sufficient amounts (28). A transition between the two carbides occurs when

(Mo + 1/2W) wt % equals 6.0 (49,50).  $M_7C_3$  carbides are not found in Ni- and Ni-Fe-base superalloys and will not be discussed here. Carbides can be beneficial to superalloy mechanical properties by blocking dislocation motion or pinning grain boundaries (51). Some early superalloys and many modern stainless steels are strengthened by a general carbide precipitation. However, carbides contain elements that would otherwise contribute to  $\gamma'$  and  $\gamma''$  precipitation or to solid solution strength. Grain boundary carbide precipitation can provide some strengthening. They also serve as stress concentrators and potential crack paths (45,52,53). Overall, carbides can be considered deleterious to superalloy properties. The presence of some carbides is unavoidable, and heat treatment modifications are necessary to reduce their effect on properties. The mechanisms behind the effects of B and Zr are not as well understood as for C. It has been shown that B and Zr occupy grain boundary sites, apparently preventing the formation of a continuous carbide film (4,6,8,54,55,56). This strengthens the alloy (57,58). The presence of Si and Mn have been shown to promote damaging phase formation (59,60). P encourages the general precipitation of carbides (48,61). The formation of sulfides can cause problems during thermomechanical processing (hardspots, stringers, etc.), so the S level is kept to a minimum in superalloys (28,58).

The  $\gamma$ ,  $\gamma'$ ,  $\gamma''$ , carbides and borides are geometrically close packed phases. The atomic structure of the lattice is isotropic. Under certain compositional conditions structures that are

topologically close packed (TCP) can form. Differences in atomic size and electronic charge cause a collapse of the smaller atoms into regions between the larger constituent atoms. This results in an anisotropic structure that is very complex, with up to 30 atoms to a unit cell. The anisotropic structure can lead to a plate morphology. For several reasons, TCP phases are deleterious to superalloy properties (62). TCP phases remove elements from the matrix that otherwise might form the strengthening phases ( $\gamma'$  or  $\gamma''$ ). The TCP phases also remove elements that influence the strengthening mechanisms of the precipitated phases (e.g. altering lattice constants and reducing the effect of coherency strains). The sharp tips of TCP plates are stress concentrators that could initiate cracks. Their plate morphology provides good paths for fracture (2). These phases also remove elements from the matrix around, weakening the alloy in this region and permitting easier fracture. The result of the presence of TCP phases in superalloys is a reduction in strength and ductility and a lower stress rupture ductility. The documented TCP phases include  $\sigma$  (sigma), Laves,  $\chi$  (chi),  $\mu$  (mu), G and R phases (62). The  $\sigma$  and Laves phases are the most frequently observed of these (48,63,64,65).

The  $\sigma$  phase has a stoichiometry that can range from  $A_7B$  to  $AB_7$ . In most cases  $\sigma$  has a composition of  $AB$ , where A is Cr or Mo and B is Ni, Fe or Co (48,62). The  $\sigma$  phase can be prevented by decreasing the Al, Ti, Mo, Cr and Co in the alloy. Each of these elements contributes to  $\sigma$  formation. Increasing the Ni content will

decrease the tendency for these elements to form  $\sigma$  by diluting them and keeping them in solution (15,17,67,68). The Laves phase has an  $A_2B$  stoichiometry with a structure based on  $Zr_2Mg$ . Here A can be Fe, Co or Ni and B is Ti, Cb or Ta (Figures 5 and 6). In some of the early generation superalloys and high temperature stainless steels Laves was a primary strengthening phase. In more recent superalloys, the elimination of Laves is preferred. The Laves phase in Ni-Fe-base superalloys ( $Fe_2Cb$ ,  $Fe_2Ti$ ) is promoted by increased Cb and Ti. The presence of Si and Mn also increase the precipitation of Laves (58,60,61,69,70). Si and Mn decrease the solubility of Cb and perhaps Ti in superalloys, making more Cb or Ti available for Laves formation. This phase is more prevalent in superalloys that were not properly solution heat treated or homogenized after casting. The Laves phase can be prevented through the reduction of Cb, Ti, Si and Mn or by increasing the Ni content (58,61). This increased Ni provides a greater opportunity for  $\gamma'$  precipitation rather than Laves formation. The remaining TCP phases are found much less frequently in Ni- and Ni-Fe-base superalloys. TCP phases will nucleate at high energy sites such as grain boundaries. Many of the elements necessary for the formation of these phases occur in abundance at grain boundaries. Only small differences exist between the structures of  $\sigma$  and  $M_{23}C_6$  and it has been shown that  $\sigma$  nucleates from  $M_{23}C_6$  at grain boundaries (71). In these carbides M is Cr, Mo, W and Fe.

The greater the processing deformation of an alloy the greater

the strain energy in the alloy. There is greater precipitation at larger deformation. The dislocation structure of a deformed alloy make precipitation more favorable. The precipitated phases include strengthening phases and deleterious phases. It has been demonstrated that the  $\sigma$  phase (FeCr) will precipitate at dislocations and twin boundaries. The precipitation of  $\sigma$  is therefore enhanced by deformation (17,67,68,71,72).

### Processing of Superalloys

Superalloys are used as castings and in various wrought forms. Cast superalloys have a higher Ni content to stabilize the austenitic matrix. Cast superalloys, whether polycrystalline, directionally solidified or single crystals, are used in the highest temperature applications. The highest temperature alloys are directionally solidified (DS) or single crystals. The DS alloys reduce the effect of grain boundary creep by eliminating transverse grain boundaries. Single crystal superalloys eliminate all grain boundaries. Other creep mechanisms will dominate in these two cases, but they are activated at higher temperatures and/or stresses. The result is superalloys that are significantly more creep resistant than polycrystalline cast or wrought superalloys.

The addition of Fe to Ni-base superalloys reduces the maximum use temperature but makes thermomechanical processing more feasible (2,55). The wrought superalloys are useful in fabricating parts for intermediate temperature use. Thermomechanical processing can take a variety of forms. Superalloys are forged, extruded, rolled to

sheets or bars, machined, welded, etc. at temperatures ranging from room temperatures to well above the solvus temperature of all phases (54). This presents an obvious challenge for microstructural control. Methods exist to control grain and microstructure in wrought superalloys during processing. These methods rely on the presence of grain boundary phases to prevent grain growth and recovery during the processing. Pinning grain boundaries helps retain the strain energy developed in the alloy. This strain energy can enhance the precipitation of  $\gamma'$  and  $\gamma''$  phases. Precipitation reactions in superalloys are enhanced by increased strain energy of the alloy. Greater deformation imparts greater strain energy into the material. Upon heat treatment the strain energy is a mechanical contribution to the activation energy for precipitation. Greater deformation processes contribute more energy to precipitation. This also means that precipitation of the overaged phase is more likely (52,73). The strain energy is in the form of plastic deformation of the grains. This generates a large number of dislocations and twins. These are favorable sites for  $\gamma''$  precipitation.

The wrought superalloys that rely on a grain boundary phase to control structure and grain size are categorized by the controlling phase. These categories are (2,51,74,75): (1) FCC-Ni<sub>3</sub>Al- $\gamma'$  control, (2) HCP-Ni<sub>3</sub>Ti- $\eta$  control or (3) Orthorhombic - Ni<sub>3</sub>Cb- $\delta$  control. In the first case the  $\gamma'$  precipitate that strengthens the Ni-base alloy is also the stable phase. Processing requires that the material be heated just into the  $\gamma'$  precipitation region during

deformation. The  $\gamma'$  precipitate at the grain boundaries prevents recovery or grain growth. The HCP- $\eta$  phase controls the structure in Ni-Fe-base alloys where Ti additions result in  $\gamma'$  strengthening and  $\eta$  is the overaged phase. These alloys are processed at temperatures just above the  $\gamma'$  solvus but below the  $\eta$  solvus. The  $\eta$  phase precipitates at grain boundaries, providing grain control. Holding at the temperature would promote  $\eta$  growth, perhaps out of the grain boundaries. In Ni-Fe-base alloys containing sufficient Cb to promote  $\gamma''$  precipitation, an analogous procedure is used. These superalloys are processed at temperatures above the  $\gamma''$  and  $\gamma'$  solvus but below the  $\delta$  solvus (76). The stable  $\delta$  phase precipitates at grain boundaries during processing, preserving the grain structure. The  $\eta$  or  $\delta$  precipitation is useful in moderation because it is a ductile phase, improving the stress rupture ductility of the material. At temperatures above the  $\eta$  and  $\delta$  solvus temperatures there is evidence that MC and  $M_6C$  carbides can prevent grain boundary motion (53). The MC carbides precipitate during solidification and cannot be completely dissolved during processing.

The temperatures during processing are a critical parameter in Ni-Fe-base superalloys (51,77,78). If the temperature is too low significant  $\gamma'$  or  $\gamma''$  precipitation can occur. This would harden the alloy and make deformation processing more difficult. At temperatures that are too high, the overaged, structure controlling phases may grow, decreasing the potential strength of the alloy. In the extreme case, at temperatures above the  $\eta$  or  $\delta$  solvus, considerable

recovery, recrystallization and grain growth can occur. The larger grain size and reduced strain energy in the wrought material reduces the potential strength and ductility because of a lack of  $\eta$  or  $\delta$  at the grain boundaries of the alloy. At higher deformation temperatures, greater deformation is required to obtain a uniform grain structure (79). The recrystallization that occurs at these temperatures must be prevented by greater deformation. Large deformation at low temperatures can result in some softening of the material (80). During the large deformation some mechanical energy is converted to heat, resulting in adiabatic heating of the alloy. This can soften the structure as a result of  $\delta$  precipitation or a loss of continuum at grain boundaries.

#### Inconel Alloy 718 - Physical Metallurgy

As mentioned previously, the superalloy of concern in this investigation is Inconel Alloy 718. This Ni-Fe-base superalloy has a nominal composition of:

	<u>Ni</u>	<u>Fe</u>	<u>Cr</u>	<u>Co</u>	<u>Al</u>	<u>Ti</u>	<u>Cb</u>	<u>C*</u>	<u>Si*</u>	<u>Mn*</u>	<u>P*</u>	<u>S*</u>
wt % bal.	19.5	18.6	--	0.55	0.90	5.30	0.04	0.35	0.15	0.15	0.15	0.15
at % bal.	19.8	20.4	--	1.14	1.08	3.25	0.190	0.68	0.17	0.29	0.29	0.29

(\* maximum)

The alloy contains sufficient Cb to promote the precipitation of the BCT  $\gamma''$  strengthening phase. It is a wrought alloy that has been in use since the early 1960's. The maximum use temperature of the

alloy is 650°C (1200°F). The proper Ni content for a Ni-21Cr-balance Fe alloy was determined by Eiselstein (37,38). From similar compositions containing Cb, Ti and Al Eiselstein determined that 53 wt.% Ni provided the peak solution and age strength (Figure 7). Eiselstein and Boesch & Canada determined the proper amounts of hardening elements (Cb+Ta, Ti, Al) to optimize the strength of a Ni-21Cr-19Fe base alloy. Eiselstein found that above 6.5 wt.% Cb the ductility of the alloy began to rapidly decrease. Boesch & Canada confirmed this; above 6.0 wt.% Cb the reduction in area became constant (Figure 8).

At a Cb level of 4 wt.% Eiselstein determined that the properties of a 53Ni-21Cr-19Fe-base alloy were optimized with a 1.2 wt.% (Al + Ti) addition (Figure 9). The Al/Ti ratio was 1 in this case. In the case of Cb and Ti + Al, the strength of the alloy increased with increased hardener content. Above some level an incremental solute addition will have a decreasing effect on strength. At higher levels, the alloy may begin to exhibit the properties of a brittle material.

The physical metallurgy of Inconel Alloy 718 is very complex. Besides the precipitation of  $\gamma'$  and  $\gamma''$ , the overaged phase,  $\delta$ , is found. Grain boundary precipitation of  $\delta$  and  $M_{23}C_6$  are reported. MC and  $M_6C$  carbides are present within grains (40). Some undesirable and damaging phases have been reported, primarily  $\sigma$  and Laves (Figure 10) (47,65,81,82).  $M_3B_2$  borides and M(CN) carbonitrides are also possible. Small compositional changes in the

alloy can shift the balance of these phases. The effect of the elements contained in Alloy 718 are shown in Table II. The effect of temperature on the phases in Alloy 718 are shown in Table III.

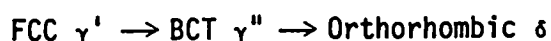
#### Solution and Age Alloy 718

Inconel Alloy 718 is used in two process conditions: (1) in the solution and age heat treated condition and (2) in the direct age heat treated condition. Solution and age heat treated Alloy 718 is used in applications where creep resistance to 650°C (1200°F) is required. The direct age or "Minigrain" alloy is used when lower temperature yield and tensile strength maximization are needed (83). Both processes start with cast Alloy 718, which is homogenized at 1175°C (2150°F) for 24-48 hours (26,84). In the solution and age alloys the material is rolled or otherwise thermomechanically processed to the appropriate dimension at a temperature high enough to make processing easy. The alloy is then solution heat treated at 1010°C (1850°F) for 2 hours (2,74). This temperature is above the solvus temperature of all phases and above the recrystallization temperature of Alloy 718. After air cooling to room temperature, the alloy is age heat treated at 730°C (1350°F) for 8 hours, furnace cooled at 38°C (100°F) per hour to 620°C (1150°F) and held for 8 hours, then air cooled (Figure 11). In the solution and age heat treated condition, Alloy 718 is among the strongest superalloys at room temperature (3). The use temperature of Alloy 718 is limited but some modification of the structure through heat treatment is possible to improve the temperature capability of the alloy (85).

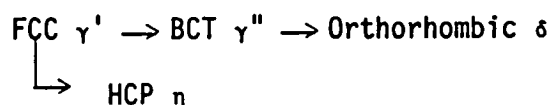
The heat treatment variations for Alloy 718 are dependent upon the application. Superior stress rupture ductility and notch fatigue resistance are attained by a solution heat treatment below the  $\delta$  solvus and not above the recrystallization temperature (Figure 12). The  $\delta$  phase forms at grain boundaries initially, providing a ductile constituent at these sites. There is an effect of grain size on precipitation; larger grain Alloy 718 has coarser  $\delta$  than a finer grained Alloy 718 (16,77,86,87). Solution heat treating the alloy at temperatures above the recrystallization temperature will dissolve all the  $\delta$  phase and increase the grain size. After aging this results in an alloy with good strength, creep resistance, lower ductility and reduced ductility in notched fatigue (1,2,86). The larger grain Alloy 718 has lower strength and slightly greater ductility than the alloy solution heat treated at temperatures below the  $\delta$  solvus (53,61,86). The loss in ductility at elevated temperatures results from the lack of grain boundary  $\delta$  and the presence of carbides at the grain boundary.

The aging heat treatment also has a marked effect on the properties of Alloy 718. The optimum aging temperature precipitates a fine uniform  $\gamma''$  throughout the alloy, avoiding the overaged phase and coarsened  $\gamma''$ . At temperatures just high enough to initiate  $\gamma''$  precipitation, a nonuniform  $\gamma''$  distribution can occur (92). A large amount of  $\gamma''$  occurs near grain boundaries and other high energy regions. An aging cycle that is high enough to cause  $\gamma''$  coarsening and  $\delta$  precipitation will be weaker from a loss of coherency strains

as a result of  $\gamma''$  area loss and Cb consumption by  $\delta$ . The best aging heat treatment was described previously. The cycle promotes uniform  $\gamma''$  precipitation at the higher initial temperature and precipitates growth at the lower temperature, without further  $\gamma''$  nucleation. This two step age heat treatment also reduces the risk of precipitating unwanted phases. The precipitation sequence in Alloy 718 is not firmly established. Some investigators suggest BCT  $\gamma''$  is an intermediate phase between FCC  $\gamma'$  and Ortho.  $\delta$  (91). The precipitation sequence in this case would be:



However, FCC  $\gamma'$  can overage to form HCP  $\eta$ . This requires an additional step:



Other work indicates that  $\gamma'$  precipitates first in Alloy 718 then  $\gamma''$  precipitates, independent from  $\gamma'$  (6,40). The overaged phases would form separately,  $\eta$  from  $\gamma'$  and  $\delta$  from  $\gamma''$ . It is indicated that  $\gamma''$  precipitate on  $\gamma'$  particles. This "compact" morphology has not been generally documented and the overaging process is not clear (90). The first investigators determined that the strengthening phase in Alloy 718 was  $\text{Ni}_3\text{Cb}-\gamma'$ , implying an FCC structure (7,38,39). Later investigations determined the strengthening phase was BCT  $\gamma''$  (11,12,13,14).

The presence of a tensile or compressive stress during aging heat treatment has an effect on the  $\gamma''$  morphology and thermal

stability (78). The application of an elastic tensile stress during aging heat treatment will promote growth of the  $\gamma''$  discs oriented with their long axis in the direction of the stress. The presence of a compressive stress will promote growth of  $\gamma''$  oriented with their long axis perpendicular to the stress axis (78). The optimum mechanical properties of Alloy 718 were developed with a processing schedule involving the following steps (52,75,88): (1) solution heat treatment; (2) predeformation age at a temperature above 705°C (1300°F) for 8 hours; (3) deformation processing and; (4) final age at a temperature below 705°C (1300°F) for 8 hours.

This schedule was shown to provide the optimum stress rupture properties and tensile strength (51,73,77,89). The predeformation age insures a random  $\gamma''$  distribution after deformation. A reduction in ductility occurs as the result of the strain energy imparted to the alloy and the small grain size of the deformed material.

#### Direct Age Alloy 718

The "Minigrain" process mentioned previously takes advantage of the smaller grain size that results from the deformation processing to develop an alloy with very high yield and tensile strength. The special processing of Alloy 718 takes advantage of the strain energy in the alloy developed during thermomechanical processing (51). The thermomechanical processing can take place in three distinct temperature regimes. First, at or near room temperature, deformation will develop a great deal of strain energy. This will provide the alloy with very high strength, but will also undergo recovery at lower

temperatures (73). Second, the warm working region is at temperatures where all phases are dissolved and above the recovery temperature but below the recrystallization temperature (2,74,75,77).

Thermomechanical processes are easier in this temperature region. Third, above the recrystallization temperature the least difficult processing occurs. There is considerable grain growth before and during processing. The maximum use temperature of the processed alloy increases with increasing processing temperature.

These three processing temperature regions, in combination with the solvus temperatures for the phases present in Alloy 718 and the structure controlling phases described previously, make possible a unique processing schedule to optimize tensile properties in this alloy. This processing takes advantage of the strain energy in the alloy during thermomechanical processing,  $\gamma''$  precipitation and a very small grain size to improve strength.

In this processing schedule, the as-homogenized material is forged to an intermediate size. It is then rehomogenized, upset forged and reforged to a near net shape. It is then rehomogenized, and the procedure continues until the proper grain structure is developed. Each rehomogenization heat treatment is at 980-995°C (1800-1825°F). This is at or above the  $\delta$  phase solvus and above the  $\gamma''$ ,  $\gamma'$  and Laves phase solvus, but below the recrystallization temperature. Forging temperatures are between 910 and 940°C (1675-1725°F) (26). During the heat up, prior to the forging, some  $\delta$  precipitation occurs mostly at grain boundaries. The  $\delta$  phase

will help the grains retain their structure during the forging operations, not permitting any pancaking of grains. Rehomogenization drives the  $\delta$  back into solution without initiating significant recrystallization. The upset forging operation prevents grain elongation and insures a uniform grain size. In this manner, a very small (1-10  $\mu\text{m}$ ) "Minigrain" Alloy 718 can be obtained. After the desired grain size is developed by the appropriate repetitions of the forming cycle, the material is subjected to the 730°C (1350°F) for 8 hour, furnace cool at 38°C (100°F) per hour and the 620°C (1150°F) for 8 hour aging heat treatment (83). The most conspicuous difference between this processing treatment and the solution and age heat treated material is the lack of a true solution heat treatment. This provides the Minigrain material with its alternative name: Direct-age Alloy 718.

The very small grain size of Minigrain Alloy 718 limits its use temperature to 540°C (1000°F). This compares with the maximum of 650°C (1200°F) for solution and age Alloy 718 (83). The grain size also limits its ductility. Above this temperature a significant drop in tensile properties occurs. The constant  $\delta$  precipitation and resolutioning means a higher initial  $C_b$  level is required in Minigrain processed alloys to promote adequate  $\gamma''$  precipitation during the age cycle (26,92). Minigrain Alloy 718 is most attractive in moderate temperature applications where tensile strength is the controlling property (93). The greatest use of this form of the alloy is in fasteners that undergo low-cycle-fatigue

(LCF). The LCF life of a material is determined largely by the tensile and yield strength of the material (93,94,95,96).

#### Deformation of Alloy 718

At low temperatures, the deformation of Alloy 718 is by planar slip (4,23,87,96,97). This mechanism is typical of FCC metals. The interaction of the FCC matrix and the FCC precipitate with different composition, etc. results in two reactions (98). First, the precipitates can be sheared (6). The first of a pair of dislocations passes through the particle. This decreases the stacking fault energy of the particle (9). In order to restore order in the  $\gamma''$  precipitate, a series of dislocations must pass through the particles because the BCT structure of the  $\gamma''$  precipitates means that only 1/3 of the potential slip systems are available to restore order in the particle. Second, subsequent dislocations are unable to pass through the faulted particles and must form dislocation loops around the precipitates (43,89). These Orowan loops will coalesce and form twinned regions (10). Within the twins, the stacking faults result in particles that no longer maintain the  $DO_{22}$  structure of the  $\gamma''$  precipitates. Within these twinned regions, and in slip planes, the  $\gamma''$  precipitates are dissolutioned.

During tensile straining the alloy will undergo the deformation mechanisms described above. This has a strong influence on the mechanism involved in LCF deformation (99). Deformation in LCF is also by Orowan loop formation (43). The extent of damage is controlled by the fatigue strain amplitude. As the fatigue cycles

continue, the deformation bands cause some work hardening, which, for a given strain, increases the stress on the material. This results in a peak stress on the alloy before plastic deformation begins. The less the plastic deformation in the tensile portion of the cycle, the lower the peak stress and the more cycles required to reach the peak stress. As the LCF progresses, deformation bands develop, indicating dissolution of  $\gamma''$  precipitates (43, 96). The loss of precipitates softens the material, decreasing the tensile stress on the material. The greater the plastic deformation component of the cycle, the greater the potential softening beyond the peak stress.

At elevated temperatures the hardening-softening phenomenon is not observed in LCF (43,8,95,96). In this case, the highest stress is at the start of the test. Deformation bands are able to form immediately, softening the alloy by  $\gamma''$  dissolution. At higher temperatures there is a greater thermal component of the activation energy to dissolution the  $\gamma''$  precipitates and cause softening (100). The higher the temperature, at a given strain amplitude, the fewer cycles required to produce a peak hardness. The creep deformation of wrought Alloy 718 is by diffusional creep or grain boundary sliding (80). Diffusional creep, or Nabarro-Herring creep, requires a net movement of atoms through the grains (101,102,103). It is increased by a small grain size, higher stress, higher lattice diffusion and higher temperature (104,105). Grain boundary sliding (Coble creep) is enhanced by small grain size (to increase grain boundary area), wide grain boundary regions (where vacancy diffusion

occurs), higher grain boundary diffusion and higher temperature. A greater grain size sensitivity exists in Coble creep than in Nabarro-Herring creep. Coble creep occurs, for a given temperature, at a lower stress. As a result, in wrought alloys with a smaller grain size than most cast materials, Coble creep is the controlling creep mechanism. Coble creep occurs by a net flow of atoms away from the grain boundaries transverse to the applied stress (104). The smaller grain size materials offer more grain boundaries with this orientation, further enhancing this creep mechanism (Figure 13).

To improve the creep resistance of wrought superalloys, grain boundary sliding must be reduced or eliminated (106). Reduction in the mass transfer along grain boundaries is possible by phases precipitated at the grain boundaries. This precipitation is promoted by various heat treatment and thermomechanical processes. Creep resistance of Alloy 718 is improved by a solution heat treatment that produces a large grain size with a continuous carbide film at grain boundaries. Large grains reduce the grain boundary area. The carbide film reduces mass transfer and vacancy motion along the grain boundary. In Alloy 718 this film is composed of  $M_{23}C_6$  and/or MC carbides (1,48). While reducing the creep rate, the carbide film reduces stress rupture ductility. The carbides are brittle and serve as stress concentrators as well as crack initiation sites. Because the carbides fracture in a low energy mode, during crack formation the film provides a convenient crack path. In an effort to improve stress rupture ductility, some investigators have

employed a two step age heat treatment (51,77,86). After a proper solution heat treatment at somewhat lower temperatures than described previously, the alloy is aged at a temperature intermediate between the typical age temperature and the solution temperature. This, in conjunction with the lower solution heat treatment temperature, results in a smaller grain size and precipitation of the  $\delta$  phase at grain boundaries. As noted previously, the smaller grain material precipitates a finer  $\delta$  phase (16). The  $\delta$  phase inhibits atomic motion at grain boundaries in the same manner as the carbide film. However, the  $\delta$  phase is more ductile than the carbide film. A reduction in creep resistance, and also a large increase in stress rupture ductility, results from this treatment. Depending upon the desired properties, the appropriate heat treatment can be selected.

Other investigators have determined that the use of B or Zr additions to wrought superalloys improves creep resistance (8,49,54, 55,56,57). As discussed previously, B and Zr have been observed to segregate to grain boundaries, occupying vacancy sites. The increase in difficulty in atomic motion and the breakup of the carbide film improved the stress-rupture life and ductility. Lastly, more recent work has been conducted on making a powder metal form of Alloy 718. This would offer the attraction of composition control to prevent the formation of deleterious phases (55,99,107,108,109,110,111).

#### Purpose of the Investigation

Columbium and three other elements, Cr, Co and Ta, have been identified as metals that are vital to the aerospace industry.

Over 90% of each of these materials is imported (Figure 14). This situation led to wide swinging supplies and price fluctuations that are potentially very harmful to the national defense industry (Figure 14). As a result of this situation, the National Materials and Minerals Policy, Research and Development Act of 1980, was adopted. This act focused attention on the supply-price vulnerability of these strategic metals. A program was established by the National Aeronautics Space Administration (NASA) to investigate three areas of the strategic metals problem (112).

- i) Understanding the role of strategic materials in Ni-base superalloys in order to reduce their levels through substitution of other, less "strategic" materials.
- ii) Investigate materials processing concepts to improve the properties of alloys with reduced strategic element content.
- iii) Identify potential alternate materials containing no strategic elements.

This investigation was undertaken to address the first two objectives above with respect to Inconel Alloy 718. The objective was to determine the amount of Cb that could be removed and, with or without substitution elements, still maintain the tensile and stress-rupture properties of the standard Inconel Alloy 718.

## PROCEDURE

Alloy Composition

A series of alloys were investigated as substitutes for Inconel Alloy 718. The fourteen alloys studied are listed in Table IV. The first alloy corresponds to the composition of the standard Alloy 718. Alloy 1b is also the standard alloy, but it contains 0.04 wt % B. Alloys 2a through 2f have a nominal 3.00 wt % Cb rather than the standard 5.30 wt. %. At this lower Cb level, additions of W, W + V, B and increased Mo were made to the alloys. Alloys 3a through 3d contained 1.10 wt % Cb. Additions of W, W + V and increased Mo were also made to these alloys. It was anticipated that the substitutions for the reduced Cb levels would allow these lower Cb alloys to maintain the properties of standard Alloy 718. The effects of all of these elements on Alloy 718 are listed in Table II.

The additions of W, V and Mo were selected because of their proximity to Cb on the periodic table. Some evidence exists that W, V and Mo partition to the strengthening precipitates in superalloys (50, 112). It is documented that W and Mo are potent solid solution strengtheners and that V forms a stable carbide of the MC type (1). W and Mo also contribute to the formation of  $M_{23}C_6$  and  $M_6C$  carbides (1). The B addition was selected to improve grain boundary strength by eliminating carbide films in these areas. This element also improves the room temperature and stress rupture ductility (54,56,57,58,63,113).

Alloys 4 and 5 contained Ti as a substitution for the reduced Cb. Alloy 4 contained 3.49 wt % Cb with a Ti addition of 1.10 wt %. This was the maximum Ti addition within the Alloy 718 specification, in contrast with a typical 0.87 wt % Ti addition. Alloy 5 had 3.89 wt % Cb and Ti addition of 1.27 wt %. It was hoped that the increased Ti would promote the formation of  $\text{Ni}_3\text{Ti}-\gamma'$  to substitute for the reduced  $\text{Ni}_x\text{Cb}-\gamma''$  precipitation (114,115,116).

#### Processing of Alloys

These alloys were vacuum cast from a set of seven 30-pound split heats. The additions were made in separate ladles. Addition elements were from commercially pure materials. Each of the split heats was cast into a 15 pound cylindrical mold 3 inches in diameter. The top of each mold had a 2.25 inch diameter pouring cup that collected low density impurities and provided some feeding to the ingot. After casting, the pouring cup and about 1.5 inches of the cylinder were cut off. These cylinders were then homogenized at 1095 (2000°F) for 1.5 hours. The cylinders were rolled to plates. Several passes were made on the mill to square the sides of the cylinders. Then passes with increasing reduction were made until the billet had been rolled to a 0.5 inch thick plate. After each roll pass, the piece was reheated to remain soft enough to be rolled without difficulty. When rolling was completed, the plates were transferred to a furnace at 980°C (1800°F) for 30 minutes and air cooled.

After a review of previous work, several solution and age heat

treatment cycles were selected for study on these alloys (38,39,45, 51,86,88,117). The heat treatments were based upon that used for standard Alloy 718. The solution heat treatments, all of which were for 2 hours, had temperatures ranging from 870 to 1095°C (1600-2000°F). The age heat treatment cycles were at temperatures ranging from 650 to 870°C (1200-1600°F), and for times ranging from 5 to 100 hours. Table V lists the times and temperatures for each solution and age heat treatment. The most favorable temperature for  $\gamma''$  precipitation in Alloy 718 has been shown to be about 705°C (1300°F) (28,90,118). Higher age temperatures were included to examine the effect of overaging on the phases and structure of the modified alloys. Solution heat treatment temperatures were varied to examine their effect on homogenization, grain size, and solvus temperatures in the lower Cb alloys. All heat treatments were conducted in air. Samples of the alloys, approximately 0.5 inch cubes, were cut from the bar stock. Temperatures were monitored by Chromel-Alumel thermocouples. All alloys were air cooled from the solution heat treatment and age heat treatment temperatures.

Further thermomechanical processing was applied to some of the alloys to improve their yield and tensile strength. The as rolled alloys were reheated to 955°C (1750°F) and held for 30 minutes. The pieces were then rolled in two passes to 0.25 inches thick. These plates were then aged directly. The direct age heat treatment was intended to retain a small grain material. No solution heat treatment was employed to produce grain growth. A series of age

heat treatments were examined to determine the the optimum time and temperature with respect to mechanical properties. All age cycles involved two steps. The upper temperature age cycles included temperatures between  $675^{\circ}$  ( $1200^{\circ}\text{F}$ ) and  $760^{\circ}\text{C}$  ( $1400^{\circ}\text{F}$ ) for 5 to 40 hours. These specimens were then furnace cooled to temperatures between  $675^{\circ}\text{C}$  ( $1200^{\circ}\text{F}$ ) and  $595^{\circ}\text{C}$  ( $1100^{\circ}\text{F}$ ) and held for 5 to 40 hours. The differences in the processing schedules of the Alloys and the effects on structure and properties are listed in Table VI.

#### Evaluation of Alloys

Microstructural analyses was performed with Scanning Electron Microscopy (SEM). The structures examined required resolution greater than that possible with optical microscopy. A JEOL-35CF SEM was used for all microstructure analysis. Specimens were polished with standard grinding and polishing procedures. Two etchants were primarily used: solution of 92 vol. % HCl, 5 vol. %  $\text{H}_2\text{SO}_4$  and 3 vol. %  $\text{HNO}_3$  for general microstructural examination; and an electroetch of 10 vol.% HCl in Methanol with a current density of  $10\text{-}15\text{ mA/cm}^2$  was used to examine the finer precipitates in the alloys (82).

Phases were identified by powder diffraction of extracted phases. Two proceduces were used to extract different phases. Carbides, borides,  $\sigma$ , Laves and other TCP phases were extracted in a solution of 10 vol. % HCl in Methanol with a current density of  $20\text{-}100\text{ mA/cm}^2$  (119,120). The  $\gamma'$ ,  $\gamma''$  and  $\delta$  phases were removed by a 10 vol.% HCl in water with 10g of Tartaric acid with a current

density of 20-100 mA/cm<sup>2</sup>. After the specimens were ground and rough polished, they were cleaned and rinsed with Methanol. Specimens were suspended in the electrolytic solution by a Chromel wire spot welded to the piece. The cathode was an encircling foil of Ta. The current was applied for 15 minutes to clean the specimen, the specimen was weighed and replaced into fresh electrolyte. The extraction current was applied for 2.5 to 4.0 hours depending on the alloy and the type of extraction. After the extraction was complete, the specimen was ultrasonically cleaned in a similar solution, dried and reweighed. A semi-quantitative measure of the phases could be made based upon the weight differences before and after extraction. The extracted phases were filtered out of the electrolyte and air dried. X-ray diffraction, using a Cu source with a 1.54 Å wavelength was used to generate diffraction traces. Phase identification was by comparison with ASTM Diffraction Index cards, results of ASTM E-4 Committee data, and literature values. (13,47,90,119,120,121).

Initial evaluation of the solution and age and the direct age alloys was performed by Rockwell "C" hardness tests. It has been shown that a good correlation exists between the  $R_c$  hardness and yield strength of polycrystalline metals. Alloys that were considered to be potential substitutes for Alloy 718 were tested further. The room temperature mechanical properties were determined on a Baldwin or an Instron Tensile machine. During tests on the Baldwin machine, stress-strain curves were determined from data gathered in two ways. When possible, a diametral strain gage and

load cell were used. A plot of the load vs diameter change was made on an X-Y plotter. With other specimens, a dial diametral strain gage was used and load-diameter changes were plotted by hand to determine yield strength. From these measurements, stress-strain curves were determined. On the Instron machine, the load-extension curves were determined by a load cell and monitoring crosshead motion.

Elevated temperature tensile properties were measured using a tube furnace surrounding the specimen while in the Instron or Baldwin machine. Thermocouples were placed in contact with the specimen and temperatures were held within  $\pm 1.5^{\circ}\text{C}$  ( $3^{\circ}\text{F}$ ) of the desired temperature. Stress rupture tests were conducted on BLW lever type creep machines. Temperatures were maintained by resistance heating tube furnaces surrounding the specimen. Temperatures were monitored by two thermocouples attached to the specimen and held to within  $1.5^{\circ}$  ( $3^{\circ}\text{F}$ ) of the desired temperature. Tests were conducted at stresses to produce fracture in about 100 and 50 hours in the standard Alloy 718. These stresses then applied to the modified alloys at the same temperatures. The time to fracture was then measured. Table VII indicates the tests, temperatures, and stresses for the tests on the alloys. Tensile tests were conducted at room temperature ( $25^{\circ}\text{C}$  or  $77^{\circ}\text{F}$ ), 540, 595 and  $650^{\circ}\text{C}$  (1000, 1100,  $1200^{\circ}\text{F}$ ). Stress rupture tests were conducted at the same elevated temperatures.

## RESULTS

Heat Treatment - Solution and Age Alloys

Alloy 1a, the standard Inconel Alloy 718, was processed to determine the optimum solution and age heat treatment cycle. The criteria used to establish the proper solution temperature were: complete dissolution of  $\gamma'$ ,  $\gamma''$ ,  $\delta$  and any TCP phases that had been present during casting or rolling; uniform distribution of  $\gamma'$  and  $\gamma''$  after aging; a uniform grain structure of the appropriate size and; grain boundaries containing a minimal amount of precipitates. Each solution heat treated alloy was aged at 705°C (1300°F) for 100 hours. Figures 15 through 18 show the effect of the solution temperature on segregation in alloy 1a. At solution temperatures below 1040°C (1900°F) substantial segregation, non uniform  $\gamma''$  precipitation, significant  $\delta$  precipitation, and a duplex grain structure occurs. At 1040°C (1900°F) and above, segregation is not present and a uniform precipitate distribution is obtained. Some grain growth at 1040°C (1900°F), and substantially more at the higher temperatures, was observed. These structures indicate that the complete solution temperature for Alloy 718 is between 980 and 1040°C (1800 and 1900°F). The structures indicate that the recrystallization temperature in the standard alloy is also between 980° and 1040°C (1800 and 1900°F). The solution temperature for  $\delta$  is about 997°C (1825°F). The recrystallization temperature for Alloy 718 is about

1003°C (1835°F). Assuming that the solution temperature and recrystallization temperature change with composition, substantial differences in these temperatures could exist between the Cb-poor and Cb-rich regions. This behavior occurred in modified Alloy 718 since the solution and recrystallization temperature rises with increased Cb content as shown in Table VI. At 1040°C (1900°F), the grain size is an acceptable ASTM 4-7 (50-200  $\mu\text{m}$ ). In combination with the above evidence it is indicated that a solution temperature above the standard Alloy 718 solution temperature was appropriate. All alloy 1a and 1b solution heat treatments were at 1040°C (1900°F).

Alloy 2a, with lower Cb content, was similarly affected by solution heat treatment temperatures. Less segregated material occurs in these alloys. Since the only difference between alloy 1 and 2 is a reduction in Cb, this indicates that many Cb-based phases are forming. The precipitate distribution in alloy 2 is uniform at temperatures above 980°C (1800°F). At or below this temperature some non uniform precipitation, a slight precipitation of undesirable phases and a variable grain structure occurred. The solution and recrystallization temperatures were lower in these lower Cb alloys, but, the decrease was not substantial. The grain size for a 980°C (1800°F) solution temperature was ASTM 4-7 (50-150  $\mu\text{m}$ ). To insure homogenization and a uniform grain size and precipitate distribution, alloy 2a was solution heat treated at 1040°C (1900°F).

Alloy 3a contained 1.10 wt.% Cb. Some nonuniform precipitation was noted at a 925°C (1700°F) solution temperature. At 980°C (1800°F) no evidence of segregation of Cb or other elements existed but only intermediate grain growth occurred between 925°C and 980°C. This indicated that the recrystallization temperature of the 1.10 wt.% Cb alloys was near 980°C. Accordingly, alloys 3a through 3d were solution heat treated at 980°C (Table VIII).

The effects of the additions of W, W + V and increased Mo on the recrystallization temperature and the dissolve of  $\gamma''$ ,  $\gamma'$ ,  $\delta$  and the TCP phases was negligible. Figures 19 through 22 show alloys 2a through 2f after a 1040°C (1900°F) solution heat treatment. No significant difference in the structures of these alloys existed after this solution treatment. This was expected since the substitution elements were not strong carbide formers but primarily solid solution strengtheners. These elements, while they might have formed some undesirable TCP phases during thermomechanical treatments, were in solution during the 1040°C (1900°F) heat treatment. Figure 23 shows that this same situation occurred for alloys containing 1.10 wt.% Cb. No structural variation existed after solution treatment among alloys 3b through 3d. The phases present in the Cb-rich regions of the segregated alloys did not increase in volume when other elements were added. This indicates that the substitution elements did not participate in the precipitation of these phases.

Alloy 1 was also examined for the optimization of the aging heat treatment cycle. The decision on the best heat treatment was made

based on: the size of the  $\gamma'$ ,  $\gamma''$  phases and their relative distribution; the presence of any carbides, borides or TCP phases; the coarsening of  $\gamma''$  or any other signs of overaging, such as abundant  $\eta$  precipitation and denuded regions around grain boundaries and the  $\sigma$  phase (Table IX). At low aging temperatures, after a complete solution heat treatment, the nucleation of the metastable  $\gamma''$  and  $\gamma'$  phases occurs. A small amount of growth occurs at low age temperatures. In general, the metastable phases will precipitate at dislocation sites, because: (1) the solute concentration is usually higher at dislocations; (2) the shear deformation, needed to match the precipitate structure, is present; (3) density differences at dislocations can more easily accomodate a new phase density.

As the aging temperature is increased, the competition between the nucleation of new sites and the growth of the phases that were present increases. At higher temperatures the growth component becomes more dominant and the precipitates will grow faster and coarser. At sufficiently high temperatures, the nucleation of stable phases will occur. Specimens of alloy 1 solution heat treated at 1040°C (1900°F) and aged at 650°C (1200°F) for 100 hours had structural components that were difficult to distinguish. It was not possible to resolve the  $\gamma''$  or  $\gamma'$  precipitates in this case. Later evidence will support the hypothesis that the precipitates are too fine to have been resolved in the SEM. The  $\gamma''$  and  $\gamma'$  precipitates were resolved after aging at 705°C (1300°F) for 100 hours. The grain boundaries have a continuous film of  $\text{Ni}_3\text{Cb}-\gamma$  and/or a carbide precipitate. No

denuded zone occurred around the grain boundaries. The  $\gamma''$  precipitates are distributed uniformly throughout the alloy. The  $\gamma''$  particle size was more uniform after the 100 hour age time than after the 50 hour age. The doubling of the age time developed a more uniform distribution and size. After aging at  $760^{\circ}\text{C}$  ( $1400^{\circ}\text{F}$ ) for 25, 50 or 100 hours, the  $\gamma''$  precipitates were significantly larger than after 50 or 100 hours at  $705^{\circ}\text{C}$  ( $1300^{\circ}\text{F}$ ). The grain boundaries had a heavier, continuous  $\text{Ni}_3\text{Cb}-\delta$  film. Some denudation existed at the region adjacent to the grain boundaries. Some  $\delta$  grew out of the grain boundaries and into the bulk of the grains in both a cellular and Widmenstätten morphology as shown in Figure 17. Aging alloy 1 at  $815^{\circ}\text{C}$  ( $1500^{\circ}\text{F}$ ) for 10 or 25 hours produced an abundance of  $\delta$  precipitation. Figure 17 shows a characteristic structure after this heat treatment. Massive regions of cellular  $\delta$  nucleated at grain boundaries and grew into the bulk of the grains. Some Widmenstätten  $\delta$  was also present. Large areas surrounding these cells, that do not contain any precipitates, exist because the  $\text{Ni}_3\text{Cb}-\delta$  has removed the Cb from the areas, preventing any  $\gamma''$  precipitation. The  $\gamma''$  precipitates were very coarse with some regions of little or no  $\gamma''$  precipitates. After aging alloy 1 at  $870^{\circ}\text{C}$  ( $1600^{\circ}\text{F}$ ) for 5 or 10 hours, massive amounts of  $\delta$  phase and very little  $\gamma''$  or  $\gamma'$  were precipitated. The  $\delta$  phase had both the cellular and Widmenstätten morphologies and was surrounded by large denuded zones. The  $\gamma''$  particles were not distributed uniformly and were large. The grain boundary regions were not well defined because of the growth of the  $\delta$

phase. Figures 24 and 25 graphically illustrate the effect of solution temperature on the structure of alloys 1a, 2a and 3a.

The initial screening of alloy 1a to determine the heat treatment that optimized its properties used Rockwell "C" hardness measurements. All specimens were solution heat treated at 1040°C (1900°F). The optimum hardness was obtained with the 650 and 705°C (1200 and 1300°F) age heat treatments. The structural and hardness considerations indicated that the 705°C (1300°F) was the optimum age heat treatment. Thus, the complete solution-and-age heat treatment for alloy 1 was: 1040°C solution for 2 hours, air cool; 705°C age for 100 hours, air cool.

A similar series of age heat treatment trials was undertaken for alloys 1b and 2(a-f) and 3(a-d). The microstructure of alloy 1b was similar to that of alloy 1a. The B addition had no effect on the aging characteristics of the  $\gamma''$  or  $\delta$  phases. At the lower age temperatures, the B may have occupied grain boundary sites but this effect was not detectable. At higher age temperatures, the B had no significant effect on the overaged phase precipitation at grain boundaries or the growth of the phase into the grains. The  $R_C$  hardness of alloy 1b was the same for alloy 1a. Since  $R_C$  hardness indicates the relative yield strength, it would be expected that alloy 1b would have a similar yield strength as alloy 1a. This was apparently due to the B preventing an embrittling grain boundary carbide.

The optimum structure for alloy 2a was the result of the 705°C

(1300°F) age heat treatment also. This was expected, since alloys 1a and 2a had similar solution temperatures, the alloys would behave similarly to the same age heat treatment. The  $\gamma''$  distribution in alloy 2a was uniform and similar throughout the alloy. Greater precipitation of the  $\gamma'$  phase occurred than in alloy 1a. No  $\gamma'$  denuded zone was present around grain boundaries. The structures of alloys 2b through 2f were also optimized by the 705°C (1300°F), 100 hour age. The characteristic structures of these alloys are shown in Figures 18 through 22.

The hardness of alloys 3a through 3f also optimized by the 1040°C (1900°F) 2 hour solution and 705°C (1300°F) /100 hour age heat treatment. The highest hardness of the reduced Cb alloys was about  $R_c 19$ . The variation in hardness between alloy 2a with no substitutions for the Cb, and the alloys with substitutions was only one hardness point, indicating little additional hardening as the result of W, W + V or Mo addition. These elements were not contributing to  $\gamma''$  precipitation; only Cb, and Ti contributed to the precipitation. As a result, nearly a 50% drop in hardness occurred when the Cb content of Alloy 718 was reduced from 5.30 wt.% to 3.00 wt.%. The structure of alloy 3a was difficult to analyze. The grain structure was similar to the higher Cb alloys but the grain boundaries had fewer precipitates, at a given age temperature, than the higher Cb alloys. Little evidence existed of  $\gamma''$  precipitation in the alloy, but significant  $\gamma'$  precipitation was detected. The structure of alloy 3a was optimized by a 705°C (1300°F) age for

100 hours after a 980°C (1800°F), 2 hour solution heat treatment. The structures of alloys 3b through 3d were similar to that for alloy 2a. The structures of these alloys were also optimized by a 705°C (1300°F) age temperature. The hardness of the alloys containing 1.10 wt.% Cb were consistently 60% lower than the hardness of the standard Alloy 718. They were also 25% below the hardness of the 3.00 wt.% Cb alloys. The W, W + V or Mo addition did not contribute to an increase in the hardness of alloys 3a through 3d after aging at 705°C (1300°F) for 100 hours.

The heat treatment of alloys 4 and 5 followed the same series of trials as for alloys 1 through 3. The structures that satisfied the criteria for solution and age alloys discussed previously resulted from a solution heat treatment of 980°C (1800°F) for 2 hours and an age heat treatment of 705°C (1300°F) for 100 hours. The structures of alloys 4 and 5 are shown in Figures 26 and 27. The grain size was similar to alloys 1 through 3. The precipitate distribution was uniform throughout the material. An increase in the amount of MC carbides occurred within the grains in alloys 4 and 5. These alloys had no grain boundary carbide films or evidence of any other deleterious phases ( $\delta$ , Laves).

#### Hardness Screening - Solution and Age Alloys

A linear relationship between the  $R_c$  hardness and the Cb content of Inconel Alloy 718 is shown in Figure 28. The variation in hardness was the result of: (1) the solution heat treatment temperature; (2) the aging heat treating temperature and; (3) the substitutions and

additions made to compensate for the reduced Cb levels. Even with these parameters, a clear linear relationship between the hardness and Cb content occurs. A line along the top of the shaded region has the equation:

$$R_C = 5.22 (\text{wt.\% Cb}) + 18.5$$

This is the best case hardness that could be obtained from Inconel Alloy 718 and alloys with lower Cb contents. From the results of the hardness test it was determined that, regardless of the added elements and the heat treatment, the 1.10 wt.% Cb alloys would never have sufficient strength to substitute for the standard Inconel Alloy 718. Therefore, alloys 3a through 3d were excluded from further property characterizations but they remained part of the structure characterization.

The  $R_C$  hardness for alloys 4 and 5 were excluded from Figure 28. A comparison of the hardness of these alloys with the other solution and age heat treated alloys is shown in Figure 29. Increased Ti and Cb has raised the hardness of these alloys above that of the other alloys. An equation describing the dependence of these alloys on Cb was not determined because of the small range of data.

#### Tensile Properties - Solution and Age Alloys

The room temperature tensile properties are shown in Table Xa and b. These are the properties of the alloys given a 1040°C 2 hour 705°C 100 hour heat treatment. The yield and tensile strength of

alloy 1a, the standard Alloy 718, was in agreement with specified values for the alloy. The addition of B to the standard alloy, alloy 1b, increased the yield and tensile strength and while the ductility increased. The B occupies vacancy sites at grain boundaries preventing the precipitation of weaker phases, such as  $\delta$ , and inhibits the formation of embrittling continuous carbide films. Thus the B addition strengthens and improves the ductility of Inconel Alloy 718.

The yield and tensile strengths of the lower Cb alloys were consistently about 15% lower and the ductility higher than those for the standard alloy. The addition of Mo to the 3.00 wt.% Cb alloy increased the tensile strength slightly. The addition of B to these alloys seemed to improve only the yield strength, ductility of the alloy decreased. This is the opposite of the anticipated effect on ductility. Similar, but smaller, effects resulted from coincident additions of Mo and B. The addition of W and W+V had very similar effects on the tensile properties. The yield and tensile strengths increased about 6 - 10% and the ductility decreased compared to the alloy with no substitutions. The effect of Cb on the room temperature strength of the alloys is shown in Figure 19. The room temperature tensile properties of the alloys containing increased Ti were above the expected levels for the Cb content (Table Xb and Figure 30). The substitution of Ti for reduced Cb improved the tensile strength over a reduced Cb alloy with standard Ti levels. The ductility of the higher Ti alloys was comparable to the standard solution and age Alloy 718.

The elevated temperature tensile properties of the solution and

age alloys are listed in Table XI and shown graphically in Figures 31 and 32. The strength of alloys 1a and 1b decreased rapidly at temperatures above 540°C (1000°F). The effect of B on the tensile strength decreased at elevated temperatures. The decrease in the strength of alloys 4 and 5 was linear between room temperature and 650°C (1200°F). At room temperature and 650°C (1200°F) alloys 1a and 5 had similar strength. At intermediate temperatures, the difference in strength is large. The response of alloy 4 was the same as alloy 5. The displacement of alloy 4 to a lower strength was the result of lower Cb + Ti content. The alloys containing predominantly Cb soften rapidly at temperatures above 540°C (1000°F). The alloys containing Cb and significant Ti do not soften as rapidly at temperatures up to 650°C (1200°F). The Ti addition improved the elevated temperature strength of these alloys. Alloys 2a through 2f and 3a through 3d were tested at room temperature and 650°C (1200°F). At 650°C, these alloys exhibited a strength 21-28% lower than at room temperature.

The elevated temperature ductility of alloys 1a and 1b decreased to a minimum between room temperature and 540°C (1000°F). Above 540°C, ductility increases to a level comparable to that at room temperature. The ductility of these alloys was more strongly influenced by temperature than was the strength. At 540°C the tensile strength was 6-8% lower than at room temperature while the ductility was 50% lower. At all temperatures the alloy containing B was more ductile than the standard alloy. The lower Cb alloys

containing B, 2b and 2d, were less ductile than alloy 2a at room temperature and more ductile at 650°C (1200°F).

#### Stress Rupture Properties - Solution and Age Alloys

The stress-rupture test results are shown in Tables XIIa and b. The test temperatures used were: 540, 595 and 650°C (1000, 1100 and 1200°F). Two stress levels were tested at each temperature to yield lives of 50 and 100 hours. Test specimens of alloys 1a and b were available only for testing at one temperature. Testing of alloys 1a and b was conducted at 595°C (1100°F) at both stress levels. Estimates were made of the stress-rupture life of these alloys at 540 and 650°C (1000 and 1200°F). The stresses selected at 540 and 650°C were below the yield strength of alloy 1a by a factor proportional to the test stresses at 595°C and literature values. At 540°C, the strength of alloy 1a was superior to alloys 4 and 5. The selected stress at this temperature was above the yield strength of both alloy 4 and 5. At temperatures above 540°C, the yield strength of alloy 1a decreased sharply. The stress-rupture properties of the alloy also decreased. Alloy 4 sustained the same stress as alloy 1a for a similar time. This alloy had only 3.49 wt.% Cb, and an addition of 1.10 wt.% Ti. Alloy 5 had a life at the same stress of over 400 hours, more than 4 times the life of the standard alloy. The standard alloy with an addition of B had a life over 400 hours. The standard alloy withstood a stress calculated to result in a 50 hour life at 595°C for about 20 hours. Alloy 4 had a similar life. Alloys 1b and 5 maintained the stress for 7 times longer. At higher

temperatures the stress rupture strength of Alloy 718 decreases rapidly. At 650°C (1200°F) the approximate stress sustained by alloy 1a for 100 hours was applied to alloy 4 for 75 hours and alloy 5 for 175.5 hours. The stress to cause failure in alloy 1a after 50 hours resulted in fracture in alloy 4 after a similar time, 33 hours. Alloy 5 fractured after twice the time. It was expected that alloy 1b would have a life, at each stress, less than that for alloy 5, because, at 650°C the strength of alloy 1b was much less than at 595°C and a large decrease in stress rupture properties was expected.

#### Heat Treatment - Direct Age Alloys

The room temperature tensile test results indicated that the lower Cb alloys would not be adequate substitutes for solution-and-age heat treated Inconel Alloy 718. The strength dependence on Cb was too great for solid solution strengtheners to recover the loss in properties at lower Cb levels. The effect of solid solution elements is more pronounced in applications where strain energy and deformation processing are important strengthening components. In these applications, the yield and tensile strength of the material are the primary considerations. The creep resistance of the material is of less significance.

The specification for the mechanical properties required of this high strength alloy, as shown in Table XIII, includes an age heat treatment schedule to be followed to obtain the appropriate properties. The direct-age heat treatment is performed on the warm- or hot-rolled pieces. The schedule is: 730°C (1350°F) for 8

hours, furnace cool at  $38^{\circ}\text{C}$  ( $100^{\circ}\text{F}$ ) per hour to  $620^{\circ}\text{C}$  ( $1150^{\circ}\text{F}$ ) and hold for 8 hours at  $620^{\circ}\text{C}$  ( $1150^{\circ}\text{F}$ ). Figure 32 shows an example of this "Minigrain" or direct-age Alloy 718. The grain size is about  $10\text{ }\mu\text{m}$  and meets the specified hardness for the minigrain material.

The alloys studied in the investigation were processed at temperatures below the  $\delta$  solvus. During the processing, the  $\delta$  phase pinned grain boundaries and retained a small grain size. There was a significant amount of segregation in these alloys. After heat treating, the structures of the alloys were similar to the as received material, with considerable segregation. Regions with high Cb concentrations had very small grains, due to the  $\delta$  precipitation at grain boundaries. Because of the lack of complete  $\delta$  precipitation at grain boundaries, the grain size in areas low in Cb was considerably larger. The lower Cb alloy structures had less segregation present since Cb was primarily responsible for the segregation seen in alloy 1a. The 1.10 wt.% Cb alloys had virtually no segregation after the rolling process. In both the 3.00 and 1.10 wt.% Cb alloys, it was difficult to resolve the precipitates in the alloy. Further aging beyond the specified time coarsened the  $\gamma''$  and  $\gamma'$  precipitates to permit resolution.

#### Hardness Screening - Direct Age Alloys

The Rockwell "C" hardness test results for these direct-age alloys are shown in Figure 34. A decrease in hardness was noted with a lower Cb content. Plotting these hardnesses with those for the solution and

age specimens indicates less of a dependence on Cb content in the direct-age condition. The equation describing the maximum attainable hardness in the direct-age alloys is:

$$R_C = 2.63 (\text{wt.\% Cb}) + 34.5$$

Thus, not only is the direct age hardness vs Cb curve displaced upward from the solution and age curve, but the slope of the curve is less. This indicates a lower dependence of hardness or strength on the Cb content in the direct age condition than in the solution and age condition. It was clear from this hardness data that alloys 3a through 3d would not attain the properties of the standard Alloy 718. Therefore these alloys were not considered further for applications as direct age substitute alloys. Based upon this data, it also appeared that the lower (3.00 wt.%) Cb alloys could substitute for Alloy 718 in direct age applications if the alloys were reprocessed and further strain energy were imparted to the material. This would also reduce the grain size of the alloys. Accordingly, these alloys were reprocessed by warm rolling at 967°C (1775°F). The resulting structures of these alloys are shown in Figures 35 through 38.

#### Reprocessed Alloys

These structures illustrate that the proper processing schedule was not maintained. The structure of alloy 1a, before aging, shows abundant  $\gamma''$  precipitation. No grain size increase occurred, indicating no recrystallization. After aging, the structure of alloy 1a was

similar to that before aging. The majority of the precipitation that was possible had already occurred. The structure of the reprocessed and direct age alloy 1b was very similar to that of 1a. The B addition had no effect on the structure of the base alloy. The 3.00 wt.% Cb alloys exhibited a similar structure before and after the age heat treatment (Figures 39 through 42). The  $R_C$  hardness of these rerolled and directly aged alloys as a function of Cb content is shown in Figure 34. When compared with the original direct age alloy, it is noted that a significant increase in  $R_C$  hardness occurred. The slope of the line describing this curve is:

$$R_C = 2.55 (\text{wt.\% Cb}) + 37.5$$

The hardness curve was displaced by the reprocessing and the slope of the line decreased, indicating a greater hardness sensitivity to the Cb content.

#### Tensile Properties - Direct Age Alloys

The room temperature tensile properties of the original direct age and reprocessed direct age alloys are shown in Tables XIV and XV. The reprocessing of alloys 1a, b, 2a, b, e, f increased the yield strength of each alloy, but had no effect on the room temperature tensile strength. The ductility of each of the alloys decreased to a level below the specification for Minigrain or direct age material (Table XIII). The elevated temperature tensile properties of the direct age alloys are shown in Table XVI and Figures 43 and 44. In general, the

effect of temperature on each of the alloys was the same. Between room temperature and about 540°C (1000°F) there was a 10-15% decrease in tensile strength. A decrease in tensile ductility occurred over this temperature range. The tensile strength of each alloy decreased an additional 9-15% between 595°C and 650°C (1100-1200°F). Figure 43 indicates this accelerated weakening at the higher temperatures. The tensile ductility of the alloys remained constant or increased slightly between 595 and 650°C (1100-1200°F).

The reprocessed alloys with lower Cb were slightly stronger than the original direct age alloys, at 650°C (1200°F) as shown in Table XVII. The ductility of the reprocessed alloys is about 50-70% of the original direct age alloys at this temperature. This is consistent with the room temperature ductility, where only the base alloys had an increase in ductility after reprocessing. Figure 44 indicates the effect of Cb on room and elevated temperature tensile strength of alloy 1a and 2a. The original direct age alloys and the reprocessed alloys showed an identical response to temperature. In both cases the tensile strength increased slightly because of the presence of W and W + V. At intermediate temperatures, the reprocessed alloys containing W + V had tensile strengths that were significantly greater than the unalloyed material. At 650°C (1200°F), however, the strength in the alloys containing W or W + V decreased below the unalloyed material. Apparently the effect of these elements occurred mostly at elevated temperatures, but their effect is negated at temperatures at or above 650°C (1200°F).

The reprocessed, direct age standard alloy that contained B (1b), was stronger than the standard alloy at room temperature and elevated temperatures. The effect of B was more pronounced at room temperature and 650°C (1200°F) than at the intermediate temperatures. The B addition to the reprocessed alloys with lower Cb helped the alloy retain significant ductility at room temperature. The effect of B on the room and elevated temperature strength of the lower Cb alloy was insignificant.

The differences in strength between the reprocessed, direct age alloy containing W and W + V were varied. At room temperature and at 650°C (1200°F), the differences were insignificant. At 540°C and 595°C (1000, 1100°F) the W + V containing alloy was stronger than the W containing alloy. Differences in ductility were consistent with expected results, higher strength materials had lower ductility.

#### X-ray Diffraction of Extracted Phases

Table XVIII through XXIII lists the results of X-ray diffraction studies on extracted phases. The phase identity and lattice parameters are listed. The as-rolled material contained carbides, Laves phase, and, in some cases, borides. The carbides extracted were all MC type, where M is Cb or Ti. The lattice parameter of the MC carbides decreased as the Cb level decreased. Qualitative chemical analysis indicated that the Ti:Cb ratio in these carbides increased with larger amounts of TiC as the Cb decreased. Since Ti has a smaller atomic size, the MC carbide lattice parameter decreases. The relative amount of Cb available for carbide formation may be reduced

from the formation of the  $\text{Fe}_2\text{Nb}$  - Laves phase and the  $\gamma'$ ,  $\gamma''$  phases. Thus, at lower Cb, the influence of TiC on the measured lattice parameter is more dominant. Quantitative measures of the amounts of TiC and NbC were not made. The addition of W + V to the lower Cb alloys decreased the lattice parameter of the MC carbides. Since the W alone produced no effect and has a smaller atomic volume than V or Cb, the W was probably not involved in the carbide formation. The W was probably in the  $\gamma$  structure as a solid solution strengthener.

In the as-rolled condition, some Laves phase formation was detected. It occurred in alloys with high Cb, and low Cb alloys with W added and W + V added. Some Laves was detected in the lower Cb alloys containing increased Mo and B additions. Significant segregation was present in the as-rolled alloys and these phases occurred in the Cb rich regions. Thus it would be improper to describe precisely the effect of Cb content on Laves formation in the alloys in this condition. The presence of W and B may have reduced the mobility of the elements that contribute to Laves formation. The only boride formation occurred in the alloys with B additions. The diffraction trace was the result of an  $\text{M}_3\text{B}_2$  type boride. The M in the phase was Mo, Fe and perhaps Cb. Borides form on solidification of the molten alloy. They are typically redissolved during heat treatment. No evidence of the  $\text{M}_{23}\text{C}_6$  or  $\text{M}_6\text{C}$  carbides was obtained even in the high W alloys; and  $\delta$  or other TCP phase formation was not observed.

The solution and age alloys contained MC carbides and Laves phase

in every alloy. The MC solution temperature is very near the melting point of the alloy, so it was not surprising that this carbide remained in the structure. The MC carbides had a lattice parameter slightly greater than those in the as-rolled alloys. The same relative effects of alloying and Cb content are seen in the solution and age alloys as in the as-rolled. It is assumed that the difference in lattice parameter is from a shift in the diffraction trace and not due to any chemistry differences. The Laves phase was present in all of the alloys. Very little variation in the lattice parameter in the extractions was measured. In some cases the extraction indicated that Laves existed but in volumes too small to measure the lattice parameter. The Laves phases had lattice parameters near those in the as-rolled alloys. The only boride detected in the solution and age alloys was in the standard alloy with a B addition. This was an  $M_3B_2$  type boride with the same lattice parameter as in the as-rolled alloy. The other borides were apparently completely dissolved during solution heat treatment.

X-ray diffraction analysis results of the higher Ti alloys are also shown in Tables XIX and XX. The MC carbides have lattice parameters that were smaller than for the lower Ti (and lower Cb) alloys. This indicates a dominance of Ti in the formation of the carbide phase. With Cb increased from 3.49 to 3.89 wt.% and higher Ti, the MC carbide lattice parameter increased. The Cb content of alloy 4 was higher than in alloy 2a but the Ti content was also increased. It appears that Ti is more likely to form MC carbides than

Cb. This has been described by other investigations. No measureable amounts of Laves or borides were precipitated in these alloys, either before the solution heat treatment or after the age heat treatment. The  $\gamma''$ ,  $\gamma'$  phase extraction analysis was much more ambiguous than the secondary phase precipitation. There is almost complete overlap of reflected peaks in  $\gamma'$  FCC and  $\gamma''$  BCT X-ray diffraction. Only one plane of reflection difference existed between the  $\gamma'$ -FCC structure and the  $\gamma''$ -BCT structure. This reflection, on the (020) plane, is weak. In order to distinguish this peak in X-ray diffraction, the particles must be very coarse. To obtain very coarse  $\gamma''$  particles requires an age heat treatment that produces a significant amount of overaged  $\delta$ -orthorhombic phase. The reflections from this phase also interfere with the identification of the  $\gamma''$  phase. As a result, X-ray peak measurements were not used for relative volume measurements. The solution and age alloys also showed evidence of  $\gamma''$  precipitation along with  $\gamma'$  precipitation. Not much extracted material was available and the precipitates were fine causing significant peak splitting and making it impossible to calculate the lattice parameters of the  $\gamma'$  and  $\gamma''$  phases. Some evidence of  $\eta$  precipitation was observed.

Alloys (1a, b, 2a, b, e, f) that were reprocessed retained an MC carbide precipitate. The lattice parameter was slightly different from the original as-rolled carbide lattice. The Laves phase may have been dissolved during the rolling operation as little evidence of it was observed in the re-rolled material. The only boride in evidence was in the lower Cb alloy with B added. In the direct age alloys, no

change was noted in the MC carbides phase. Laves phase precipitation occurred in all the low-Cb alloys containing W and W + V. The lattice parameter of the Laves phase did not change, where peaks were strong enough to measure the parameter accurately. The 1a, b, 2a, b, e and f alloys, processed by the direct aging-heat, had a relatively strong  $\gamma''$  peak. The  $\gamma'$  lattice parameter decreased with a decrease in the Cb content. Since some substitution for Cb occurs into the  $\gamma'$ -FCC lattice, the absence of Cb may have caused the lattice to shrink somewhat. This may result in lower mismatch and more stable  $\gamma'$  at high temperature. The overaged  $\delta$ -orthorhombic phase was not observed in the direct-age alloys. This was not expected since the processing of these alloys was designed to promote precipitation at grain boundaries. Again, interference between  $\gamma''$  and  $\delta$  peaks probably resulted in the apparent lack of  $\delta$ . Photomicrographs confirm the presence of the phase in these alloys.

## DISCUSSION

This section will explain the factors influencing the structure of Inconel Alloy 718 and the effects of chemistry modification on that structure. The influence of these structures on the mechanical properties will then be discussed.

Strengthening of Alloy 718

The primary strengthening phase in Inconel Alloy 718 is the precipitated BCT- $\gamma''$  with some FCC- $\gamma'$  precipitation present. The predominant strengthening mechanisms in superalloys have been described previously. They are: coherency strains in  $\gamma''$  strengthened alloys and ordering and anti phase boundary formation in  $\gamma'$  strengthened materials (25,33,34,98). The  $\gamma''$  coherency strains are the result of BCT ( $\gamma''$ ) - FCC ( $\gamma$ ) lattice mismatch (11,12,13,23,54,61,108). The precipitates in these alloys are interfaced with the matrix in the orientation:

$$\{100\}_{\gamma''} \parallel \{100\}_{\gamma}; \{001\}_{\gamma''} \parallel \langle 001 \rangle_{\gamma}$$

The mismatch results in a very high strength material at intermediate temperatures (below  $0.4T_M$ ) and down to cryogenic temperatures.

Strains are 2.5-2.8% in the "c" direction and 0.2-0.28% in the "a" direction. Coherency strains also account for the slow precipitation rate and low volume fraction ( 0.2) of  $\gamma''$  in Alloy 718. At elevated temperatures a stronger tendency exists for  $\gamma''$  particles to coarsen, reducing the coherency strains and reducing the alloy strength.

A determination of the mismatch between the precipitate and the matrix can be made with the following equation (6,27,36):

$$\text{Mismatch} = \delta = \frac{a_{0\gamma''} - a_{0\gamma}}{a_{\gamma}}$$

or, more precisely, taking into account the disc shape of the  $\gamma''$  precipitate:

$$= \frac{(a_{0\gamma''} - a_{0\gamma}) + (C_{0\gamma''} - a_{0\gamma})}{a_{0\gamma}} = \frac{a_{0\gamma''} + C_{0\gamma''} - 2a_{0\gamma}}{a_{0\gamma}}$$

where  $a_{0\gamma}$  is the matrix lattice parameter,  $a_{0\gamma''}$  is the precipitate lattice spacing in the "a" direction and  $C_{0\gamma''}$  is the lattice spacing in the "c" direction. The strain that this mismatch produces is determined by:

$$\text{Strain} = \epsilon = \delta \cdot \frac{1 + \nu}{1 + 2k + \nu(1-4k)}$$

where  $\nu$  is Poisson's ratio and  $k$  is the ratio of the shear modulus of the lattice and the precipitate. Assuming  $\nu = 1/3$  and  $k = 1$ , then  $\epsilon = 2/3 \delta$ .

Superalloys strengthened by FCC-  $\gamma'$  precipitation have lower coherency strains and rely on other mechanisms to provide elevated temperature strength. The lower coherency strains result in a precipitate that is more resistant to overaging and is stable at higher temperatures. The lower coherency strains also result in a much faster precipitation rate.

#### Modification of Alloy 718 strengthening

The development of a superalloy with a Cb content lower than Inconel Alloy 718 and comparable properties can proceed along several paths. First, solid solution strengtheners can be substituted for the reduced precipitation strengthening. Second, the  $\gamma''$  precipitate that remains can be stabilized or strengthened. Third, an equal replacement of  $\gamma'$  for the reduced  $\gamma''$  can be made through the addition of  $\gamma'$  forming elements. The last two options must be carefully controlled to prevent altering the precipitation characteristics of the alloy. In the first case, the contribution of matrix solid solution strengtheners to the overall strength of a precipitation hardened superalloy is less than 10%. The strengthening effects are stable at elevated temperatures, however, and may have a significant contribution to strength at these temperatures. However, the initial creep mechanism encountered by these materials at high temperatures is grain boundary sliding a mechanism not influenced by those elements. The use of solid solution elements would also require the use of grain boundary stabilizers. The amount of these elements required could lead to the formation of deleterious, unpredicted, phases such as carbides, borides and TCP phases.

The stabilization of the  $\gamma''$  precipitates, the second option mentioned above, would require the reduction of the coherency strains between the matrix and the precipitates. The distortion of the Ni-base alloy matrix lattice by Fe and Cr is similar to the distortion of the Ni-Fe-base alloy matrix by Mo and W. When Fe and Cr distorted the lattice,  $\gamma''$  precipitation became possible (6). By a similar mechanism Mo and W additions could increase the precipitation and stability of  $\gamma''$  in lower Cb alloys. This has been accomplished in  $\gamma'$  hardened alloys through additions of W and Mo (122). These are solid solution elements that may cause enough deformation of the matrix lattice to achieve better matching with the precipitate. The most potent element for altering the lattice is Cb (6). This element would thermodynamically rather form  $\gamma''$  or  $\gamma$  precipitates. The reduction of coherency strains in modified Alloy 718 would make  $\gamma''$  precipitation easier by reducing nucleation and growth barriers. This may severely alter the precipitation characteristics of the alloy, however, and result in an alloy that could not substitute for Alloy 718 in some applications. Lastly, the substitution of  $\gamma'$  forming elements for the reduced  $\gamma''$  forming elements could help the alloy maintain the properties of the standard alloy. Again, care must be taken to avoid changing the aging characteristics of the alloy. The logical element choice for this substitution is Ti. This would promote the  $\text{Ni}_3\text{Ti} - \gamma'$  precipitate. The proper Ti addition must be determined by the ratio of the  $\gamma'$  and the  $\gamma''$  forming elements. The  $\gamma'$  producing elements in Ni-Fe-base superalloys are Ti and Al. Ti substitutions were chosen over Al

substitutions because of the stronger tendency to form  $\gamma'$ . Al in Ni-Fe-base superalloys partitions between  $\gamma'$  ( $\text{Ni}_3(\text{Ti},\text{Al})$ ) and environmental protection; with no  $\text{Ni}_3\text{Al}$  formation. In Alloy 718, another technique has been exploited to increase the  $\gamma''$  precipitation (36,87). Because Cb is such a potent carbide former, the effective Cb content of Alloy 718 is decreased by the stoichiometric requirement of MC carbides. Table XXIV indicates the amount of Cb remaining, in the alloys investigated, after the MC carbide requirement has been satisfied. The Cb removed would probably be less than this amount because other elements, especially Ti and V, are also MC formers. However, any Cb removal would be reflected in reduced  $\gamma''$  precipitation. The use of a low C Alloy 718 has been explored as a method of reducing Cb content while maintaining the precipitation characteristics of the standard alloy (83). The work that has been done in this area gave no clear indication of how the reduced MC carbide content will affect the thermomechanical processing of the alloy. As mentioned previously, MC carbides provide some grain size control during processing, especially at temperatures above the  $\delta$  solvus (Figure 12).

#### Structures - Solution and Age Alloys

The effect of each of these substitutions could be seen in this investigation. The alloys studied had a variety of substitutions for the reduced Cb content. Additions of Mo and W were made to the lower Cb alloys (2e, c and 3b, c). These elements provide some solid solution strength and there is evidence that W may join the  $\text{Ni}_x\text{Cb}-\gamma''$  structure. These additions had a larger effect on mechanical

properties at elevated temperatures than at room temperature. This would indicate some solid solution strengthening but not enough to recover the properties of the standard Alloy 718. The W and Mo could have another effect, as mentioned previously. Solid solution elements expand or contract the lattice of the matrix. This alters the mismatch between the precipitate and the matrix. Reduction of the coherency strains should stabilize the precipitates at elevated temperatures, providing a higher use temperature. The precipitation characteristics of the alloy would also change; precipitation of the  $\gamma''$  would be faster than in the base alloy. The presence of relatively large atoms in the matrix lattice will reduce the diffusion rate of elements through the lattice. A slower precipitation rate and inhibited formation of the overaged phase result. Competition results from the effect of solid solution elements in alloys precipitating a BCT phase in an FCC matrix. The elements may speed precipitation by reducing coherency strains or may slow it by reducing diffusion. The solid solution elements would, in both cases, stabilize the metastable precipitate. The hardening rates of the alloys containing W and Mo are shown in the graph in Figure 45 and 46. The alloy with the W addition showed some apparent nucleation and growth of the hardening precipitate in a shorter time than the lower Cb alloys with no additions (2a). At longer times, however, the hardness of the alloys is the same. The Mo addition did not change the precipitation rate in the lower Cb alloys (2c,3b). It was not possible to determine the morphology of the precipitates (spherical  $\gamma'$  or disc  $\gamma''$ ) at the

shorter age times in these alloys. In the 1.10 wt.% Cb alloys (3a-d) the effect of the W and Mo additions was similar to the 3.0 wt.% Cb alloys. These alloys (3b,c) attained a peak hardness earlier than alloy 3a. This effect will be discussed later.

The influence of substituting Ti for the reduced Cb was also examined. Literature data indicated a definite effect of the  $\text{Ti+Al/Cb}$  ratio on the precipitate structure (114,115,116). Scanning Electron Microscope studies indicate a change in the predominant phase precipitating in alloys 1,2 and 3. Figures 47 through 49 indicate that  $\gamma''$  is the primary precipitate in alloy 1 (the standard alloy). A mixture of  $\gamma''$  and  $\gamma'$  is apparent in alloy 2 (with 3.00 wt.% Cb). The  $\gamma'$  phase is dominant in alloy 3 (1.10 wt.% Cb). Figure 50 is a plot of the (Ti+Al) content of alloys of this study and from the literature normalized by the Cb content and the Cb content, with the type of dominant precipitation (115,117,123). Definite  $\gamma''$  and  $\gamma'$  regions, defined by the Ti, Al and Cb levels exist. Figure 51, with fewer data points, indicates the effect of Ti and Cb on the overaged phase. In this case Al is not of concern because only Ti forms the overaged  $\text{Ni}_3\text{Ti}-\eta$  phase. Again, definite regions of  $\gamma$  and  $\eta$  precipitation are present. The effect of the particular overaged phase on properties is not known, but, to insure consistency throughout, it was decided to retain an overaged phase with a  $\delta$  or  $\delta + \eta$  structure. Examination of the SEM micrographs and X-ray diffraction data indicate that, in alloys 1 and 2, the overaged phase is  $\delta$ . In the micrographs of alloy 2, Figure 47, a zone around the grain boundary that is denuded of  $\gamma''$

precipitates occurs. No  $\gamma'$  (spherical particle) denuded zone is present, indicating that only Cb is removed from the bulk grain to form the grain boundary precipitates (125). This observation and the existence of the  $\gamma$  phase in the X-ray diffraction trace indicate a dominance of this phase over the  $\eta$  phase. The  $\delta$  phase was not detected in alloy 3 (by X-ray diffraction) and the precipitate was not found in the microstructure. The graph in Figure 51 indicates that the overaged phase should be  $\eta$ . Qualitative chemical analysis by EDAX indicates this could be the case since a greater amount of Ti occurs in the grain boundary precipitates of alloy 3 than the other alloys.

Table XXV lists the elements responsible for precipitation in alloys 1, 2 and 3. The ratios of Ti+Al and Ti to Cb and their effects on the metastable and stable phases, respectively, are also shown. From these ratios and the graphs in Figure 50, it was possible to determine Ti and Cb levels to substitute  $\gamma'$  for the decreased  $\gamma''$  precipitate while still maintaining a slow precipitation reaction.

#### Precipitation Sequence

The hardening rate of alloy 2a was similar to that of the standard Alloy 718 (Figure 52). The ratio of (Ti+Al) to Cb in alloy 2a could be tolerated while still maintaining the slow precipitation. It was necessary to also increase the Cb content over that of alloy 2. As a result of this analysis, two alloys were developed. The increased Ti and Cb were maintained in a ratio to promote  $\gamma'' + \gamma'$  precipitation. The  $\gamma'$  precipitate was anticipated to be a smaller part of the room temperature strength, but, because of the superior elevated temperature

stability of  $\gamma'$ , it should be a larger contributor to high temperature properties. Microstructural analysis on alloys 4 and 5 confirmed the effect of the  $\text{Ti+Al/Cb}$  ratio on the precipitate morphology. Figures 53, 26 and 27 shows the structure of alloys 4 and 5 after solution and age heat treatment. The precipitates are a combination of discs and spherical particles ( $\gamma''$  and  $\gamma'$ ). The volume fraction ( $\gamma'' + \gamma'$ ) was less than the lower Cb alloys. This may have been caused by a higher than expected C content. The nominal C content was within specified levels but, locally, the level may have been higher. The hardening rates of alloys 4 and 5 were comparable to that for alloy 2 (Figure 54). This would indicate a similar precipitation sequence. SEM photomicrographs of alloys 1a, 2a, 3a, 4a and 5 after solution heat treatment and aging for 10, 100 and 1600 minutes show the precipitation characteristics of these alloys. Some  $\gamma'$  precipitation in alloys 1a, 3a and 13a was apparent after 100 minutes at  $695^{\circ}\text{C}$  ( $1300^{\circ}\text{F}$ ). After 10 minutes at this temperature, a small increase in  $R_c$  hardness took place but no observed precipitation occurred in any of the alloys. The precipitates were probably too small to be resolved. After 1600 minutes at the aging temperature more complete microstructures were developed. Alloy 1a had a structure similar to the alloy aged 100 hours (6000 minutes) at this temperature. Some  $\eta$  precipitation at the grain boundaries was noted. Alloy 3a had a  $\gamma' + \gamma''$  precipitate after 1600 minutes. Alloy 3a had little overall precipitation, but according to the hardening rate curve, it had reached its full hardness. The precipitates may have been too fine to

be seen, only being resolved after 100 hours (Figure 30). Alloys 4 and 5 had substantial  $\gamma' + \gamma''$  precipitation after 1600 minutes of aging at 695°C (1300°F).

These structures confirm the relative precipitation rates of the  $\gamma'$  and  $\gamma''$  phases. The  $\gamma'$  phase precipitates first, because of the lower barriers to nucleation and growth, and then  $\gamma''$  precipitates. The  $\gamma''$  provides the more significant contribution to strength. The hardening rate curve indicates that a difference in the precipitation sequence in alloys 4 and 5 may exist. Alloy 4 appears to reach a higher hardness than alloy 5 in 100 minutes. After 6000 minutes, however, alloy 5 exhibits the greater hardness and strength (Figure 54). The  $\gamma'$  phase may precipitate faster in alloy 3 as a result of the lower absolute Cb content, increasing its initial hardness. The contribution of Cb to the longer term hardness and strength is less in alloy 4 than alloy 5. Accordingly, after longer aging times, alloy 5 is stronger than alloy 4. X-ray diffraction analysis could confirm this. However, differences between the  $\gamma'$  and  $\gamma''$  phases cannot be readily determined in X-ray diffraction. Literature information, however, confirms this type of sequential precipitation and relative contribution to strengthening (114,115,116).

#### Tensile Properties - Solution and Age Alloys

The room temperature tensile properties of alloys 1a, 2a and 3a indicate the strong dependence of Alloy 718 on Cb content. The relationship is the same as for the hardness. The beneficial effect of B on the tensile properties is also evident. Additions of Ti to

the reduced Cb alloys improved the strength of the alloy to a level above this linear relationship. The Ti promotes the formation of  $\gamma'$  which may have contributed to the improved strength. The grain boundary strength of the alloys is also important. Alloy 1a contained  $\gamma$  and carbide precipitation at grain boundaries. These phases would be expected to improve the tensile properties of alloy 1a at room temperature. Alloy 5 did not exhibit the same grain boundary phases. The lack of grain boundary strengthening phases in alloy 5 indicate that the improved strength of the alloy is the result of  $\gamma'$  precipitation strengthening. The alloy did retain the ductility of alloy 1a.

The decrease in strength in alloy 1a at temperatures above 540°C (1000°F) is the result of two phenomena. First,  $\gamma''$  strengthening decreased as the particles began to coarsen. Second, grain boundary regions became weaker. Up to 540°C, the decrease in strength is gradual while the ductility decreases substantially. In this temperature range, the coherency strains between the  $\gamma''$  particles and the matrix increase. The grain boundary regions are still strong at these temperatures. As a result, the decrease in strength is small while the material becomes less ductile. At temperatures above 540°C, grain boundary strength decreases rapidly and the  $\gamma''$  particles begin to coarsen, accelerating the decrease in the coherency strain effect. As the temperature increases, this coarsening accelerates and the grain boundaries are further weakened. Strength decreases more rapidly and ductility increases at these temperatures. The B addition improved the strength and ductility of the standard

alloy at all temperatures. The presence of B at the grain boundaries prevented the formation of phases that would exhibit low energy fracture, stabilizing these regions at high temperatures and allowing the grain boundaries to retain their ductility. This results in a stronger, more ductile alloy.

The strength of the lower Cb alloys was more affected by solid solution elements at elevated temperatures than at room temperatures. The W and W + V additions to the 3.0 wt.% Cb alloys were twice as effective at increasing strength at elevated temperatures than at room temperatures. The room and elevated temperature strength of the low Cb alloys were not affected by Mo additions. B also had a more significant effect at elevated temperatures. Coincident additions of Mo and B were less effective at elevated temperature than at room temperature. Interactions between the Mo and B are unlikely because of the relatively low temperatures involved. At elevated temperatures the solid solution elements provide a more significant component of the overall strength of the alloys than at room temperature because the contribution of  $\gamma''$  precipitation to overall strength is less in alloys with reduced Cb contents. The effect of  $\gamma''$  is also reduced somewhat at temperatures over 595°C (1100°F) so the solid solution elements have a more pronounced effect at these temperatures.

The tensile strength of the high Ti alloys did not exhibit the rapid decrease in strength at temperatures over 540°C (1000°F). As described above, this is the result of two phenomena. The  $\gamma'$  precipitates provide strengthening at temperatures above the limit of

$\gamma''$  strengthening. Grain boundary strength also accounts for a large portion of the strengthening of these of these alloys. The grain boundary regions of the highest Ti alloys did not contain the phases that were evident in the standard alloy. At intermediate temperatures, the  $\gamma''$  strengthening is significant and the grain boundaries of alloy 1a were stable. As a result, at intermediate temperatures, alloy 1a was much stronger than alloy 5. The strengthening mechanisms in the high Ti alloys is a combination of  $\gamma'$  and  $\gamma''$  effects. At lower temperatures the coherency strain effects of  $\gamma''$  probably dominate. At high temperatures the anti-phase-boundary and ordering effects of  $\gamma'$  dominate. The lack of a sharp drop in strength at the highest temperatures and a decrease in ductility at these temperatures is strong evidence that APB and ordering effects were dominate in the alloy.

#### Stress Rupture Properties - Solution and Age Alloys

The stress rupture properties are also sensitive to the type of precipitate and grain boundary strength of the superalloy. The superior stress-rupture properties of the high Ti alloy is a result of the dominance of  $\gamma'$  strengthening and stronger grain boundaries. The stronger grain boundaries in this alloy are a result of less precipitation of carbides and  $\delta$  in these regions. At all temperatures the yield strength of the standard alloy is greater than that for the high Ti alloy. However, at temperatures above 540°C (1000°F), alloy 5 has superior stress rupture properties, indicating reduced grain boundary creep in this alloy. It would be inappropriate to separate the effects of grain boundary strength and  $\gamma'$  strengthening in the high Ti alloy.

The addition of B to the standard alloy improved its stress-rupture properties. The B may have improved the grain boundary ductility, as indicated by the ductility of alloy 1b in Table X. The addition did not significantly affect the microstructure of the alloy, however, and significant precipitation occurred at the grain boundaries. It is not clear how the B additions altered the properties of the alloy. The increased ductility of superalloys containing B does make further alloying possible. Elements that improve strength but reduce ductility could be added in conjunction with B. The new alloy would be stronger and still retain the ductility of the original alloy. The formation of undesirable phases may restrict the additions of hardening elements.

#### Alloying and Structures - Direct Age Alloys

The alloys processed with the direct age heat treatment were consistently stronger and less ductile than the solution and age alloys. This was the result of smaller grain size of the direct age alloys. The grain size is, in turn, dependent upon the temperatures used during thermomechanical processing. The micrographs in Figures 55 through 57 indicate that the proper processing schedule was not followed during the rerolling of alloys 1a, b and 2a, b, e, f. The as-rerolled alloys contained a large amount of  $\gamma''$  and  $\delta$  precipitations. This indicates that proper temperatures were not maintained during the rolling. The direct age process requires that deformation occur at temperatures above the  $\gamma''$  solvus and near, but not over, the  $\delta$  solvus, within the "warm rolled" temperature region. In this case, the temperature was not above the  $\gamma''$  solvus. As a result, the  $\gamma''$  precipitates

were coarse while  $\gamma$  was heavy and extended beyond the grain boundaries. The rolling temperature was probably above the peak  $\gamma''$  precipitation temperature and near the temperature that maximized the  $\gamma$  precipitation. In the warm rolling temperature regime, a great deal of strain energy is put into the material. Some of this is lost to the recovery processes that take place at these temperatures, while some strain energy remains in the material. This energy and the precipitation of the strengthening phases, contribute to the material strength. If the deformation temperature is not into the warm rolled temperature region, the precipitating phase is not dissolved. At these lower temperatures, the recovery processes in the alloy are not activated. More strain energy is put into the material.

The precipitation of  $\gamma$  during processing reduces the Cb available for  $\gamma''$  precipitation. Aging these alloys after the rerolling produced only a small amount of additional  $\gamma''$  precipitation. The as-rerolled hardness of the alloys were similar to those for the aged alloys. This indicates that the hardness increase was the result of the strain energy input and not from the subsequent aging heat treatment (which also was reduced as a result of the large  $\gamma$  precipitation.)

#### Processing Effects - Direct Age Alloys

The rerolling of alloys 1a, b and 2a, b, e, f increased their yield strength and decreased the ductility. The tensile strength of these alloys was not affected. This increase in flow stress was the result of increased strain energy input, while the lack of tensile strength improvement indicated that the precipitation hardening has a

greater effect on tensile strength than strain energy. This was the result of the reduced  $\gamma''$  precipitation in the direct age rerolled alloys over the original direct age alloys. More precise controls and proper temperature selection would have yielded the proper structure for a direct age alloy. The standard alloy (1a,b) should be thermomechanically processed above  $980^{\circ}\text{C}$  ( $1800^{\circ}\text{F}$ ) and below  $1000^{\circ}\text{C}$  ( $1830^{\circ}\text{F}$ ). This would dissolve  $\gamma''$  and still permit some  $\gamma$  precipitation. Some recovery will have occurred but no recrystallization will develop. In alloys 2a, b, e, and f, the recrystallization temperature is similar to that for the standard alloy. These alloys should be processed alone at temperatures around  $980^{\circ}\text{C}$  ( $1800^{\circ}\text{F}$ ). Segregation in direct age alloys has been avoided in other investigations. Homogenization of the standard alloy is possible, without grain growth, at temperatures between  $996^{\circ}\text{C}$  ( $1825^{\circ}\text{F}$ ) and  $1010^{\circ}\text{C}$  ( $1850^{\circ}\text{F}$ ). This will dissolve the  $\delta$ ,  $\gamma''$ , TCP and boride phases in the material. The alloys are held at these temperatures for 24 to 48 hours to insure homogenization. Thus, several, carefully controlled processing steps are required to obtain the proper direct age structure. These steps were described previously; here the steps are listed with the temperature range these steps require, after melting, casting and homogenization (26): (i) extrusion (or forging, rolling, etc.) at  $980\text{--}1000^{\circ}\text{C}$  ( $1800\text{--}1820^{\circ}\text{F}$ ), (ii) upset forging, (iii) homogenization at  $996\text{--}1010^{\circ}\text{C}$  ( $1825\text{--}1850^{\circ}\text{F}$ ), repeat (i) through (iii) until the desired grain size is developed. Once the proper grain size is attained, the alloy is given the two step age heat

treatment; 730°C(1350°F)/8 hours; furnace cool at 38°C (100°F) per hour; hold at 620°C (1150°F)/8 hours; air cool.

#### Tensile Properties - Direct Age Alloys

The direct age alloys were consistently stronger and less ductile than the solution and age alloys. The direct age alloys in this study were 12 to 15% stronger than the corresponding solution and age alloy. The ductilities were about 50% of the solution and age alloys. The reduced Cb alloys, reprocessed and direct aged, were not as strong as the standard Alloy 718. The decrease in room temperature strength was comparable to that for the original direct age alloys and less than that for the solution and age alloys. The effect of B, W and W+V additions were, surprisingly, more pronounced in the solution and age alloys. The similarity of tensile properties for the original direct age and the reprocessed direct age alloys indicates that the rolling operation was not successful because of the improper rolling temperature. The effect of reduced Cb in the solution and age alloys is to reduce  $\gamma''$  precipitation and weaken the alloy. A similar response is apparent in the direct age alloys. The  $\gamma''$  precipitate is a major strengthener in these alloys. The strain energy imparted to the material displaces the entire curve to a higher base strength; but the dependence on Cb is unaltered. Standard Alloy 718 was strengthened by the B addition, apparently by strengthening the grain boundaries. No corresponding decrease in ductility occurred in alloy 1b. At elevated temperatures this alloy maintained its superiority in strength and ductility.

The effect of temperature on direct age alloys is similar for the two Cb levels. The 3.0 wt.% Cb alloys were shifted 10-15% below the strength of the standard alloy at elevated temperatures. The alloys containing W and W+V were slightly stronger, at room temperature, than the same alloy with no additions. The B addition to the lower Cb alloy had no effect on strength at any temperature. Apparently the B provides no strength to the grain boundaries of these lower Cb alloys. It did not improve the strength of the original direct age alloy either. An increase in ductility in the alloy occurred both in the original and reprocessed alloys as a result of the B addition. The B may prevent continuous carbide film formation, but, due to the reprocessing conditions, weaker, denuded, grain boundaries could not be avoided. At the highest temperatures the lower Cb alloys had very similar ductility. At elevated temperatures, only the alloy with W+V additions was able to remain stronger than the low Cb alloy with no additions. The effect of the W addition diminished at temperatures of 540°C (100°F). The expected solid solution effects of W were not evident. Based upon the similar high temperature strengths of alloy 2a and 2e, the predominant strengthening mechanism in these alloys is coherency strains between  $\gamma''$  and  $\gamma$ . Solid solution strengtheners and the presence of  $\gamma'$  precipitates had no effect on strength of the direct age alloys. The lack of influence by V or W+V together was not clear. Vanadium is a strong MC carbide former. The formation of significantly more carbides may have prevented the recovery processes or delayed them to higher temperatures. The V may stabilize grain boundary carbides

but this is unlikely because of the presence of the  $\gamma$  phase at grain boundaries in direct age alloys.

As seen in the solution and age alloys the tensile ductility of the direct age alloys decreased at intermediate elevated temperatures. The decrease in ductility between room temperature and  $595^{\circ}\text{C}$  ( $1100^{\circ}\text{F}$ ) was the result of increased coherency strains between the precipitate and the matrix. Competing against the coherency strain mechanism are softening mechanisms activated by the higher temperature. The result could be a weaker less ductile alloy at intermediate temperatures. At the highest test temperature,  $650^{\circ}\text{C}$  ( $1200^{\circ}\text{F}$ ), the coherency strains have been overcome by the grain boundary weakening and coarsening. Coarsening reduces precipitate surface area and promotes the formation of non-coherent phases or  $\gamma$ . The result, as shown here and in other studies, is a large decrease in tensile strength over a particular temperature range. For all the alloys in this direct age study, this temperature range is between  $560^{\circ}\text{C}$  ( $1050^{\circ}\text{F}$ ) and  $650^{\circ}\text{C}$  ( $1200^{\circ}\text{F}$ ). At  $650^{\circ}\text{C}$  ( $1200^{\circ}\text{F}$ ), regardless of alloying additions, the lower Cb alloys had essentially the same strength and ductility. This further indicates that the predominant strengthening mechanism in direct age alloys is  $\gamma''$  precipitation and the grain boundary strength. Solid solution effects are negligible in direct age alloys at the maximum service temperatures. Surprisingly, the softening temperature of the direct age alloys was the same as that for the solution and age alloys,  $560^{\circ}\text{C}$ .

Segregated regions rich in Cb and some other elements are also

prone to the formation of deleterious phases. The as-rolled and direct age heat treated alloys contained significant amounts of the Laves phase as the result of this segregation. During processing, a heat treatment to dissolve these phases is essential. The Laves phase apparent from the X-ray diffraction analysis was much finer and more disperse throughout the microstructure. The severe segregation could also promote the formation of carbides that do not normally occur in more homogeneous alloys. The Mo + W content has been shown to have a strong effect on the carbide structure. Accordingly, Mo + W content may exceed the threshold amount to change the carbides while the bulk alloy would not (28,49,50). The effect of homogeneous composition on the precipitated phases is complex. Interactions between elements and phases can cause ambiguous analysis. This investigation attempted to avoid these interactions so that results could be analyzed more precisely.

#### Alloying Effects on Stoichiometry of Phases

Changes in the Ti + Al to Cb ratio affects not only the strengthening precipitates; it also influences the other phases in the alloy. As the  $Ti/Cb$  ratio increases, the MC carbide will contain greater proportions of Ti (or, conversely, less Cb). As a result, the lattice of the MC carbide will change. Since the atomic volume of Ti is less than that of Cb, a slight decrease in the lattice parameter of the MC carbides occurs as the  $Ti/Cb$  ratio increases. The lattice parameter of pure CbC is greater than that of the extracted carbide, indicating a (Ti, Cb)C even in the standard alloy 718. The decrease in the  $\gamma'$

lattice parameter at lower Cb, observed in the direct age alloys, did not take place in the solution and age heat treated alloys. The lattice parameter decrease may have been the result of two effects: (1) the reduced Cb content from the significant precipitation in the direct age alloys, and (2) the short age times. First, Cb has been shown to substitute into the FCC -  $\gamma'$  lattice (6,126). The lattice parameter of the  $\gamma'$  would increase in the presence of Cb. The  $\gamma$  precipitation may have reduced the available Cb in the 3.0 wt.% Cb alloys. Second, at longer aging times, as in the solution and age heat treated alloys, the  $\gamma'$  phase may reject Cb as it coarsens, reducing the strains on the  $\gamma'$  lattice as it does so. This would reduce the  $\gamma'$  lattice parameter by reducing the  $\gamma'$  Cb content. The combination of these two effects may account for the different lattice parameter behavior of the direct age and solution and age alloys.

## CONCLUSIONS

Based on the above results, the following conclusions can be made:

1. Reduced Cb contents in Inconel Alloy 718 reduces the precipitation of the primary strengthening phase,  $\gamma''$ , and promotes formation of  $\gamma'$  precipitates, at the standard Ti contents. The  $(Al+Ti)/Cb$  ratio will indicate the strengthening phase that forms. The decreased  $\gamma''$  precipitation results in a decrease in tensile strength at room temperature and 650°C (1200°F), with a linear relationship between Cb content and tensile properties. Additions of solid solution strengthening elements do not recover these properties to the level of the original alloy. Increased  $\gamma'$  forming elements, in the presence of reduced Cb, will recover some of these properties at room temperature.

2. At temperatures above 540°C (1000°F) Alloy 718 undergoes a sharp decrease in tensile properties as the result of  $\gamma''$  coarsening and reduced grain boundary strength. In the presence of increased  $\gamma'$  formers, in a reduced Cb alloy, the tensile properties exhibit a linear response to temperature between 25 and 650°C (77-1200°F) as the result of  $\gamma'$  stability and grain boundary strength. An alloy containing 3.89 wt.% Cb and 1.27 wt.% Ti exhibited stress-rupture properties superior to Alloy 718 at 595 and 650°C (1100, 1200°F).

3. Direct age alloys with reduced Cb can substitute for the standard alloy in applications where yield and tensile strength are important. The deformation processing and direct age heat treatment

must be tightly controlled to avoid undesirable structures.

4. The addition of B to solution and age heat treated Alloy 718 produced a coincident increased yield and tensile strength and an increase in ductility. The stress-rupture life of the standard alloy was improved greatly as a result of the B addition. Additions of B to solution and age alloys with reduced Cb, while not strongly influencing tensile strength, could improve the tensile and stress-rupture properties of these alloys as well.

## REFERENCES

1. R. F. Decker and C. T. Sims; The Metallurgy of Nickel-base Alloys; from The Superalloys, Sims and Hagel Eds; John Wiley and Sons, New York, 1972.
2. D. R. Muzyka; The Metallurgy of Nickel-Iron Alloys; from The Superalloys, Sims and Hagel Eds.; John Wiley and Sons, New York, 1972.
3. ASM Handbook, 9th Edition, Volume 3; American Society for Metals, Metals Park, 1980, pp. 207-268.
4. N. S. Stoloff; Fundamentals of Strengthening; from The Superalloys, Sims and Hagel, Eds, John Wiley and Sons, New York, 1972.
5. R. F. Decker; Strengthening Mechanisms in Nickel-Base Superalloys; Metals Reviews, pp. 147-170.
6. M. Naik and G. S. Ansell; Effect of Refractory Elements on the Coherency Strain and Flow Stress of Nickel-base Alloys; from Refractory Alloying Elements in Superalloys, Tien & Reichman, Eds.; ASM, Metals Park, Ohio, 1984, pp. 153-164.
7. Lecture Notes; EMMS 401, Professor R. F. Hehemann, Dept. of Metallurgy and Materials Science, Case Western Reserve University; Fall 1983.
9. R. A. Ricks, A.J. Porter and R. C. Eob; The Growth of  $\gamma'$  Precipitates in Nickel-Base Superalloys; Acta Metallurgica, 31 pp. 43-53 (1983).
10. D. Raynor and J. M. Silcock; Strengthening Mechanisms in  $\gamma'$  Precipitating Alloys; Metal Science Journal, 4 pp. 121-130 (1970).
11. P. S. Kotval; Identification of the Strengthening Phase in Inconel Alloy 718; Transactions of the Metallurgical Society of AIME, 242, pp. 1764-1765 (1968).
12. I. Kirman and D. H. Warrington; Identification of the Strengthening Phase in Fe-Ni-Cr-Nb Alloys; Letter to Editor, Journal of the Iron and Steel Institute, 205 No. 12, pp. 1264-1265 (1967).
13. A. Kaufman and S. Niedzwiedz; On the Precipitation of  $\text{Ni}_3\text{Nb}$ ; Scripta Metallurgica, 3 pp. 655-658 (1969).

14. A. Kaufman, N. J. Hoggman and H. Lipson, *Scripta Metallurgica*, 3, pp. 715-720 (1969).
15. W. J. Boesch and J. S. Slaney; Preventing Sigma Phase Embrittlement in Nickel-Base Superalloys; *Metal Progress*, July 1964, pp. 109-111.
16. J. P. Stroup and R. A. Heacox; Effect of Grain Size Variation on the Long-Time Stability of Alloy 718; *International Symposium on Structural Stability of Superalloys*, 1968, pp. 544-578.
17. R. Mihalisin, C. G. Bieber and R. T. Grant; Sigma - Its Occurrence, Effect, and Control in Ni-Base Superalloys; *Transactions of the Metallurgical Society of AIME*, 242, pp. 2399-2414 (1968).
18. W. E. Quist, R. Taggart and D. H. Polonis; The Influence of Fe and Al on the Precipitation of Metastable  $Ni_3Nb$  Phases in the Ni-Nb System; *Metallurgical Transactions*, 2, pp. 825-832 (1971).
19. M. C. Chaturvedi and D. W. Chung; Effect of Iron Addition on the Precipitation Behavior of CoNiCr Alloys Containing Nb; *Metallurgical Transactions*, 10A, pp. 1579-1585 (1979).
20. C. R. Whitney and G. Krauss; Effects of Ti and Al Variations on an Fe-Ni Superalloy, *Metals Engineering Quarterly*, Nov. 1971, pp. 25-30.
21. B. H. Kear, A. F. Giamci, J. M. Silcock and R. K. Ham; Slip and Climb Processes in  $\gamma'$  Precipitation Hardened Nickel-Base Alloys; *Scripta Metallurgica*, 2, pp. 287-294 (1968).
22. I. Kirman; Precipitation in the Fe-Ni-Cr-Nb System; *Journal of the Iron and Steel Institute*, 207 No. 12, pp. 1612-1618 (1969).
23. I. Kirman and D. H. Warrington; The Precipitation of  $Ni_3Nb$  Phases in a Ni-Fe-Cr-Nb Alloy; *Metallurgical Transactions*, 1, pp. 2667-2675 (1970).
24. A. Kaufman and A. E. Paulty; The Phase Structure of Inconel 718 and 702 Alloys; *Transactions of the Metallurgical Society of AIME*, 221, pp. 1253-1262 (1961).
25. O. H. Kriege and J. M. Baris; The Chemical Partitioning of Elements in Gamma Prime Separated from Precipitation-Hardened, High-Temperature Nickel-Base Alloys; *Transactions of the ASM*, 62 pp. 195-200 (1969).

26. Personal Communication, Herb Black, Universal Cyclops Corp.
27. Ya-fang Han, P. Deb and M. C. Chaturvedi; Coarsening Behavior of  $\gamma''$  and  $\gamma'$  Particles in Inconel Alloy 718; *Metal Science*, 16, pp. 555-561 (1982).
28. R. O. Williams; Origin of Strengthening on Precipitation: Ordered Particles; *Acta Metallurgica*, 5, pp. 24-244 (1957).
29. R. F. Decker and J. R. Mihalisin; Coherency Strains in  $\gamma'$  Hardened Nickel Alloys; *Transactions of the ASM*, 62 pp. 481-489 (1969).
30. B. Reppich; Some New Aspects Concerning Particle Hardening Mechanisms in  $\gamma'$  Precipitating Ni-Base Alloys - I. Theoretical Concept; *Acta Metallurgica*, 30 pp. 87-94 (1982).
31. B. Reppich; Some New Aspects Concerning Particle Hardening Mechanisms in  $\gamma'$  Precipitating Ni-Base Alloys-II Experiments; *Acta Metallurgica*, 30 pp. 95-104 (1982).
32. V. A. Phillips; Coherency Hardening in Ni-Al-Ti Alloys; *Scripta Metallurgica*, 2, pp. 147-152 (1968).
33. P. S. Kotval; Strengthening of Nickel-Base Superalloys by Precipitation of a Body-Centered Tetragonal  $\gamma''$  Phase;
34. J. M. Oblak, D. F. Paulonis and D. S. Duvall; Coherency Strengthening in Ni-Base Alloys Hardened by  $\text{DO}_{22}$   $\gamma''$  Precipitates; *Metallurgical Transactions*, 5 pp. 143-153 (1974).
35. J. P. Pedron and A. Pineau; The Effect of Microstructure and Environment on the Crack Growth Behavior of Inconel 718 Alloy at 650°C Under Fatigue, Creep and Combined Loading; *Materials Science and Engineering*, 56, pp. 143-156 (1982).
36. T. E. Gibbons and B. E. Hopkins; The Influence of Grain Size and Certain Precipitate Parameters on the Creep Properties of Ni-Cr-Base Alloys; *Metal Science Journal*, 5, pp. 233-240 (1971).
37. W. J. Boesch and H. B. Canada; Precipitation Reactions and Stability of  $\text{Ni}_3\text{Cb}$  in Inconel Alloy 718; *International Symposium on Structural Stability in Superalloys*; 1968, pp. 579-596.

38. H. L. Eiselstein, Metallurgy of a Columbium-Hardened Nickel-Chromium-Iron Alloy; ASTM STP 369 (1969).
39. H. J. Wagner and A. M. Hall, Physical Metallurgy of Alloy 718; DMIC Report 217 (1965).
40. W. J. Boesch and H. B. Canada; Precipitation Reactions and Stability of  $\text{Ni}_3\text{Cb}$  in Inconel Alloy 718; International Symposium on Structural Stability of Superalloys, 1968, pp. 579-596.
41. S. Floreen and R. H. Kane; Effects of Environment on High Temperature Fatigue Crack Growth in a Superalloy; Metallurgical Transactions, 11A, pp. 1745-1751 (1979).
42. W. M. Robertson; Hydrogen Permeation and Diffusion in Inconel 718 and Incoloy 903; Metallurgical Transactions, 8A, pp. 1709-1712 (1977).
43. D. Fournier and A. Pineau; Low Cycle Fatigue Behavior of Inconel 718 at 298K and 823K; Metallurgical Transactions, 8A pp. 1095-1105 (1977).
44. E. L. Raymond, Effect of Grain Boundary Denudation of Gamma Prime on Notch-Rupture Ductility of Inconel Nickel-Chromium Alloys X-750 and 718; Transactions of the Metallurgical Society of AIME; 239, pp. 1415-1422 (1967).
45. D. R. Muzyka and G. N. Maniar; Effect of Solution Treating Temperature and Microstructure on the Properties of Hot-Rolled 718 Alloy; Metals Engineering Quarterly, ASM, Nov. 1969, pp. 23-37.
46. L. R. Woodyatt, C. T. Sims and H. J. Beattie; Prediction of Sigma-Type Phase Occurrence from Compositions in Austenitic Superalloys; Transactions of the Metallurgical Society of AIME, 236, pp. 519-527 (1966).
47. H. E. Collins; Relative Long-Time Stability of Carbide and Intermetallic Phases in Ni-Base Superalloys; Transactions of the ASM, 62, pp. 82-104 (1969).
48. Precipitation Processes in Solids, Russell and Aaronson, Eds; 1976 Conference Proceedings, The Metallurgical Society of AIME.
49. H. E. Collins: Relative Long-Time Stability of Carbide and Intermetallic Phases in Nickel-Base Superalloys; Transactions of the ASM, 62 pp. 82-104 (1969).

50. R. L. Dreshfield; The Effect of Refractory Elements on the Stability of Complex Carbides in Ni-Base Superalloys; Transactions of the ASM, 61, pp. 352-354 (1968).
51. J. M. Oblak and W. A. Owczarski; Thermomechanical Strengthening of a ' Precipitation-Hardened Nickel-Base Alloy; Metallurgical Transactions, 3 pp. 617-626 (1972).
52. R. S. Cremisio, H. M. Butler and J. F. Radavich; The Effect of Thermomechanical History on the Stability of Alloy 718; International Symposium on Structural Stability of Superalloys, 1968, pp. 597-618.
53. D. R. Muzyka and G. N. Maniar; Effects of Solution Treating Temperature and Microstructure on the Properties of Hot Rolled 718 Alloy; Metals Engineering Quarterly, ASM; Nov. 1969, pp. 23-37.
54. C. P. Sullivan and M. J. Donachie Jr.; Some Effects of Microstructure on the Mechanical Properties of Nickel-base Superalloys; Metals Engineering Quarterly, ASM; Feb. 1967, pp. 36-45.
55. A. R. Knott and C. H. Symonds; Compositional and Structural Aspects of Processing Ni-Base Alloys; Metals Technology, Aug. 1976, pp. 370-379.
56. J. M. Walsh and B. H. Kear; Direct Evidence for Boron Segregation to Grain Boundaries in a Nickel-Base Alloy by Secondary Ion Mass Spectrometry; Metallurgical Transactions, 6A pp. 226-229 (1975).
57. R. F. Decker and J. W. Freeman; The Mechanism of Beneficial Effects of B and Zr on the Creep Properties of a Complex Heat-Resistant Alloy; Transactions of the Metallurgical Society of AIME, 218, pp. 277-285 (1960).
58. R. T. Holt and W. Wallace; Impurities and Trace Elements in Ni-Base Superalloys; International Metals Reviews, Review 203, March 1976.
59. A. W. Denham and J. M. Silcock; Precipitation of Fe<sub>2</sub>Nb in a 16 wt. % Ni - 16 wt. % Cr Steel, and the Effect of Mn and Si Additions; Journal of the Iron and Steel Institute, May 1969, pp. 585-592.
60. M. C. Chaturvedi and R. W. K. Honeycombe; Precipitation of the Laves Phases in Fe-Mn-Nb Austenites; Journal of the Iron and Steel Institute, May 1969, pp. 593-597.

61. F. J. Rizzo and J. D. Buzzanell; Effect of Chemistry Variations on the Structural Stability of Alloy 718; International Symposium on Structural Stability in Superalloys; 1968, pp. 501-543.
62. C. T. Sims; The Occurrence of Topologically Close-Packed Phases from The Superalloys; Sims and Hagel, Eds, pp. 259-284, John Wiley and Sons, New York, 1972.
63. C. P. Sullivan and M. J. Donachie, Jr.; Microstructures and Mechanical Properties of Ion-base (-containing) Superalloys; Metals Engineering Quarterly, ASM; Nov. 1971, pp. 1-11.
64. J. H. Westbrook; Temperature Dependence of the Hardness of Secondary Phases Common in Turbine Bucket Alloys; Transactions of the AIME, Journal of Metals, 209 p. 898 (1957).
65. H. J. Beattie and W. C. Hagel; Intergranular Precipitation of Intermetallic Compounds in Complex Austenitic Alloys; Transactions of the Metallurgical Society of AIME, 221, pp. 28-35 (1961).
66. F. L. Ver Snyder and H. J. Beattie; The Laves and Chi Phases in a Modified 12 Cr Stainless Alloy; Transactions of the ASM, 47, pp. 211-230 (1955).
67. V. Biss, G. N. Kirby and D. L. Sponseller; The Relative Effects of Cr, Mo, W and Ta on the Occurrence of  $\sigma$  Phase in Cast Co-Ni-Cr Alloys; Metallurgical Transactions, 7A, pp. 1251-1261 (1976).
68. G. N. Kirby, D. C. Sponseller and L. H. Van Vlack; The Relative Effects of Cr, Mo and W on the Occurrence of  $\sigma$  Phase in Ni-Co-Cr Alloys; Metallurgical Transactions, 5, pp. 1477-1494 (1974).
69. H. J. Beattie and W. C. Hagel; Compositional Control of Phases Precipitating in Complex Austenitic Alloys; Transactions of the Metallurgical Society of AIME, 233 pp. 277-287 (1965).
70. K. P. Gupta, N. S. Rajan and P. A. Beck; Effect of Si and Al on the Stability of Certain Sigma Phases; Transactions of the Metallurgical Society of AIME, 218, pp. 617-624 (1960).
71. P. A. Blenkinsop and J. Nutting; Precipitation of the Sigma Phase in an Austenitic Steel; Journal of the Iron and Steel Institute, Sept. 1967, pp. 953-958.

72. J. C. Uy, C. J. Nolan and T. E. Davidson; The Hydrostatic Extension of Nickel-Base Superalloys at Room Temperature; Transactions of the ASM, 60 pp. 693-698 (1967).
73. R. A. Heacox; Influence of Cold Reduction and Heat Treatment on the Properties and Microstructure of Alloy 718 Fastener Stock, Mechanisms of Phase Transformations in Crystalline Solids, Proceedings of 1968 International Symposium; Institute of Metals, 1969.
74. D. R. Muzyka; Controlling Microstructures and Properties of Superalloys Via Use of Precipitated Phases; Metals Engineering Quarterly, ASM; Nov. 1971, pp. 12-20.
75. D. R. Muzyka; Physical Metallurgy and Effects of Process Variables on the Microstructure of Wrought Superalloys; MiCon '78, ASTM STP 672, Abrams, Maniar, Nail and Solomon, Eds.; pp. 526-546.
76. C. Hammond and S. Nutting; The Physical Metallurgy of Superalloys and Ti Alloys; Metal Science, Oct. 1977, pp. 474-490.
77. B. H. Kear, J. M. Oblak and W. A. Owczarski; Thermomechanical Processing of Nickel-Base Alloys; Journal of Metals, June 1972 pp. 25-32.
78. I. Kiman and D. M. Warrington; The Effect of Deformation on Precipitation in Ni-Base Alloys; from Mechanisms of Phase Transformations in Crystalline Solids, Proceedings of 1968 International Symposium; Institute of Metals, 1969.
79. A. J. De Ridder and R. W. Koch; Controlling Variations in Mechanical Properties of Heat Resistant Alloys During Forging; Metals Engineering Quarterly, ASM; Aug. 1965, pp. 61-64.
80. A. A. Guimacaes and J. J. Jonas; Recrystallization and Aging Effects Associated with the High Temperature Deformation of Waspaloy and Inconel 718; Metallurgical Transactions, 12A, pp. 1655-1666 (1981).
81. G. R. Speich; Precipitation of Laves Phases from Fe-Nb (Cb) and Fe-Ti Solid Solutions; Transactions of the Metallurgical Society of AIME, 224, pp. 850-858 (1962).
82. Personal Communication, John Radavich, Purdue University.

83. Personal Communication, John Domingue, Special Metals Corp., New Hartford, New York.
84. L. W. Lherbier; Melting of Superalloys, Micon '78; ASTM STP 672; Abrams, Maniar, Nail and Solomon, Eds.; pp. 514-525.
85. D. J. Bologna; Metallurgical Factors Influencing the Microfissuring of Alloy 718 Weldments; Metals Engineering Quarterly, ASM; Nov. 1969, pp. 37-43.
86. J. A. Burger and D. K. Hanink; Heat Treating Nickel-Base Superalloys; Metal Progress, July 1967 pp. 61-66.
87. J. P. Stroup and L. A. Pugliese; How Low Carbon Contents Affect Superalloys; Metal Progress, Feb 1948, pp. 96-100.
88. D. M. Gadsby; Forging and Solution Treating Alloy 718; Metal Progress, Dec. 1966, pp. 85-88.
89. M. A. Meyers and R. N. Orava; Thermomechanical Processing of Inconel 718 by Shock-Wave Deformation; Metallurgical Transactions, 7A pp. 179-190 (1976).
90. D. F. Paulonis, J. M. Oblak and D. S. Duvall; Precipitation in Nickel-base Alloy 718; Transactions of the ASM, 62, pp. 611-622 (1969).
91. C. T. Sims; Columbium in Superalloys: A Perspective; G. E. Report No. 83CRD046; Sept. 1983.
92. J. E. Coyne; Microstructural Control in Titanium- and Nickel-base Forgings; An Overview; Metals Technology, July 1977, pp. 337-345.
93. Personal Communication, William Boesch, Special Metals Corp., New Hartford, New York.
94. J. F. Barker; A Superalloy for Medium Temperatures; Metal Progress, May 1962, pp. 72-76.
95. H. F. Merrick; Low Cycle Fatigue of Three Wrought Nickel-Base Alloys; Metallurgical Transactions, 5, pp. 891-897 (1974).
96. T. H. Sanders, R. E. Fushmuth and G.T. Embly; Temperature Dependent Deformation Mechanisms of Alloy 718 in Low Cycle Fatigue; Metallurgical Transactions, 12A pp. 1003-1010 (1981).

97. M. C. Chaterwedi and Ya-fang Han; Strengthening Mechanisms in Inconel 718 Superalloy; Metal Science, 17, pp. 145-149, March 1983.
98. M. G. Stout and W. W. Gerberich; Structure/Property/Continuum Synthesis of Ductile Fracture in Inconel Alloy 718; Metallurgical Transactions, 9A, pp. 649-658 (1978).
99. N. A. Wilkinson; Technological Considerations in the Forging of Superalloy Rotor Parts; Metals Technology, July 1977, pp. 346-359.
100. M. Clavel, D. Fournier, and A. Pineau; Plastic Zone Sizes in Fatigued Specimens of Inco 718; Metallurgical Transactions, 6A, pp. 2305-2307 (1975).
101. K. Sadananda and P. Shahinian; Creep Crack Growth in Alloy 718; Metallurgical Transactions, 8A, pp. 439-449 (1977).
102. M. F. Ashby; A First Report on Deformation Mechanism Maps; Acta Metallurgica, 20 pp. 887-897.
103. M. F. Ashby, C. Gandhi and D.M.R. Taplin; Fracture Mechanism Maps and Their Construction for F.C.C. Metals and Alloys; Acta Metallurgica, 27 pp. 699-729 (1979).
104. Lecture Notes; EMMS 417, Professor R. Gibala, Dept. of Metallurgy and Materials Science, Case Western Reserve University; Spring 1982.
105. N. Kushmir, D. Eylon and A. Rosen; The Effect of Rapid Thermal Fluctuations on the Creep Rate in Inconel 718; Metallurgical Transactions, 2 pp. 2237-2241 (1971).
106. G. S. Cole and R. S. Cremisio; Solidification and Structure Control in Superalloys; from The Superalloys, Sims and Hagel, Eds.; John Wiley and Sons, New York, 1972.
107. K. Mazmili, R. Angers and G. Dufour; Phase Analysis of Sintered and Heat Treated Alloy 718, Metallurgical Transactions, 13A, pp. 5-12 (1982).
108. H. F. Merick; Effect of Heat Treatment on the Structure and Properties of Extended P/M Alloy 718; Metallurgical Transactions, 7A pp. 505-514 (1976).
109. A. Hajmili and R. Angers; Sintering of Inconel 718; International Journal of Powder Metallurgy and Powder Technology, 16 No. 3, pp. 255-266 (1980).

110. R. L. Dreshfield and J. F. Wallace; The Gamma-Gamma Prime Region of the Ni-Al-Cr-Ti-W-Mo System at 850°C; Metallurgical Transactions, 5, pp. 71-78 (1974).
111. COSAM Program Overview; NASA Technical Memorandum 83006; October 1982.
112. J. T. Brown and J. Bulina; W545-A New Higher Temperature Turbine Disc Alloy; from High Temperature Materials Hehemann and Ault Eds., John Wiley and Sons, New York, 1959.
113. R. Cozar and A. Pineau; Morphology of  $\gamma'$  and  $\gamma''$  Precipitates and Thermal Stability of Inconel 718 Type Alloys; Metallurgical Transactions, 4, pp. 47-59 (1973).
114. J. H. Moll, G. N. Maniar and D. R. Muzyka; The Microstructure of 706, a New Fe-Ni-Base Superalloy; Metallurgical Transactions, 2, pp. 2143-2151 (1971).
115. J. H. Moll, G. N. Maniar and D. R. Muzyka; Heat Treatment of 706 Alloy for Optimum 1200°F Stress-Rupture Properties; Metallurgical Transactions, 2, pp. 2153-2160 (1971).
116. N. J. Grant; Choice of High Temperature Alloys-Influence of Fabrication History; Metal Progress, May 1956, pp. 81-86.
117. R. F. Decker and R. R. DeWitt; Trends in High-Temperature Alloys; Journal of Metals, Feb. 1965, pp. 139-145.
118. M. J. Donachie and O. M. Kriege; Phase Extraction and Analysis in Superalloys - Summary of Investigations by ASTM Committee E-4 Task Group 1; Journal of Materials 7 No. 3, pp. 269-278 (1972).
119. M. J. Donachie; Phase Extraction and Analysis in Superalloys - Second Summary of Investigations by ASTM Subcommittee E04.91; Journal of Testing and Evaluation, 6 No. 3, pp. 189-195 (1978).
120. V. Ramaswamy, P. R. Swann and D.R.F. West; Observations on Intermetallic Compound and Carbide Precipitation in Two Commercial Nickel Base Superalloys; Journal of the less-Common Metals, 27 pp. 17-26 (1972).
121. A. Havalda; Influence of W on the  $\gamma'$  to  $\eta$  Transformation and Carbide Reactions in Ni-Base Superalloys; Transactions of the ASM, 62, pp. 581-589 (1969).

122. I. L. Rency, J. Lanceese and H. Aubert; Precipitation Behavior and Creep Rupture of 706 Type Alloys; Materials Science and Engineering, 38, pp. 227-239 (1979).
123. F. G. Haynes; The Use of Nb in the Development of Air-Cast Ni-Cr Alloys for High-Temperature Service; Journal of the Institute of Metals, 90, pp. 311-320 (1961-62).
124. G. K. Bouse and P. W. Schulke; Process Optimization of Cast Alloy 718 for Water Cooled Gas Turbine Application; Superalloys 1980, pp. 303-310.
125. I. Kirman and D. H. Warrington; Precipitation in Ni-Base Alloys Containing Both Nb and Ti; Journal of the Institute of Metals, 99, pp. 197-199 (1971).

TABLE I  
NOMINAL COMPOSITIONS OF NICKEL-BASE SUPERALLOYS

Alloy Designation	Nominal composition, wt %													
	C	Mn	Si	Cr	Co	Mo	W	Nb	Ti	Al	B	Zr	Fe	Others
Astroloy	0.06	-	-	15.0	15.0	5.25	-	-	3.5	4.4	0.03	-	-	-
IN-100	0.18	-	-	10.0	15.0	3.0	-	-	4.7	5.5	0.014	0.06	-	1.0 V
In-792	0.21	-	-	12.7	9.0	2.0	3.9	-	4.2	3.2	0.02	0.10	-	-
Inconel 625	0.05	0.2	0.2	21.5	-	9.0	-	3.6	0.2	0.2	-	-	2.5	-
Inconel 706	0.03	0.2	0.2	16.0	-	-	-	2.9	1.8	0.2	-	-	40	0.2 Cu
Inconel 718	0.04	0.2	0.2	18.5	-	3.0	-	5.1	0.9	0.5	-	-	18.5	0.2 Cu
Inconel X-750	0.04	0.5	0.2	15.5	-	-	-	1.0	2.5	0.7	-	-	7.0	0.2 Cu
Rene 41	0.09	-	-	19.0	11.0	10.0	-	-	3.1	1.5	0.010	-	1.0	-
Rene 77	0.15	-	-	15.0	18.5	5.2	-	-	3.5	4.25	0.05	-	1.0	-
Rene 80	0.17	-	-	14.0	9.5	4.0	4.0	-	5.0	3.0	0.015	0.03	-	-
Rene 95	0.15	-	-	14.0	8.0	3.5	3.5	3.5	2.5	3.5	0.01	0.05	-	-
Udimet 630	0.04	0.2	0.2	17.0	1.0	3.1	3.0	6.0	1.1	0.6	0.005	-	17.5	-
Udimet 700	0.07	-	-	15.0	18.5	5.0	-	-	3.5	4.4	0.025	-	0.5	-
Waspaloy	0.07	0.5	0.5	19.5	13.5	4.3	-	-	3.0	1.4	0.006	0.09	2.0	0.03 S 0.10 Cu

TABLE II  
EFFECT OF THE ELEMENTS CONTAINED IN THE ALLOYS OF THE STUDY

INCONEL ALLOY 718

<u>ELEMENT</u>	<u>CONCENTRATION (WT. )</u>	<u>MAJOR EFFECT</u>	<u>MINOR EFFECT</u>
Ni	55	MATRIX & PRECIP.	
Fe	19	MATRIX	LAVES, $M_3B_2$
Cr	18	ENVIRONMENTAL PROTECTION	$\gamma, \gamma'$ HARDENER, $M_{23}C_6$
C	0.10 MAX	CARBIDE FORMER	
Mo	3.00	$\gamma$ HARDENER	$M_6C, M_{23}C_6, M_3B_2$
Al	0.55	$\gamma'$ FORMER, ENVIR. PROTEC.	$\gamma$ HARDENER
Ti	0.87	$\gamma'$ FORMER	MC, LAVES
Cb+Ta	5.10 - 5.60	$\gamma', \gamma''$ FORMER	MC, LAVES
Si	0.35 MAX	PROMOTES LAVES	
P	0.15 MAX	PROMOTES CARBIDES	
S	0.15 MAX	SULFIDE FORMER	
Mn	0.35 MAX	PROMOTES LAVES	
B	0.003	G.B. STRENGTHENER	$M_3B_2$
W		$\gamma, \gamma'$ HARDENER	$M_6C$
V		$\gamma'$ HARDENER	MC

TABLE III  
CRITICAL TEMPERATURES IN THE PROCESSING  
OF INCONEL 718

<u>TEMPERATURES °C (°F)</u>	<u>EFFECTS</u>
675-900 (1250-1650)	$\gamma''$ PRECIPITATION
790-995 (1450-1825)	$\delta$ PRECIPITATION
1000 (1830)	RECRYSTALLIZATION TEMPERATURE
<u>NON - STRENGTHENING PHASES</u>	
760-995 (1400-1825)	$M_{23}C_6$ PRECIPITATION
870-1075 (1600-2150)	$M_6C$ PRECIPITATION
815-955 (1500-1750)	$\sigma$ PRECIPITATION
1095-1075 (2000-2150)	BORIDE PRECIPITATION
SOLIDIFICATION	MC PRECIPITATION
1260 (2300)	

TABLE IV  
COMPOSITION OF ALLOYS IN THIS STUDY

Alloy	Weight %						Atomic%					
	Ti	Cb	Mo	W	V	B	Ti	Cb	Mo	W	V	B
1a	0.87	5.32	3.10	-	-	-	1.11	3.34	1.83	-	-	-
1b	0.87	5.30	3.10	-	-	0.04	1.11	3.33	1.83	-	-	0.212
2a	0.87	3.20	3.10	-	-	-	1.17	1.91	1.85	-	-	-
2b	0.87	3.20	3.10	-	-	0.04	1.17	1.89	1.85	-	-	0.213
2c	0.87	3.10	5.80	-	-	-	1.14	1.86	2.09	-	-	-
2d	0.87	3.10	5.80	-	-	0.04	1.14	1.86	2.09	-	-	0.212
2e	0.87	3.00	2.99	3.00	-	-	1.12	1.84	1.82	1.82	-	-
2f	0.87	3.00	3.00	3.00	0.9	-	1.11	1.83	1.81	1.81	1.03	-
3a	0.87	1.10	3.10	-	-	-	1.22	0.69	1.88	-	-	-
3b	0.87	1.10	5.80	-	-	-	1.20	0.67	2.14	-	-	-
3c	0.87	1.10	3.00	3.00	-	-	1.20	0.66	1.85	1.83	-	-
3d	0.87	1.10	3.00	3.00	0.9	-	1.19	0.65	1.84	1.83	-	-
4	1.09	3.49	3.00	-	-	-	1.32	3.08	1.81	-	-	-
5	1.27	3.89	3.00	-	-	-	1.54	3.13	1.81	-	-	-

Elements Common to All Alloys:

Ni + Co	-	Balance	C	-	0.04 max.
Fe	-	19.0	Si	-	0.35 max.
Cr	-	18.0	S	-	0.15 max.
Al	-	0.55	P	-	0.15 max.
			Mn	-	0.15 max.

TABLE V  
SOLUTION AND AGE HEAT TREATMENTS  
FOR THE ALLOYS OF THIS STUDY

SOLUTION AND AGE HEAT TREATMENTS

SOLUTION TEMPERATURES °C (°F; ALL FOR 2 hr.)

1095 (2000)

1040 (1900)

980 (1800)

930 (1700)

AGE TREATMENTS

<u>TEMPERATURE</u> °C (°F)	<u>TIME</u> (hr.)
870 (1600)	5
	10
815 (1500)	10
	25
760 (1400)	25
	50
	100
705 (1300)	50
	100
650 (1200)	100

TABLE VI  
PROCESSING OF INCONEL ALLOY 718 FOR  
OPTIMUM MECHANICAL PROPERTIES

CAST ALLOY 718

SA - SOLUTION AND AGE

PROCEDURE

1. HOMOGENIZE
2. HOT OR WARM ROLL
3. SOLUTION; QUENCH
4. AGE

DA - DIRECT AGE

PROCEDURE

1. HOMOGENIZE
2. HOT, WARM OR  
COLD ROLL
3. AGE

FEATURES OF MATERIAL AFTER PROCESSING

LARGER GRAINS  
(ASTM 4-7)

HIGHER USE TEMPERATURE  
(TO 650°C (1200°F))

GREATER DUCTILITY  
(OVER 18%)

CREEP RESISTANCE  
AGE CYCLE CAN BE MODI-  
FIED TO THE APPLICATION

SMALLER GRAINS  
(ASTM 10-14)

LOWER USE TEMPERATURE  
(TO 540°C (1000°F))

LOWER DUCTILITY  
(10-15%)

VERY HIGH YIELD AND  
TENSILE STRENGTH

TABLE VII  
ALLOYS, CONDITIONS AND TESTS PLANNED IN THIS STUDY

Alloy 1(a,b)	Condition*	Tensile Tests				Stress-Rupture Tests		
		25 X	540 X	595 X	650 X	540 X	595 X	650 X
2 (a-f)	SA	X			X			
3(a-d)	SA	X			X			
4	SA	X	X	X	X	X	X	X
5	SA	X	X	X	X	X	X	X
1(a,b)	DA	X	X	X	X		X	
2(a,b,e,f)	DA	X	X	X	X		X	

\* SA = Solution and Age Heat Treatment  
DA = Direct Age Heat Treatment

TABLE VIII  
EFFECT OF SOLUTION TEMPERATURE ON GRAIN SIZE AND  
SECONDARY PHASE PRECIPITATION IN SOLUTION  
AND AGE ALLOYS WITH DECREASING Cb CONTENT

Alloy	Solution °C(°F)2 hrs.*	Grain Area ( $\mu\text{m}^2$ )	Boundary Cond.
1a	(2000)	150000	spotty, light precip.
1a	1040 (1900)	10000	light precip.
1a	980 (1800)	6000	light, even precip.
1a	940 (1700)	250**	heavier precip.(MC, $\gamma$ )
2a	(2000)	6000	light precip.
2a	1040 (1900)	6000	light precip.
2a	980 (1800)	2000**	heavier precip.
2a	940 (1700)	300	heavier precip.(MC, $\gamma$ )
3a	(2000)	1500	medium precip.
3a	1040 (1900)	2400	medium precip.
3a	980 (1800)	1000	medium precip.
3a	940 (1700)	200	spotty, heavier precip.

\* Age = 705°C (1300°F) 100 hour, AC

\*\* (Duplex; segregation)

TABLE IX  
EFFECT OF AGE TEMPERATURE ON DIMENSIONS OF  $\gamma''$  AND  
VOLUME FRACTION  $\gamma'$   $\gamma''$  AND  $\eta$  IN SOLUTION AND AGE ALLOYS

Alloy	Solution = 1900°F 2 hr. Age Temperature °C(°F)	- - - $\gamma'$	Volume% $\gamma''$	- - - $\eta$	Aspect ratio of $\gamma''$
1a	705 (1300)	-	20-25	GB*	4.0
	815 (1500)	-	15	20-30	2.75
1b	705	-	20-25	GB	4.0
	815	-	15	20-30	2.75
2a	705	20	10-15	GB	2.5
	815		5	5-10	2.33
2b	705	20	10-15	GB	2.5
	815		-	10	2.33
2c	705	20	10-15	GB	2.5
	815		-	10	2.33
2d	705	20	10-15	GB	2.5
	815		-	5-10	2.33
2e	705	20	10-15	GB	2.5
	815		-	10	2.33
2f	705	20	10-15	GB	2.5
	815		-	10	2.33
3a	705	15	-	GB	-
	815		-		-
3b	705	15	-	GB	-
	815		-		-
3c	705	15	-	GB	-
	815		-		-
3d	705	15	-	GB	-
	815		-		-

\* GB = Grain Boundary Precip.

TABLE X: a)  
ROOM TEMPERATURE TENSILE PROPERTIES OF  
SOLUTION AND AGE ALLOYS\*

<u>Alloy</u>	<u>Yield Strength</u>		<u>Tensile Strength</u>		<u>% Elongation</u>
	<u>(ksi)</u>	<u>(MPa)</u>	<u>(ksi)</u>	<u>(MPa)</u>	
1a	122.1	841.9	186.6	1286.6	16.5
1b	135.7	935.6	198.6	1369.3	19.4
2a	77.1	531.6	158.3	1091.4	30.8
2b	97.3	670.9	167.8	1156.9	24.7
2c	77.1	531.6	159.6	1100.4	36.5
2d	89.3	615.7	165.1	1138.4	28.8
2e	91.5	630.9	167.6	1155.6	30.0
2f	96.4	664.6	168.6	1162.5	27.7
3a	65.0	448.2	138.6	955.6	21.0
3b	75.5	520.6	139.6	962.5	20.5
3c	70.5	486.1	141.8	977.7	23.8
3d	75.0	517.1	140.5	968.7	21.9

\* Solution = 1040°C (1900°F) 2 hours, A.C.  
Age = 705°C (1300°F) 100 hours, A.C.

TABLE X: b)

ROOM TEMPERATURE TENSILE PROPERTIES OF  
SUPPLEMENTAL SOLUTION AND AGE ALLOYS\*

<u>Alloy</u>	<u>Yield Strength</u>		<u>Tensile Strength</u>		<u>% Elongation</u>
	<u>(ksi)</u>	<u>(MPa)</u>	<u>(ksi)</u>	<u>(MPa)</u>	
4	109.1	752.2	171.1	1179.7	25.0
5	126.1	869.4	179.9	1240.4	23.5

\* Solution = 1040°C (1900°F) 2 hours, A.C.

Age = 705°C (1300°F) 100 hours, A.C.

TABLE XI  
ELEVATED TEMPERATURE TENSILE PROPERTIES  
OF THE SOLUTION AND AGE ALLOYS\*

Alloy	Test Temperature °C(°F)	Yield Strength		Tensile Strength		% Elongation
		(ksi)	(MPa)	(ksi)	(MPa)	
1a	540 (1000)	143.7	990.8	175.1	1207.3	7.7
1b	540	157.6	1086.6	181.4	1250.7	9.8
4	540	106.4	733.6	143.6	990.1	24.0
5	540	120.8	832.9	153.7	1059.7	20.0
1a	595 (1100)	137.6	948.7	162.3	1190.0	10.7
1b	595	144.5	996.3	173.8	1198.3	12.4
4	595	105.6	728.1	141.7	977.0	21.5
5	595	119.7	825.3	151.6	1045.2	19.5
1a	650 (1200)	121.4	837.0	152.8	1053.8	12.8
1b	650	126.7	873.6	158.5	1092.8	16.5
2a	650	83.8	577.8	118.3	815.7	20.0
2b	650	92.1	635.0	132.4	912.9	23.5
2c	650	82.8	570.9	128.6	886.7	26.5
2d	650	90.7	625.4	119.3	822.5	20.0
2e	650	92.1	635.0	131.7	908.3	25.5
2f	650	90.7	625.4	132.4	912.9	25.0
3a	650	64.4	444.0	101.0	696.4	23.8
3b	650	65.9	454.4	110.5	761.9	18.9
3c	650	65.2	449.5	113.3	781.2	19.8
3d	650	63.3	436.4	110.5	761.8	23.8
4	650	104.1	717.7	137.1	945.3	16.0
5	650	117.6	810.8	148.3	1022.5	14.0

\* Solution heat treatment: 1040°C (1900°F) for 2 hours; Air Cool  
Age heat treatment: 705°C (1300°F) for 100 hours; Air Cool

TABLE XII: a)  
STRESS RUPTURE PROPERTIES FOR ALLOYS TESTED,  
100 HOUR TESTS

Alloy	Temperature °C (°F)	Stress		Life (Hr.)	% Elongation
		(ksi)	(MPa)		
1a	540 (1000)	127.0	875.6		
1b	540	127.0			
4	540	127.0			
5	540	127.0			
1a	595 (1100)	115.6	797.0	88.7	3.0
1b	595	115.6		400	*
4	595	115.6		87.5	5.0
5	595	115.6		430.8	4.0
1a	650 (1200)	90.0	620.5	100	4.0
1b	650	90.0		200	5.0
4	650	90.0		75	8.0
5	650	90.0		175.5	7.0

\* Specimen removed prior to fracture

TABLE XII: b)  
STRESS-RUPTURE PROPERTIES FOR ALLOYS TESTED,  
50 HOUR TESTS

Alloy	Temperature °C (°F)	Stress		Life (Hr.)	Elongation
		(ksi)	(MPa)		
1a	540 (1000)	130.0	896.3		
1b	540	130.0			
4	540	130.0			
5	540	130.0			
1a	595 (1100)	120.0	827.4	20.1	3.0
1b	595	120.0		164.8	3.5
4	595	120.0		60.1	4.8
5	595	120.0		147.9	3.6
1a	650 (1200)	95.0	655.0	25*	5.0
1b	650	95.0		100*	6.0
4	650	95.0		33.2	5.8
5	650	95.0		116.4	5.5

\* Estimated

TABLE XIII

GENERAL ELECTRIC SPECIFICATION FOR  
THE MINIGRAIN INCONEL ALLOY 718 (83)

Forgings supplied in the following condition:

Heat treated:

720°C  $\pm$  15° (1325°F  $\pm$  25°) for 8 hours; furnace  
cool at 38°C  $\pm$  15° (100°F  $\pm$  25°) per hour, to  
620°C  $\pm$  15° (1150°F  $\pm$  25°) and hold for 8 hours;  
air cool.

Hardness: BHN 363 to 477 or R<sub>c</sub> 39 to 50

Tensile properties:

	<u>Room Temperature</u>		<u>650°C(1200°F)</u>	
	<u>(ksi)</u>	<u>(MPa)</u>	<u>(ksi)</u>	<u>(MPa)</u>
Tensile Strength	210	1447.9	170	1172.1
Yield Strength	185	1275.5	150	1034.2
Elongation	12		12	
Reduction in Area	20		20	

TABLE XIV

ROOM TEMPERATURE TENSILE PROPERTIES OF  
THE ORIGINAL DIRECT AGE ALLOYS\*

<u>Alloy</u>	<u>Yield Strength</u>		<u>Tensile Strength</u>		<u>% Elongation</u>
	<u>(ksi)</u>	<u>(MPa)</u>	<u>(ksi)</u>	<u>(MPa)</u>	
1a	197.7	1363.1	214.7	1480.3	4.7
1b	201.4	1388.6	217.1	1496.9	5.3
2a	164.3	1132.8	186.4	1285.2	15.3
2b	149.1	1028.0	186.4	1285.2	16.5
2c	156.0	1075.6	184.6	1272.8	16.5
2d	158.9	1095.6	184.4	1271.4	16.5
2e	158.0	1089.4	189.4	1305.9	15.3
2f	161.4	1112.8	189.4	1305.9	11.8

\* Age heat treatment: 730°C (1350°F) for 8 hours; furnace cool at 38°C (100°F) per hour to 620°C (1150°F) and hold 8 hours; air cool.

TABLE XV

## ROOM TEMPERATURE PROPERTIES OF DIRECT AGED ALLOYS\*

<u>Alloy</u>	<u>Yield Strength</u>		<u>Tensile Strength</u>		<u>% Elongation</u>
	<u>(ksi)</u>	<u>(MPa)</u>	<u>(ksi)</u>	<u>(MPa)</u>	
1a	205.0	1413.4	212.8	1467.2	8.0
1b	206.8	1425.8	221.6	1527.8	10.7
2a	165.5	1141.1	183.7	1266.6	9.5
2b	159.2	1097.6	182.0	1254.8	10.5
2e	171.9	1185.2	192.0	1323.8	8.0
2f	171.9	1185.2	191.8	1322.4	7.5

\* Age heat treatment: 730°C (1350°F) for 8 hours; furnace cool at 38°C (100°F) per hour to 620°C (1150°F) and hold 8 hours; air cool.

TABLE XVI  
ELEVATED TEMPERATURE TENSILE PROPERTIES OF  
DIRECT AGED ALLOYS\*

Alloy	Test Temperature °C(°F)	Yield Strength		Tensile Strength		% Elongation
		(ksi)	(MPa)	(ksi)	(MPa)	
1a	540 (1000)	178.7	1232.1	189.7	1307.9	5.6
1b	540			134.2	925.3	6.7
2a	540	155.2	1070.0	162.3	1119.0	4.7
2b	540			162.3	1119.0	6.7
2e	540			164.6	1134.9	6.7
2f	540			175.9	1212.8	4.6
1a	595 (1100)	175.7	1211.4	183.4	1264.5	7.7
1b	595			187.8	1294.8	7.7
2a	595	150.7	1039.0	163.6	1128.0	5.6
2b	595			159.2	1097.6	7.7
2e	595			164.8	1136.3	6.7
2f	595			168.7	1163.1	7.7
1a	650 (1200)	150.3	1036.3	159.2	1097.6	10.9
1b	650			167.7	1156.3	9.0
2a	650	143.5	989.4	151.1	1041.8	7.7
2b	650			148.3	1022.5	7.7
2e	650			150.2	1035.6	7.7
2f	650			148.3	1022.5	7.7

TABLE XVII

650°C (1200°F) TENSILE PROPERTIES OF  
THE ORIGINAL DIRECT AGE ALLOYS\*

<u>Alloy</u>	<u>Yield Strength</u>		<u>Tensile Strength</u>		<u>% Elongation</u>
	<u>(ksi)</u>	<u>(MPa)</u>	<u>(ksi)</u>	<u>(MPa)</u>	
1a	160.0	1103.2	164.3	1132.8	14.1
1b	164.3	1132.8	172.8	1191.4	9.4
2a	138.1	952.2	149.3	1029.4	16.0
2b	132.6	914.2	145.2	1001.1	15.6
2c	131.7	908.0	140.5	968.7	14.1
2d	130.0	896.3	141.1	972.85	15.9
2e	134.8	929.4	146.5	1010.1	17.1
2f	135.4	933.6	145.2	1001.1	15.6

\* Age heat treatment: 730°C (1350°F) for 8 hours; furnace cool  
at 38°C (100°F) per hour to 620°C  
(1150°F) and hold 8 hours; air cool.

TABLE XVIII  
X-RAY DIFFRACTION RESULTS OF THE AS-ROLLED ALLOYS

<u>Alloy</u>	<u>MC (a; Å)</u>	<u>Laves (a, c; Å)</u>	<u>M<sub>3</sub>B<sub>2</sub> (a,c;Å)</u>
1a	4.424	4.75, 7.90	-
1b	4.422	-	5.80, 3.10
2a	4.415	-	-
2b	4.420	4.80, 7.85	5.80, 3.10
2c	4.415	-	-
2d	4.410	4.80, 7.85	5.70, 3.20
2e	4.417	4.75, 7.80	-
2f	4.410	4.80, 7.85	-
3a	4.404	-	-
3b	4.395	-	-
3c	4.395	4.80, 7.85	-
3d	4.390	4.80, 7.85	-
4	4.407	-	-
5	4.410	-	-

TABLE XIX

X-RAY DIFFRACTION RESULTS FOR SOLUTION AND  
AGE ALLOYS - SECONDARY PHASES\*

<u>Alloy</u>	<u>MC (a; Å)</u>	<u>Laves (a, c; Å)</u>	<u>M<sub>3</sub>B<sub>2</sub> (a, c; Å)</u>
1a	4.429	4.85, 7.90	-
1b	4.415	+	5.75, 3.10
2a	4.429	+	-
2b	4.416	+	-
2c	4.426	+	-
2d	4.412	4.85, 7.90	-
2e	4.415	+	-
2f	4.408	4.90, 8.05	-
3a	4.401	+	-
3b	4.389	4.80, 7.85	-
3c	4.384	4.80, 7.85	-
3d	4.384	4.80, 7.85	-
4**	4.407	-	-
5**	4.416	-	-

\* Solution = 1040°C (1900°F), 2 hours, A.C.  
Age = 705°C (1300°F), 100 hours, A.C.

\*\* Solution = 980°C (1800°F), 2 hours, A.C.  
Same Age as other alloys

+ Phase detected

TABLE XX  
X-RAY DIFFRACTION RESULTS FOR SOLUTION AND  
AGE ALLOYS - STRENGTHENING PHASES\*

<u>Alloy</u>	<u><math>\gamma'</math> (a; Å)</u>	<u><math>\gamma''</math></u>	<u><math>\eta</math></u>
1a	3.583	+	+
1b	3.598	+	+
2c	3.587	+	+
2b	3.569	+	+
2c	3.589	+	+
2d	-	-	-
2e	3.606	+	+
2f	3.602	-	+
3a	3.577	-	-
3b	3.575	-	-
3c	3.583	-	-
3d	3.580	-	-
4**		+	+
5**		+	+

\* Solution = 1040°C (1900°F), 2 hours, A.C.  
Age = 705°C (1300°F), 100 hours, A.C.

\*\* Solution = 980°C (1800°F), 2 hours, A.C.  
Same Age as other alloys

+ Phase detected

TABLE XXI  
X-RAY DIFFRACTION RESULTS FOR THE ORIGINAL  
DIRECT AGE ALLOYS - SECONDARY PHASES \*

<u>Alloy</u>	<u>MC (a; Å)</u>	<u>Laves (a, c; Å)</u>	<u>M<sub>3</sub>B<sub>2</sub> (a,c;Å)</u>
1a	4.420	4.85, 7.90	-
1b	4.422	+	+
2a	4.408	+	-
2b	4.404	-	+
2c			
2d			
2e	4.413	+	-
2f	4.410	-	-
3a	4.384	-	-
3b			
3c			
3d	4.393	-	-

\* Age = 730°C(1350°F), 8 hours, F.C. at 38°C (100°F) per hour to 620°C (1150°F) and hold for 8 hours, A.C.

+ Phase detected

TABLE XXII

X-RAY DIFFRACTION RESULTS FOR THE DIRECT AGE ALLOYS  
 ALLOYS AFTER RE ROLLING - SECONDARY PHASES \*

<u>Alloy</u>	<u>MC (a; Å)</u>	<u>Laves</u>	<u>M<sub>3</sub>B<sub>2</sub></u>
1a	4.418	+	-
1b	4.422	+	-
2a	4.406	-	-
2b	4.404	-	-
2e	4.413	-	-
2f	4.407	-	-

\* Age = 730°C (1350°F), 8 hours, F.C. at 38°C (100°F) per hour  
 to 620°C (1150°F) and hold for 8 hours, A.C.

+ Phase detected

TABLE XXIII  
X-RAY DIFFRACTION RESULTS OF THE DIRECT AGE  
ALLOYS - STRENGTHENING PHASES \*

<u>Alloy</u>	<u><math>\gamma'</math> (a; Å)</u>	<u><math>\gamma''</math></u>	<u><math>\eta</math></u>
1a	3.629	strong	
1b			
2a	3.616	strong	
2b			
2c		strong	
2d			
2e	3.595	strong	
2f	3.587	strong	
3a	3.568	-	
3b			
3c			
3d	3.577	-	

\* Age = 730°C (1350°F), 8 hours, F.C. at 38°C (100°F) per hour to 620°C (1150°F) and hold for 8 hours, A.C.

TABLE XXIV  
EFFECT OF C ON THE Cb AVAILABLE  
FOR  $\gamma''$  PRECIPITATION

<u>Alloy</u>	<u>At.%Cb</u>	<u>At.%C</u>	<u>0.8C</u>	<u>At. % Cb Available for <math>\gamma''</math>, <math>\eta</math></u>	<u>%<math>\Delta</math>Cb</u>
1a	3.33	0.197	0.158	3.17	4.8
1b	3.32	0.250	0.200	3.12	6.0
2a	2.06	0.190	0.152	1.91	7.3
2b	2.00	0.200	0.160	1.84	8.0
2c	1.96	0.196	0.157	1.80	8.2
2d	1.98	0.198	0.158	1.82	8.1
2e	1.92	0.198	0.158	1.76	8.3
2f	1.90	0.196	0.157	1.74	8.4
3a	0.720	0.152	0.122	0.600	16.7
3b	0.706	0.149	0.119	0.587	16.9
3c	0.712	0.150	0.120	0.592	16.9
3d	0.705	0.100	0.080	0.625	11.3
4	3.18	0.194	0.155	3.03	4.7
5	3.43	0.193	0.154	3.28	4.4

TABLE XXV

THE EFFECT OF AL, TI AND CB ON PHASES  
PRECIPITATED IN ALLOY 718

<u>ALLOY</u>	<u>Cb</u>	<u>Al</u>	<u>Ti</u>	$\frac{(Ti+Al)^*}{Cb}$	$\frac{Ti^*}{Cb}$	<u>PRECIPITATE</u>
Std. 718	5.20	0.55	0.85	0.690	0.300	$\gamma''(\gamma')$ ; $\delta$
CWRU						
1	5.31	0.55	0.87	0.655	0.318	$\gamma''(\gamma')$ ; $\eta$
2	3.00	0.55	0.87	1.135	0.550	$\gamma''+\gamma'$ ; ?
3	1.10	0.55	0.87	3.357	1.690	$\gamma'(\gamma'')$ ; ?
<u>NEW</u>						
4	3.49	0.53	1.09	1.090	0.580	$\gamma''+\gamma'$ ; ?
5	3.89	0.52	1.27	0.970	0.620	$\gamma''+\gamma'$ ; ?

\* Ratios are from atomic %, all others are in weight

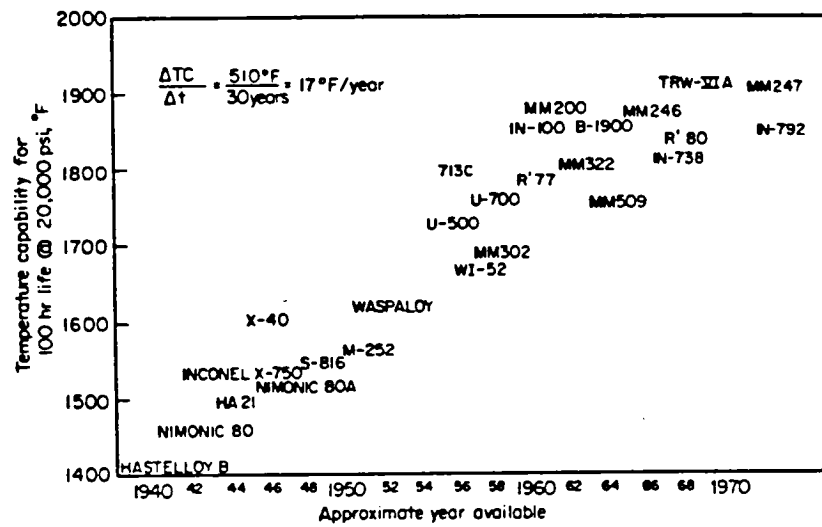


FIGURE 1: EVOLUTION OF SUPERALLOY USE TEMPERATURE (REF. 1).

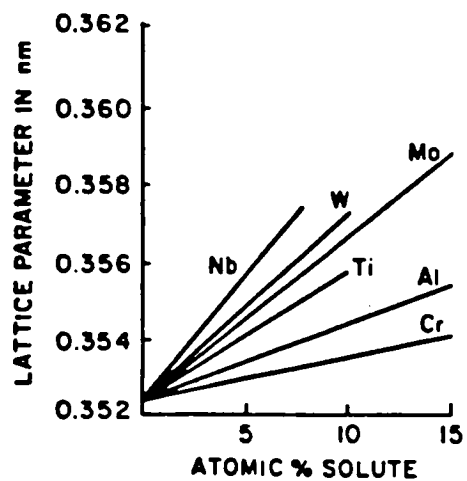


FIGURE 2: EFFECT OF SOLUTE ELEMENTS ON THE SOLID SOLUTION (Ni-BASE) LATTICE PARAMETER (6).

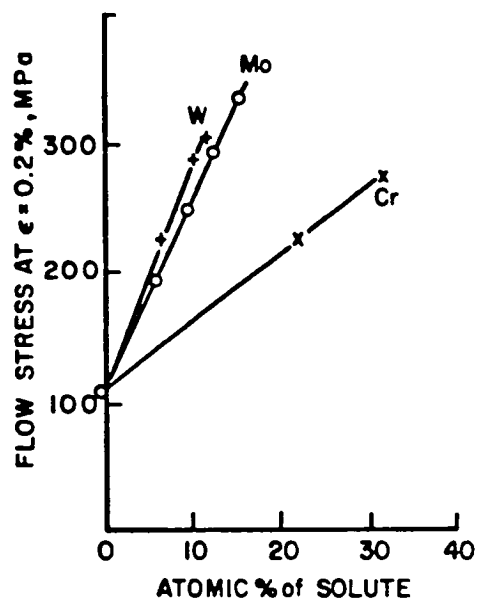


FIGURE 3: EFFECT OF SOLUTE ELEMENTS ON THE ROOM TEMPERATURE FLOW STRESS (6).

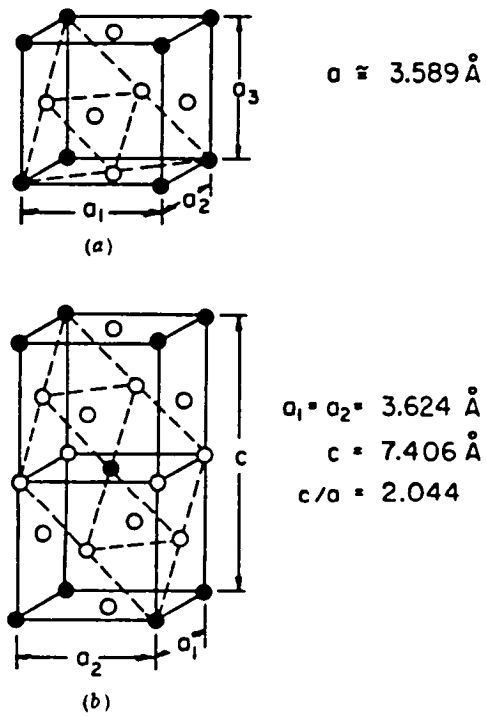


FIGURE 4: (a) FCC  $L1_2$   $Ni_3Cb$  LATTICE AND APPROXIMATE LATTICE PARAMETER; (b) BCT  $DO_{22}$   $Ni_3Cb$  LATTICE AND APPROXIMATE LATTICE PARAMETER (18).

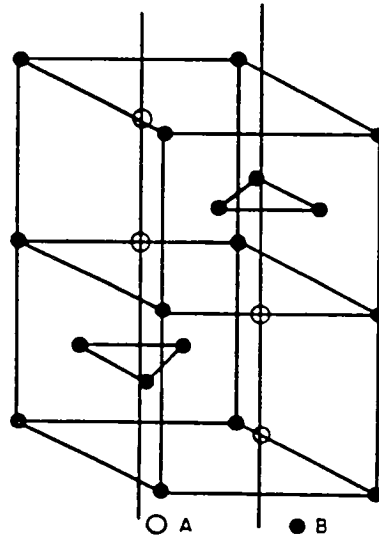


FIGURE 5: STRUCTURE OF THE LAVES PHASE  
(HERE WITH AN  $AB_2$  STRUCTURE) (66).

*A*-atoms are somewhat larger than the *B*-atoms.

	IV <sub>B</sub>	V <sub>B</sub>	VI <sub>B</sub>	VII <sub>B</sub>	VIII		I <sub>B</sub>	II <sub>B</sub>	III <sub>A</sub>		
A-group →	Ti	V	Cr	Mn	Fe	Co	Ni	Cu	Zn	Ga	← B-group
	Zr	Cb	Mo	Tc	Ru	Rh	Pd	Ag	Cd	In	
	Hf	Ta	W	Re	Os	Ir	Pt	Au	Hg	Tl	

FIGURE 6: CANDIDATE ELEMENTS FOR THE *A* AND *B* ATOMS OF THE LAVES  
PHASE (65).

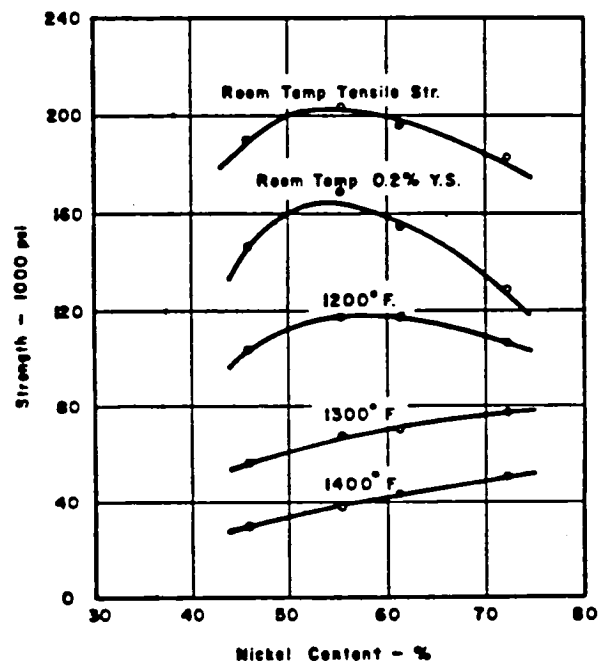


FIGURE 7: EFFECT OF Ni CONTENT ON ROOM TEMPERATURE STRENGTH AND ELEVATED TEMPERATURE 100-HOUR STRESS-RUPTURE STRENGTH (BASE COMPOSITION: Ni-Fe-15Cr-6Cb-3Mo-0.6Al-0.6Ti) (38).

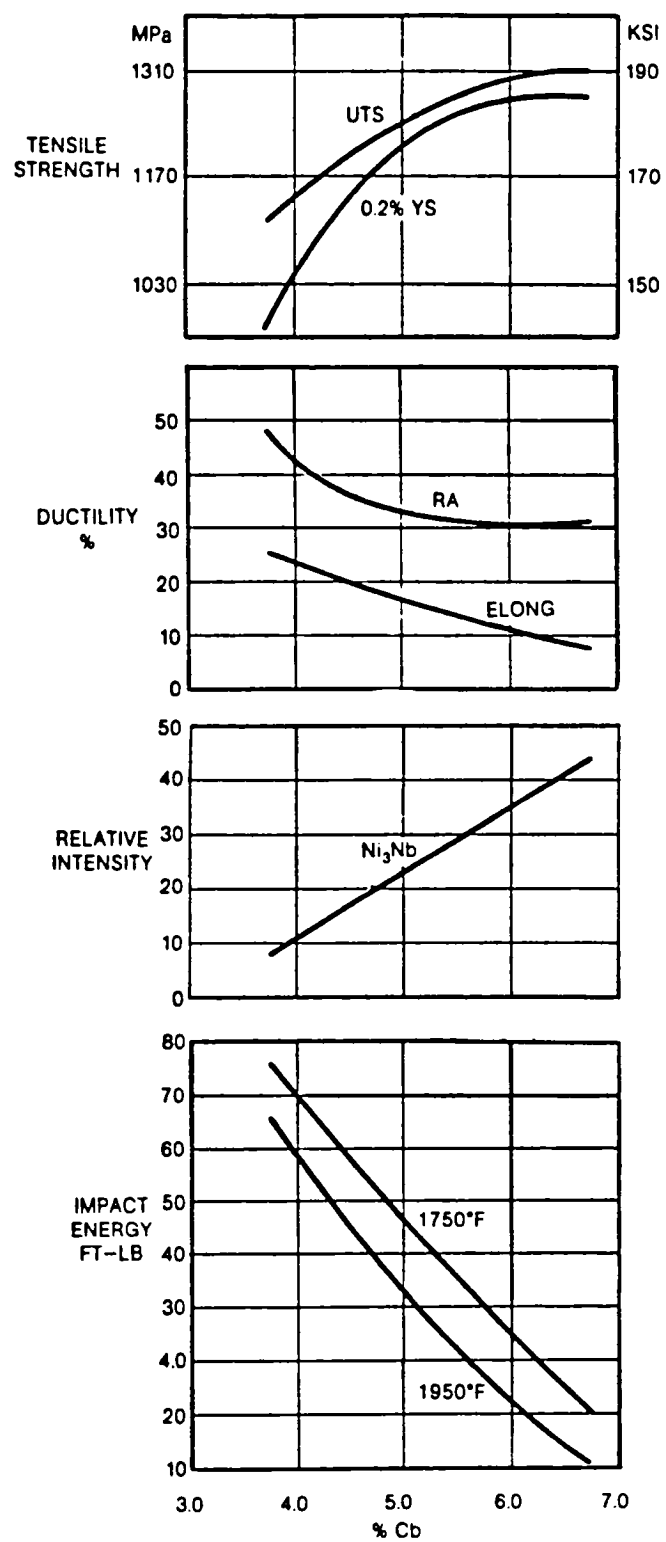


FIGURE 8: EFFECT OF Cb ON VARIOUS PROPERTIES OF INCONEL ALLOY 718 (61).

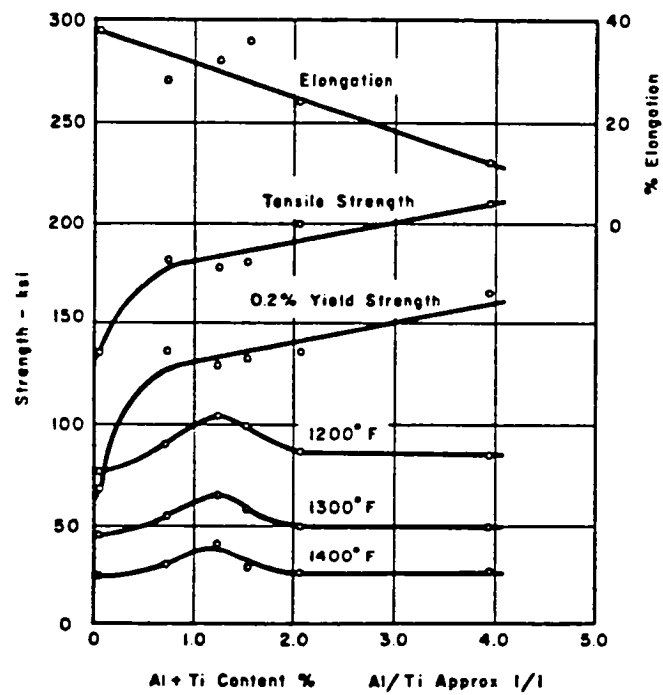


FIGURE 9: EFFECT OF (Al + Ti) ON ROOM TEMPERATURE STRENGTH AND ELEVATED TEMPERATURE 100-HOUR STRESS-RUPTURE STRENGTH (BASE COMPOSITION: 53Ni-21Cr-18Fe-4Cb-2Mo) (38).

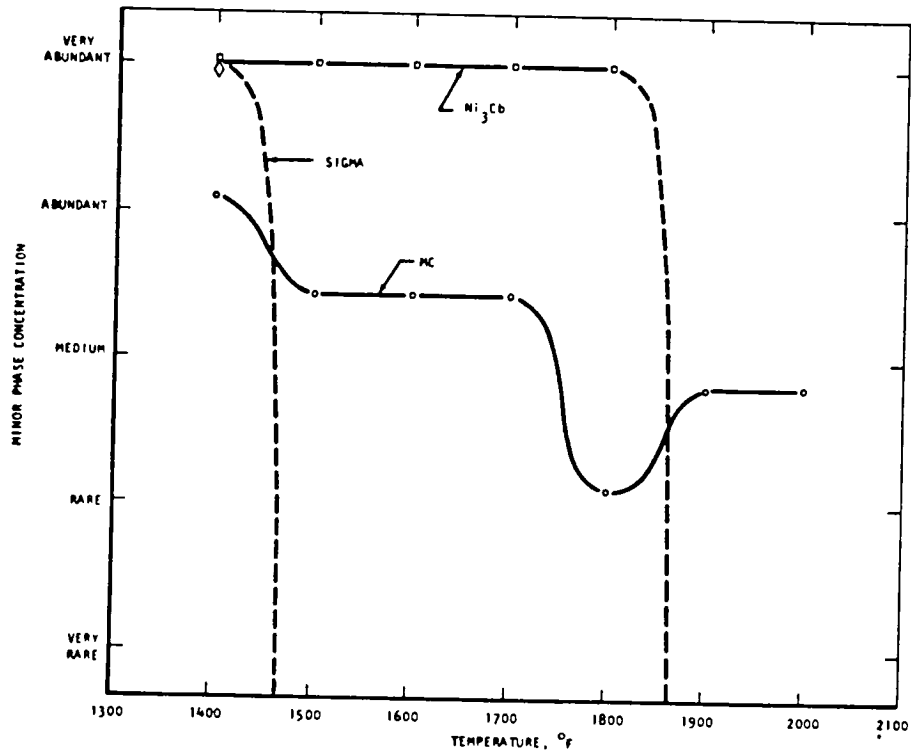


FIGURE 10: EFFECT OF TEMPERATURE ON MINOR PHASE FORMATION IN INCONEL ALLOY 718 (49).

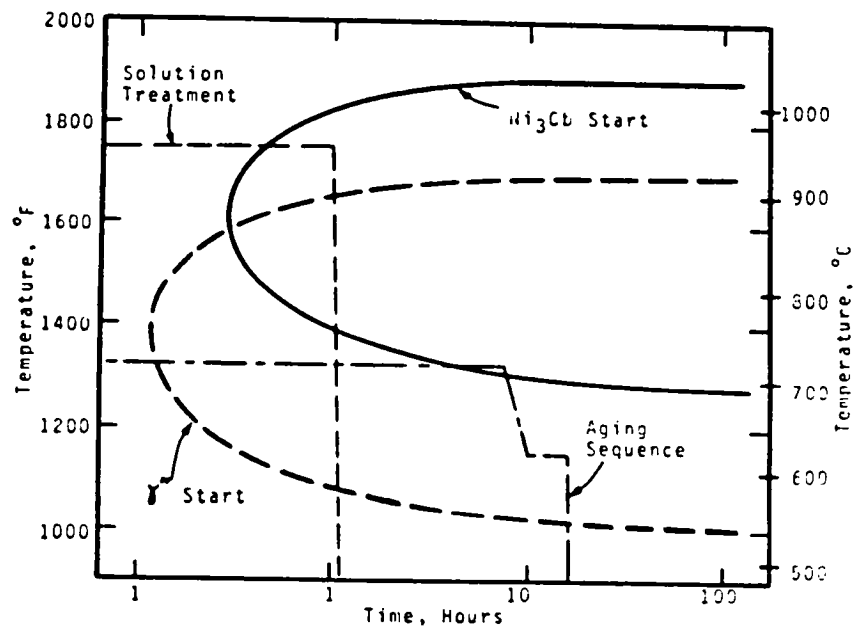


FIGURE 11: TYPICAL SOLUTION AND AGE HEAT TREATMENT OF ALLOY 718, WITH THE MAJOR PHASES PRECIPITATED (2).

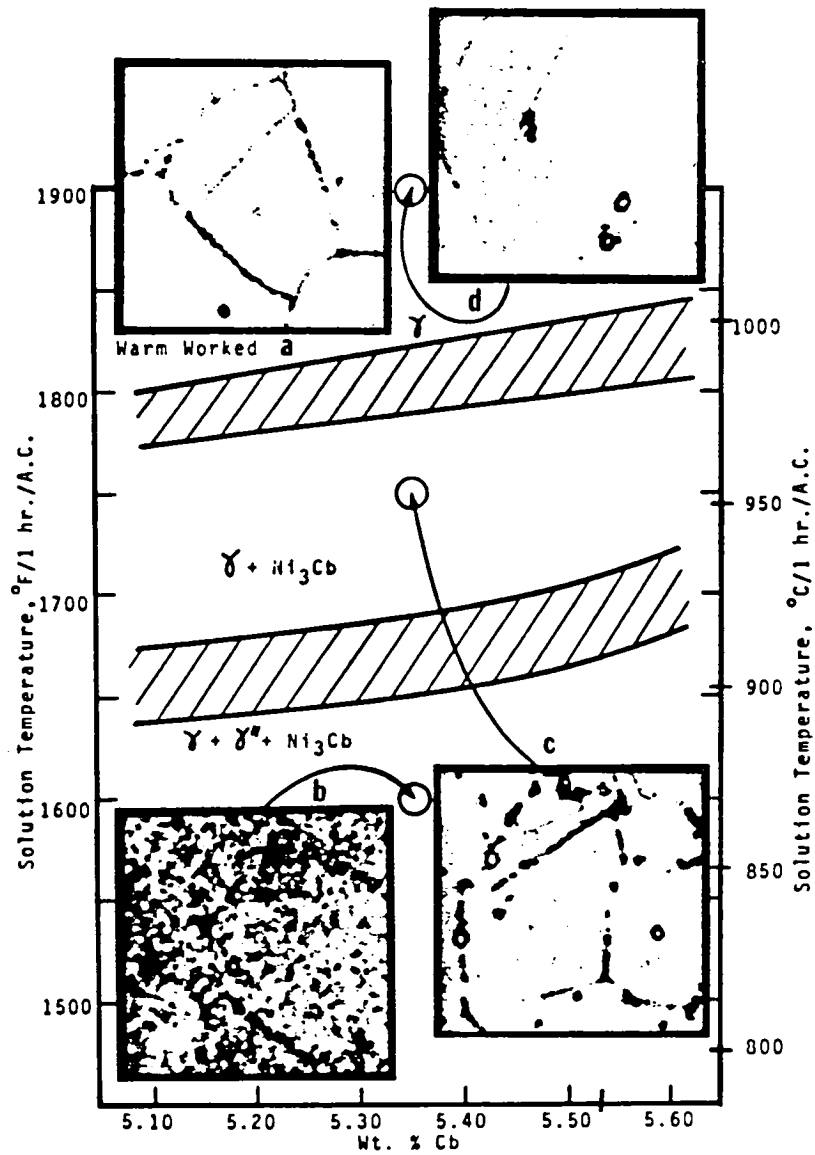


FIGURE 12: EFFECT OF DEFORMATION TEMPERATURE ON THE FINAL STRUCTURE OF INCONEL ALLOY 718 (2).

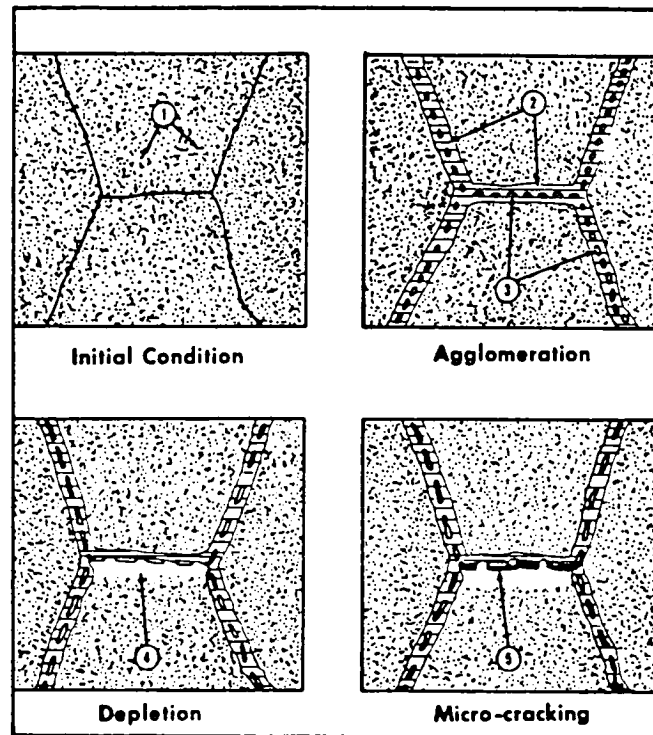


Fig. 9—Schematic representation of the steps in the mechanism of stress-rupture of the experimental alloy at 1600°F. Axis of tension is vertical. ① Intragranular  $\gamma'$ , ② Agglomerated  $\gamma'$ , ③ Agglomerated  $M_{23}C_6$ , ④ Matrix depleted of  $\gamma'$ , ⑤ Microcracks at  $M_{23}C_6$ -depleted zone interfaces.

FIGURE 13: SCHEMATIC REPRESENTATION OF THE STEPS IN THE MECHANISM OF COBLE CREEP (91).

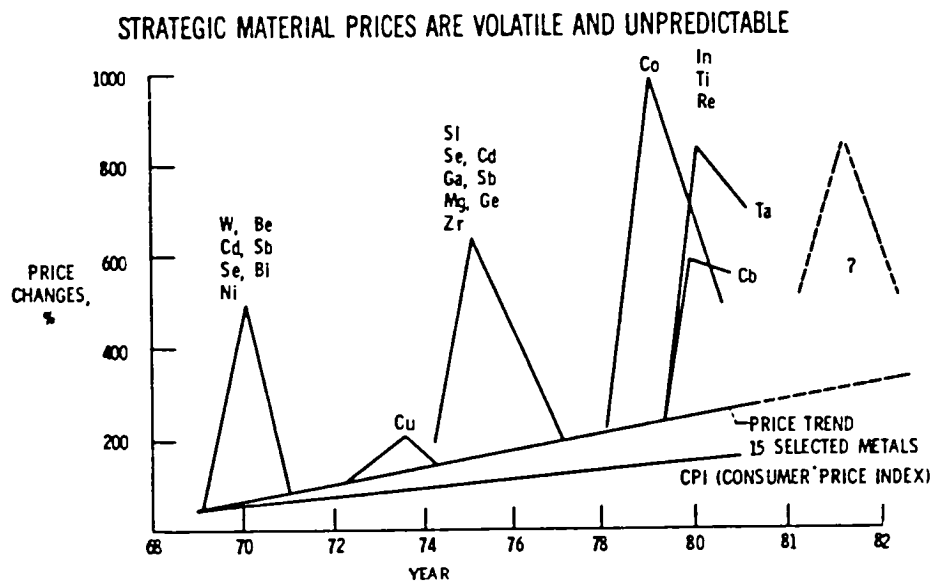
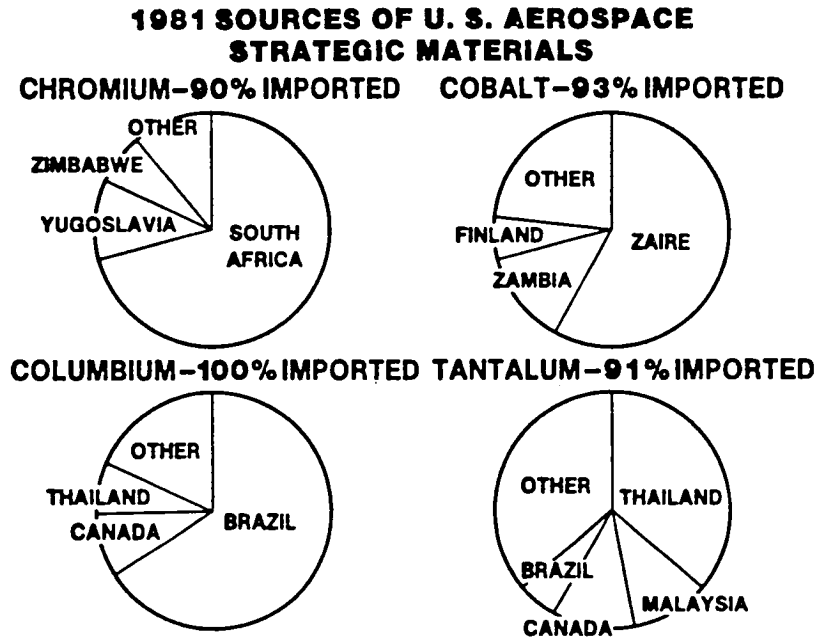


FIGURE 14: (a) SOURCES OF STRATEGIC METALS,  
(b) RECENT PRICE CHANGES OF METALS (112).

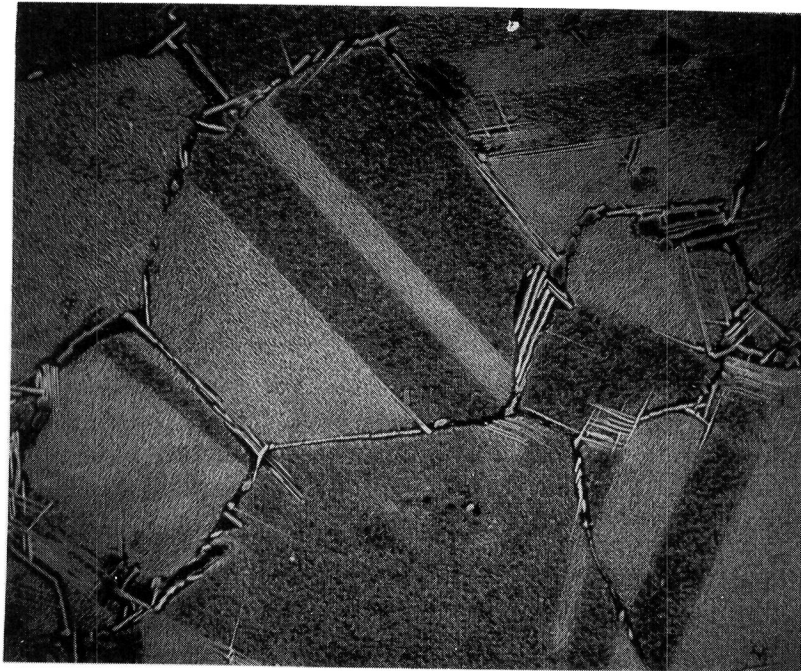


FIGURE 15: SOLUTION AND AGE HEAT TREATED ALLOY 1a.  
SOLUTION: 1040°C (1900°F), 2 HOURS;  
AGE: 705°C (1300°F), 100 HOURS. 5000X.

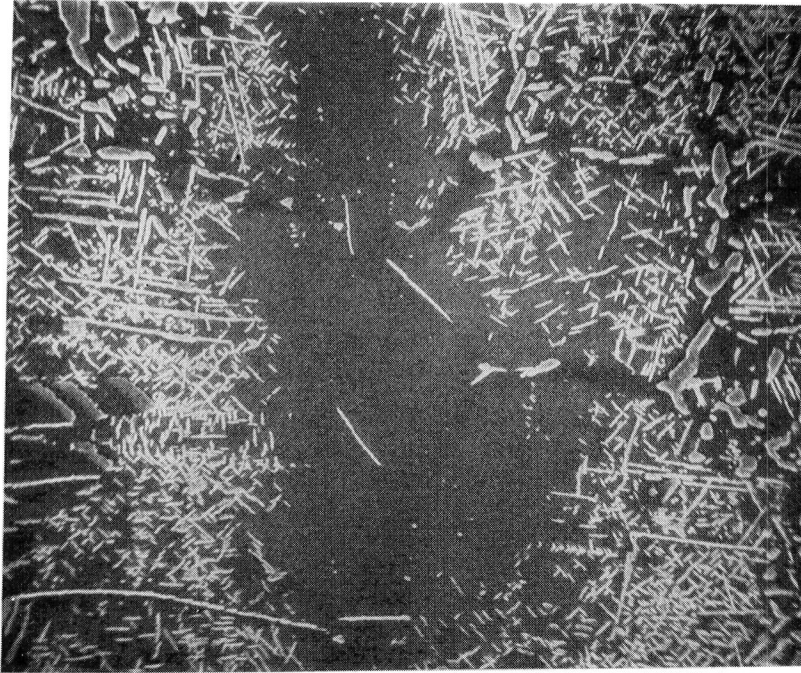


FIGURE 16: SOLUTION AND AGE HEAT TREATED ALLOY 1a.  
SOLUTION: 930°C (1700°F), 2 HOURS;  
AGE: 705°C (1300°F), 100 HOURS. 10000X.



FIGURE 17: SOLUTION AND AGE HEAT TREATED ALLOY 1a.  
SOLUTION: 1040°C (1900°F), 2 HOURS;  
AGE: 815°C (1500°F), 25 HOURS.

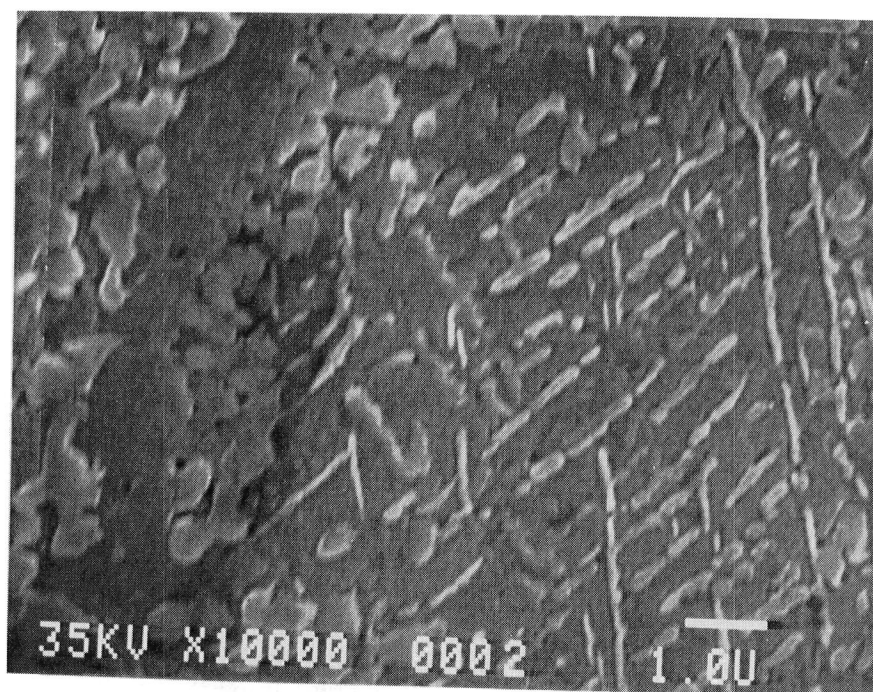


FIGURE 18: SOLUTION AND AGE HEAT TREATED ALLOY 1b.  
SOLUTION: 1040°C, 2 HOURS;  
AGE: 705°C, 100 HOURS.

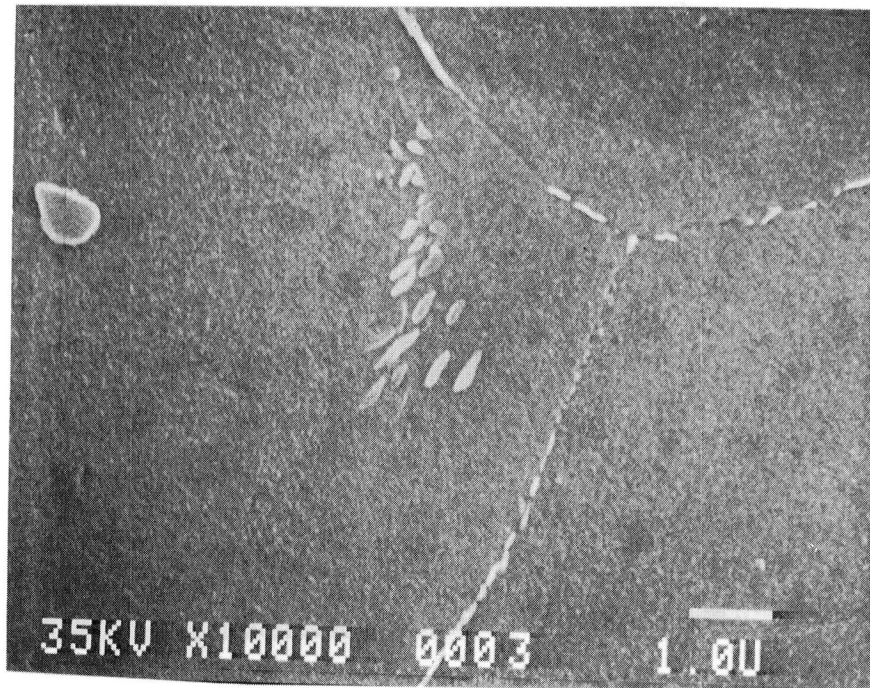


FIGURE 19: SOLUTION AND AGE HEAT TREATED ALLOY 2a.  
SOLUTION: 1040°C, 2 HOURS;  
AGE: 705°C, 100 HOURS.

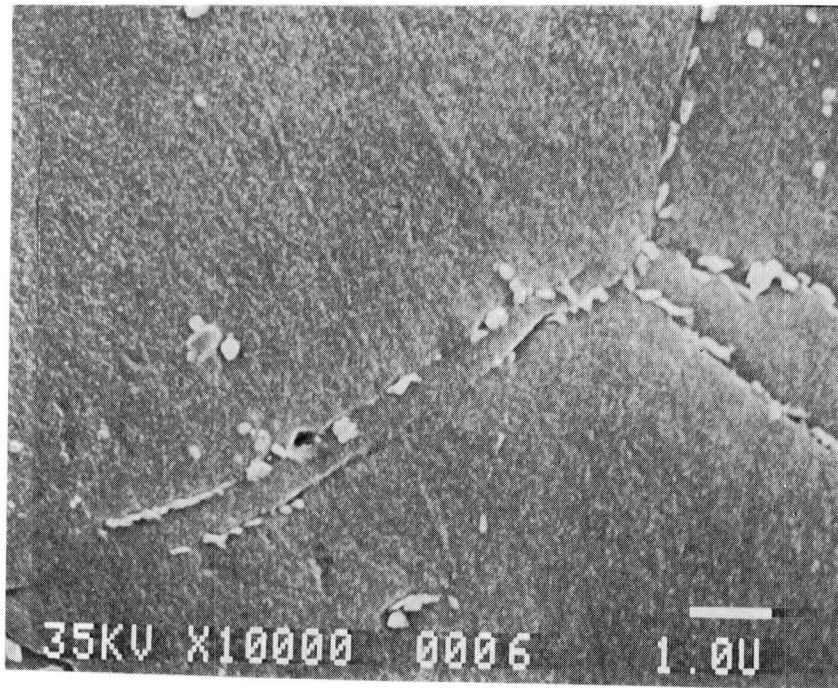


FIGURE 20: SOLUTION AND AGE HEAT TREATED ALLOY 2b, c and d.  
SOLUTION: 1040°C, 2 HOURS;  
AGE: 705°C, 100 HOURS.

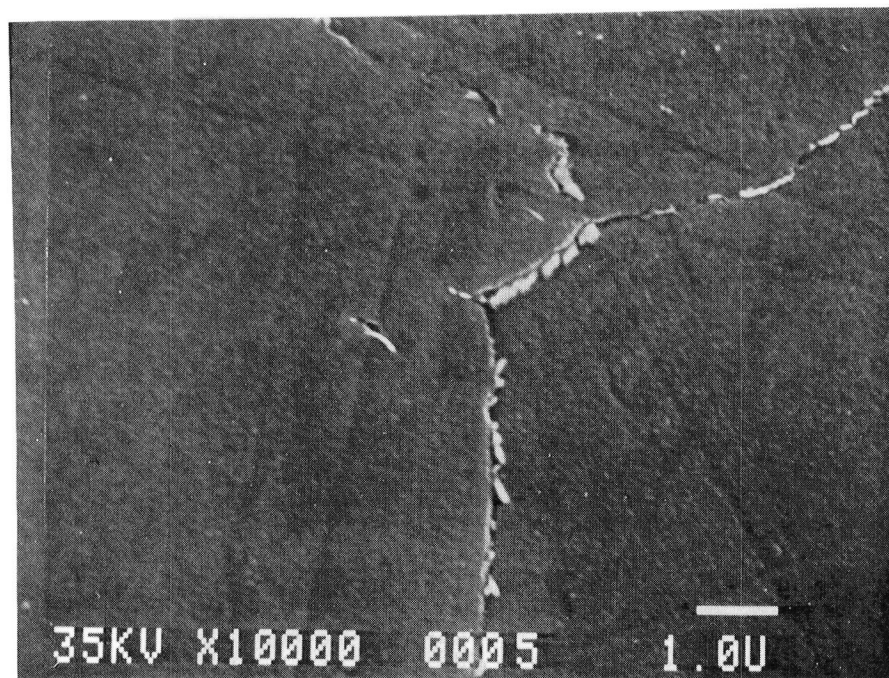


FIGURE 21: SOLUTION AND AGE HEAT TREATED ALLOY 2e.  
SOLUTION: 1040°C, 2 HOURS;  
AGE: 705°C, 100 HOURS.

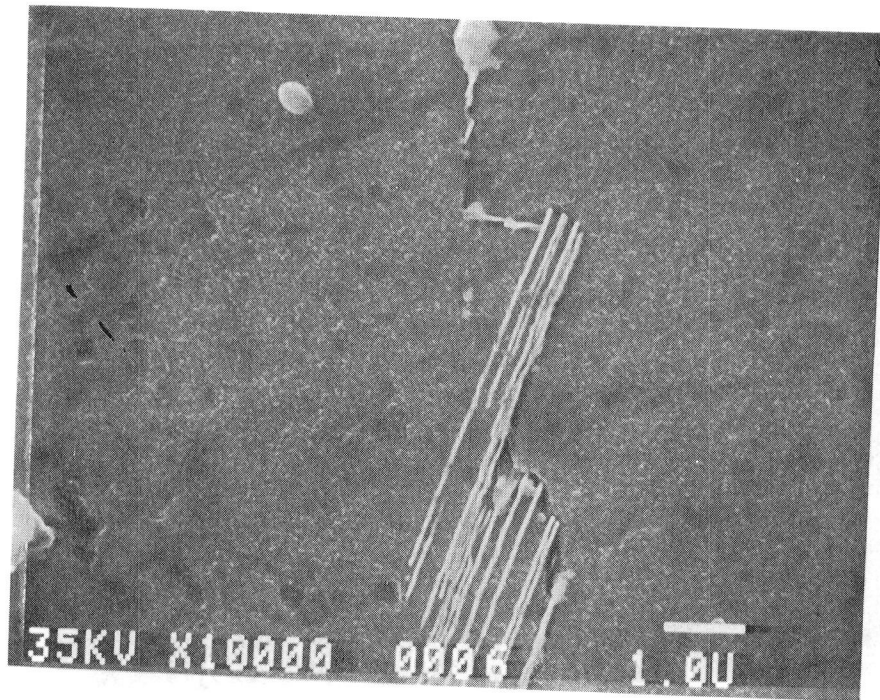


FIGURE 22: SOLUTION AND AGE HEAT TREATED ALLOY 2f.  
SOLUTION: 1040°C, 2 HOURS;  
AGE: 705°C, 100 HOURS.

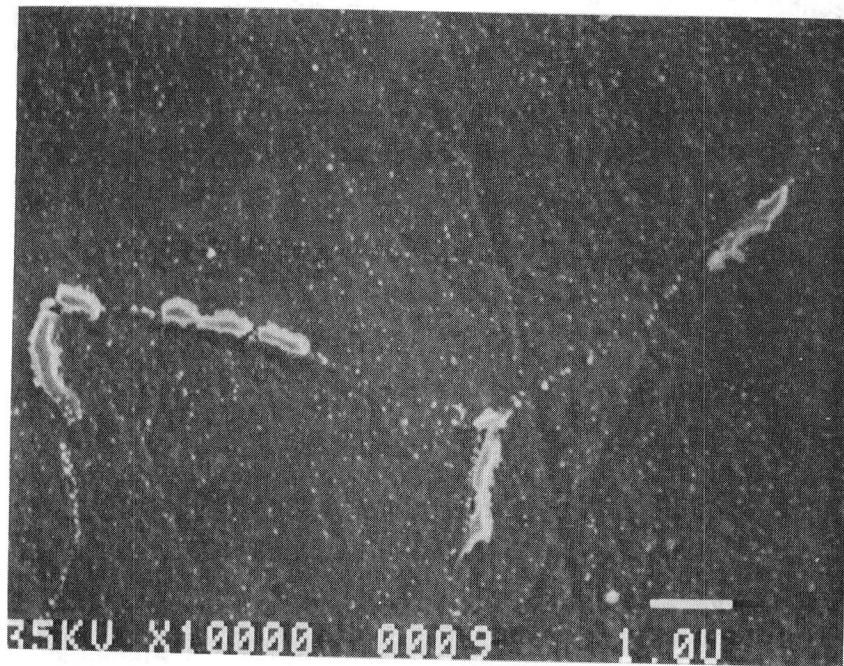


FIGURE 23: SOLUTION AND AGE HEAT TREATED ALLOY 3a, b, c and d.  
SOLUTION: 980°C (1800°F), 2 HOURS;  
AGE: 705°C (1300°F), 100 HOURS.

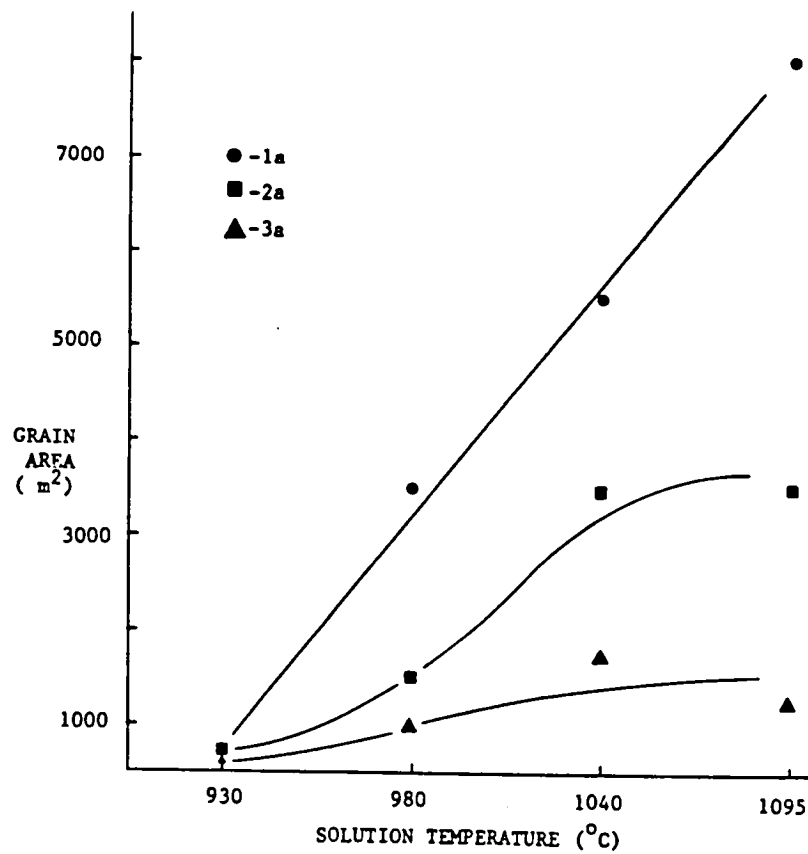


FIGURE 24: GRAIN SIZE OF ALLOYS STUDIED AS A FUNCTION OF SOLUTION TEMPERATURE FOR VARIOUS Cb CONTENTS.

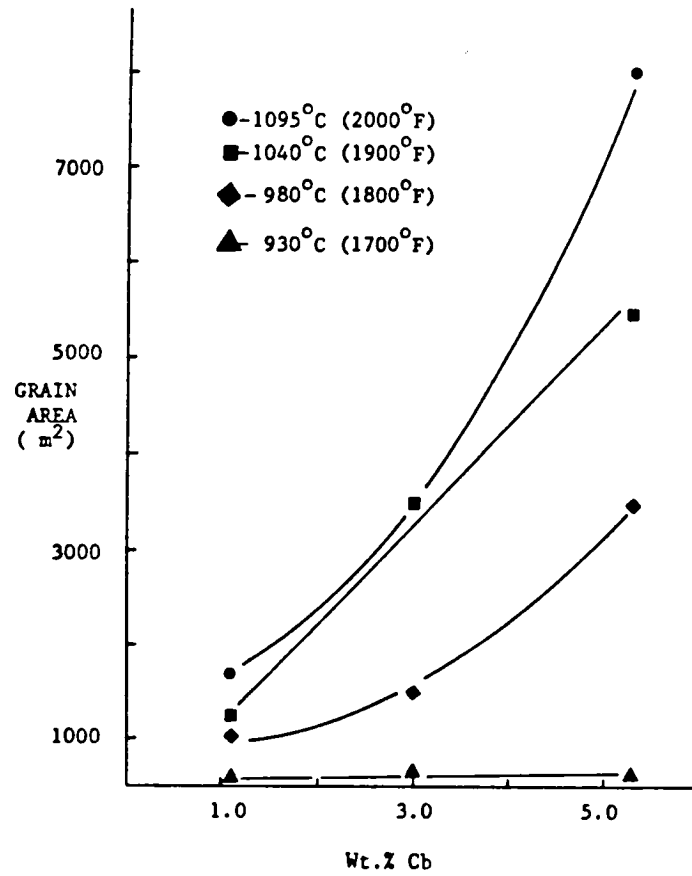


FIGURE 25: GRAIN SIZE OF ALLOYS STUDIED AS A FUNCTION OF CB CONTENTS FOR VARIOUS SOLUTION TEMPERATURES.

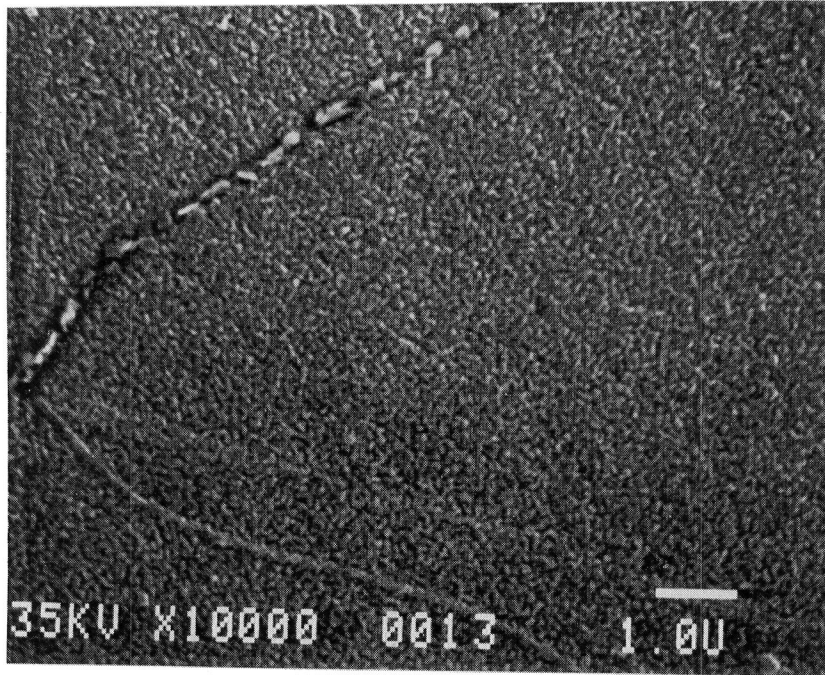


FIGURE 26: SOLUTION AND AGE HEAT TREATED ALLOY 4,  
SOLUTION: 980°C (1800°F), 2 HOURS;  
AGE: 705°C (1300°F), 100 HOURS.

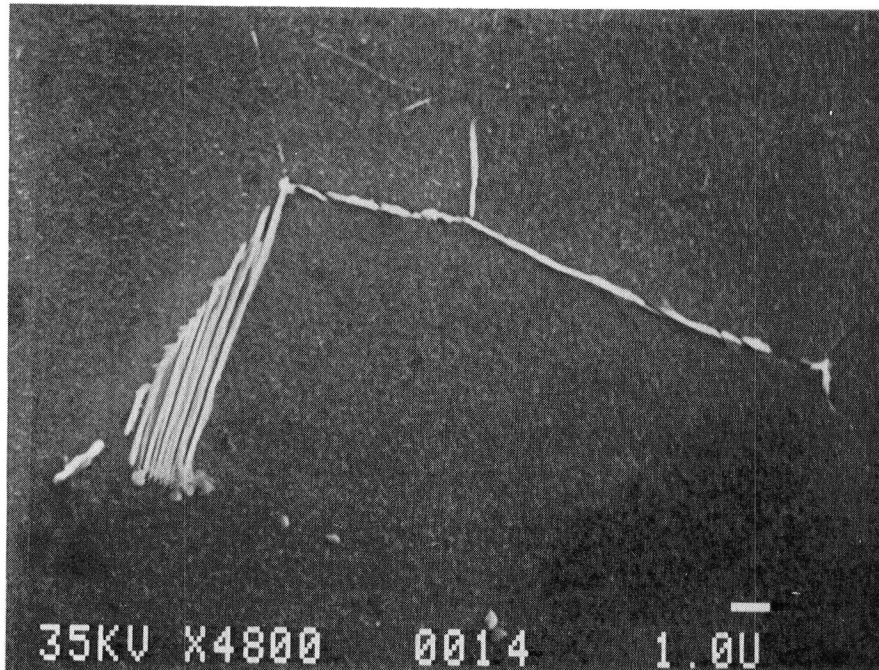


FIGURE 27: SOLUTION AND AGE HEAT TREATED ALLOY 5.  
SOLUTION: 980°C, 2 HOURS;  
AGE: 705°C, 100 HOURS.

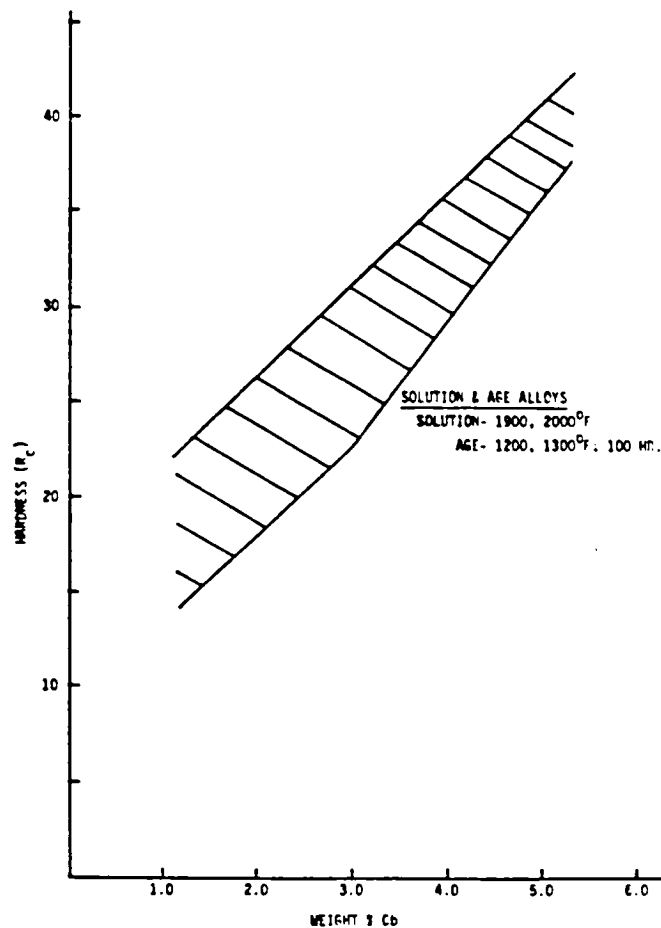


FIGURE 28: HARDNESS OF ALLOYS STUDIED AS A FUNCTION OF Cb CONTENT IN SOLUTION AND AGE CONDITION. RANGE OF HARDNESS IS SHOWN.

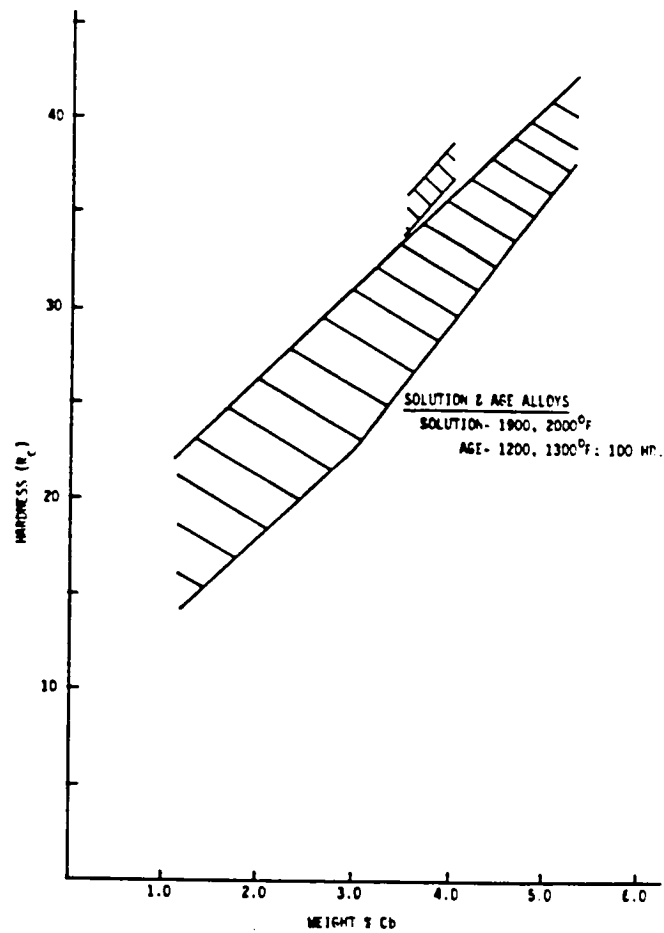


FIGURE 29: HARDNESS OF ALLOYS STUDIED AS A FUNCTION OF CB CONTENT IN SOLUTION AND AGE CONDITION. RANGE OF HARDNESS IS SHOWN.

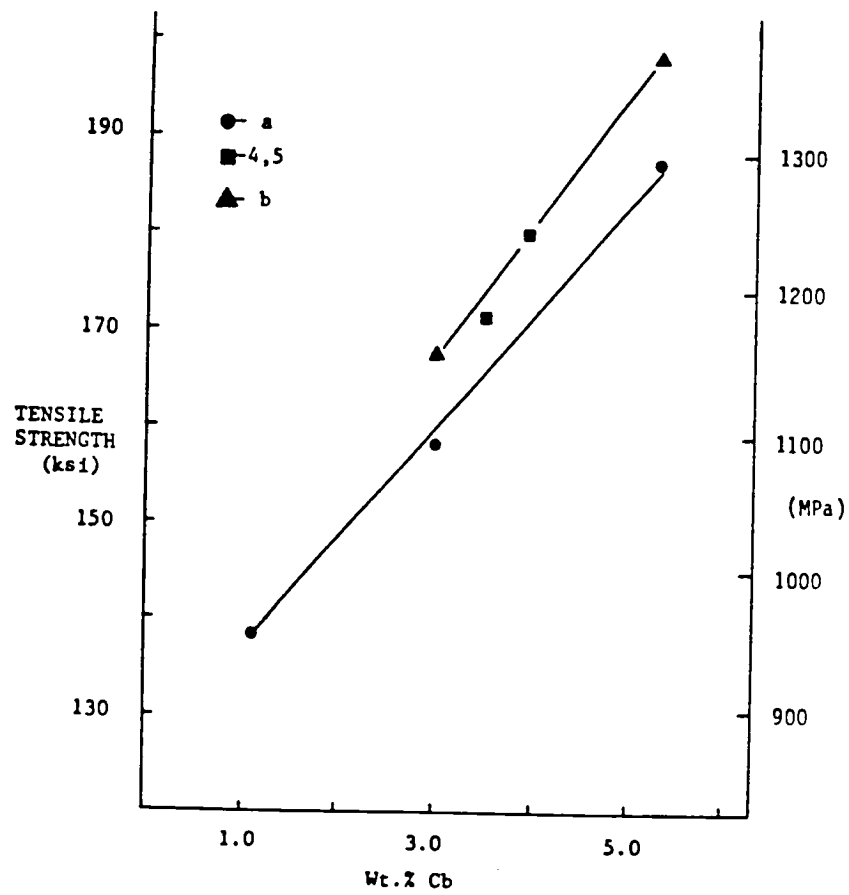


FIGURE 30: TENSILE STRENGTH OF ALLOYS STUDIED AS A FUNCTION OF Cb CONTENT.

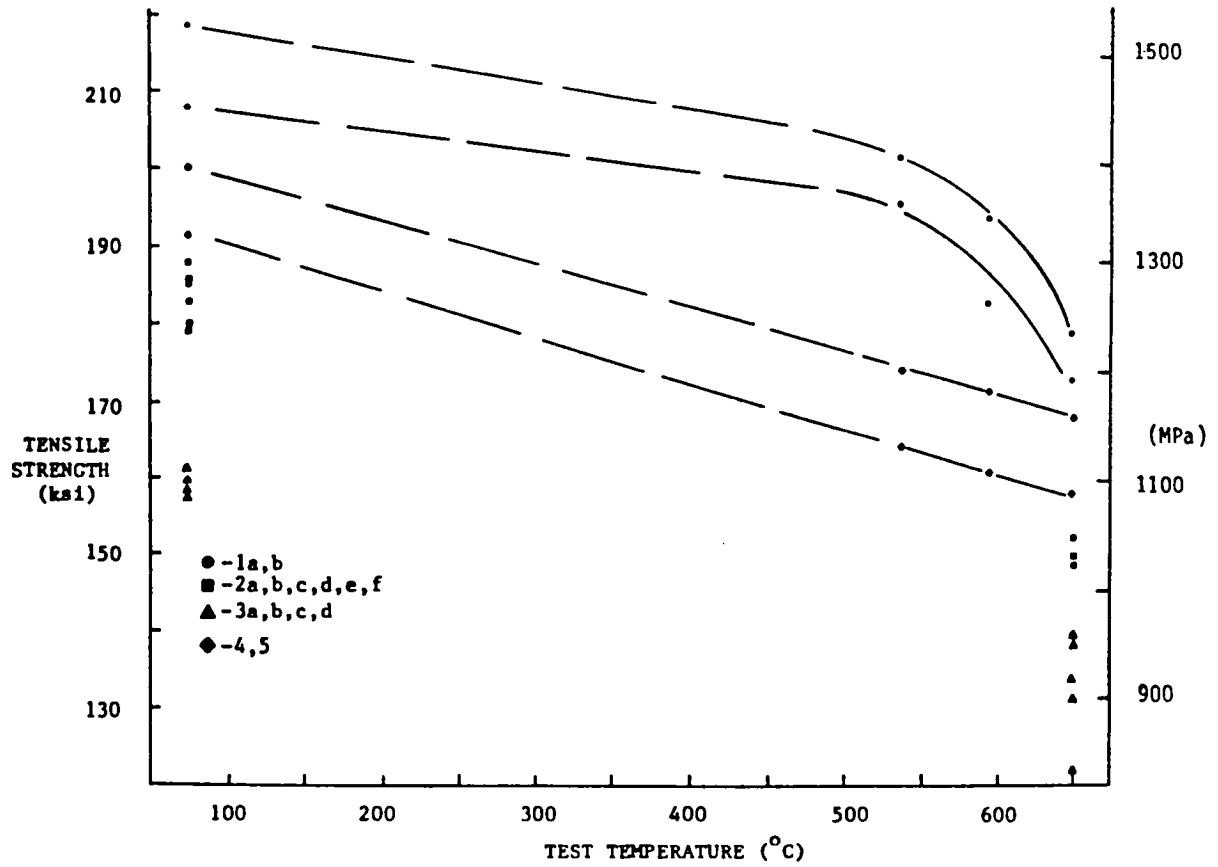


FIGURE 31: TENSILE STRENGTH OF SOLUTION AND AGE ALLOYS AS A FUNCTION OF TEMPERATURE.

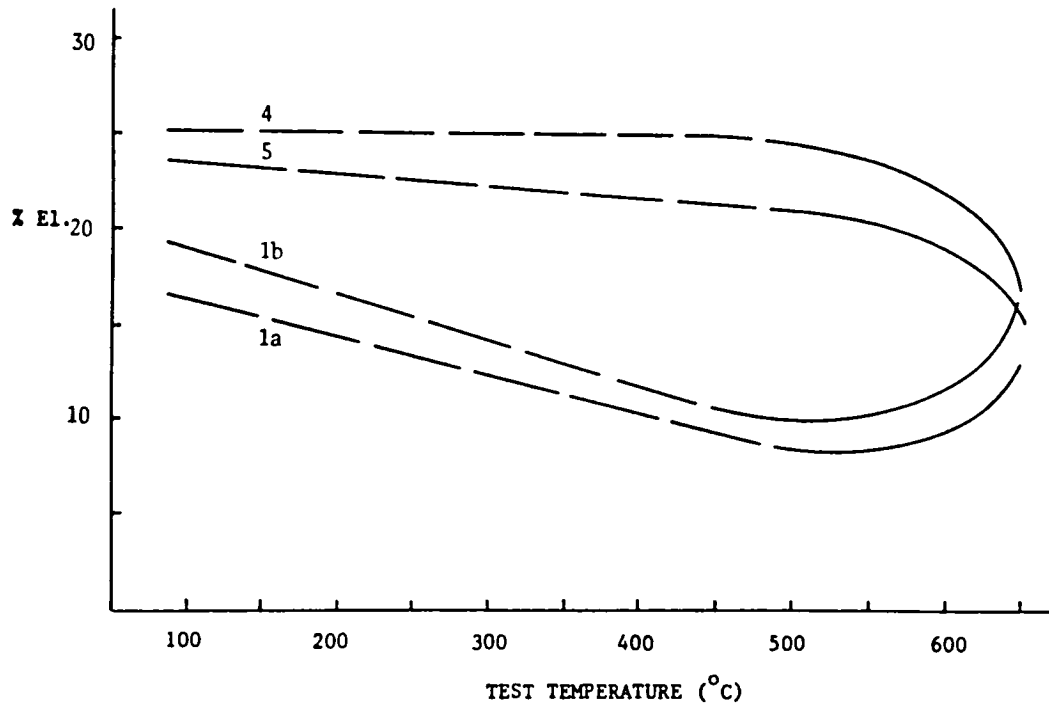


FIGURE 32: TENSILE DUCTILITY OF SOLUTION AND AGE ALLOYS AS A FUNCTION OF TEMPERATURE.

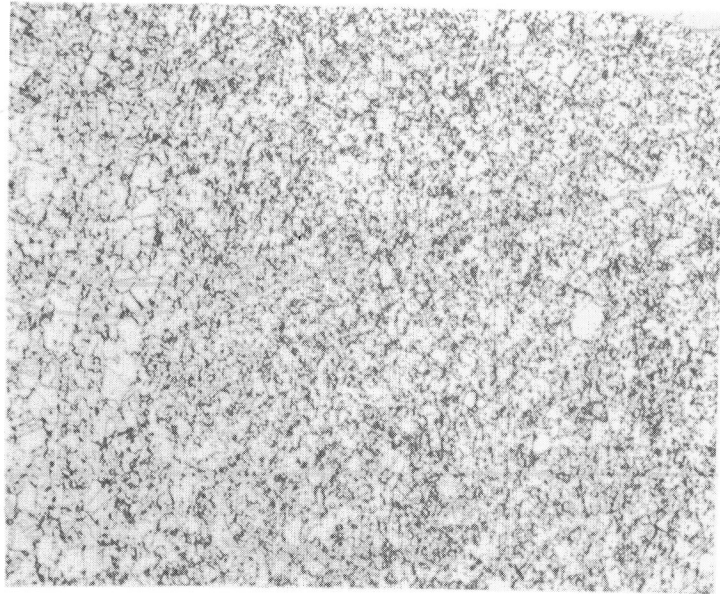


FIGURE 33: MINIGRAIN STRUCTURE OF ALLOY 718.

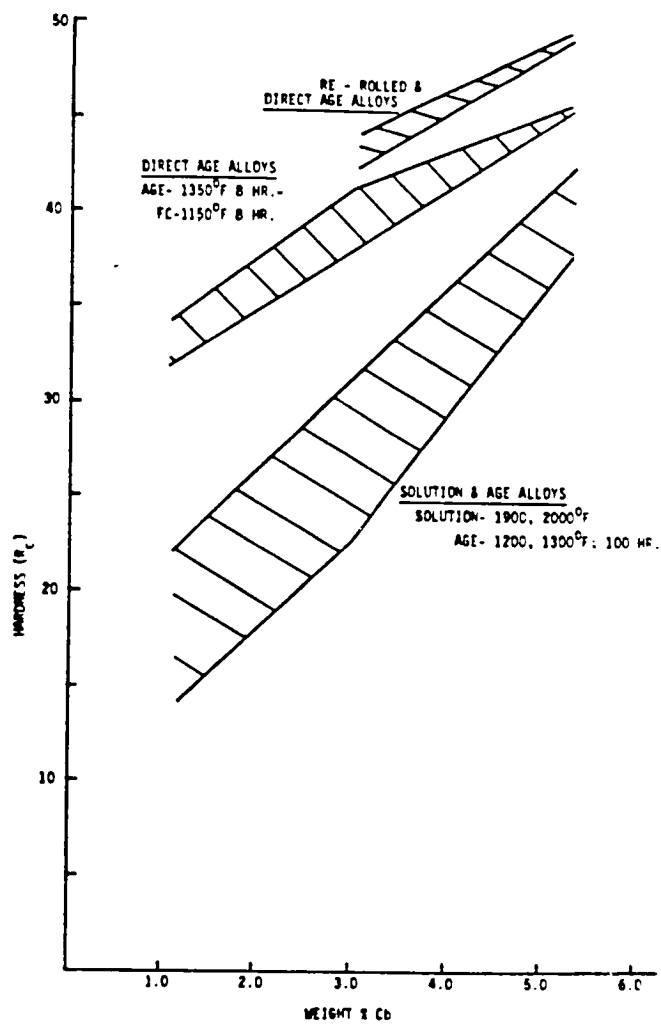


FIGURE 34: HARDNESS OF ALLOYS STUDIED AS A FUNCTION OF Cb CONTENT IN VARIOUS PROCESS CONDITIONS. RANGE OF HARDNESS IS SHOWN.

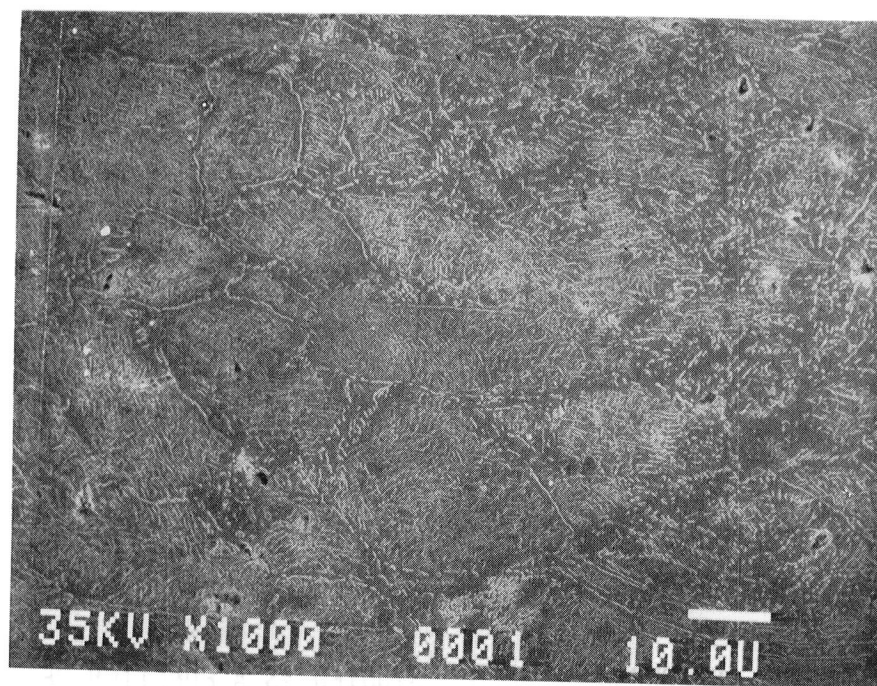


FIGURE 35: REPROCESSED ALLOY 1a;  
BEFORE AGE HEAT TREATMENT.

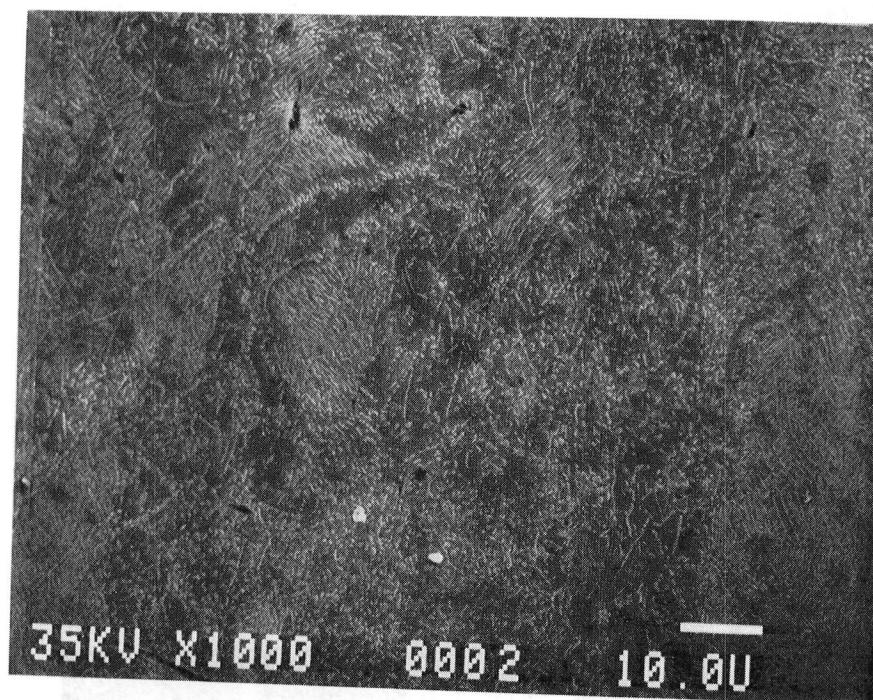


FIGURE 36: REPROCESSED ALLOY 1b;  
BEFORE AGE HEAT TREATMENT.

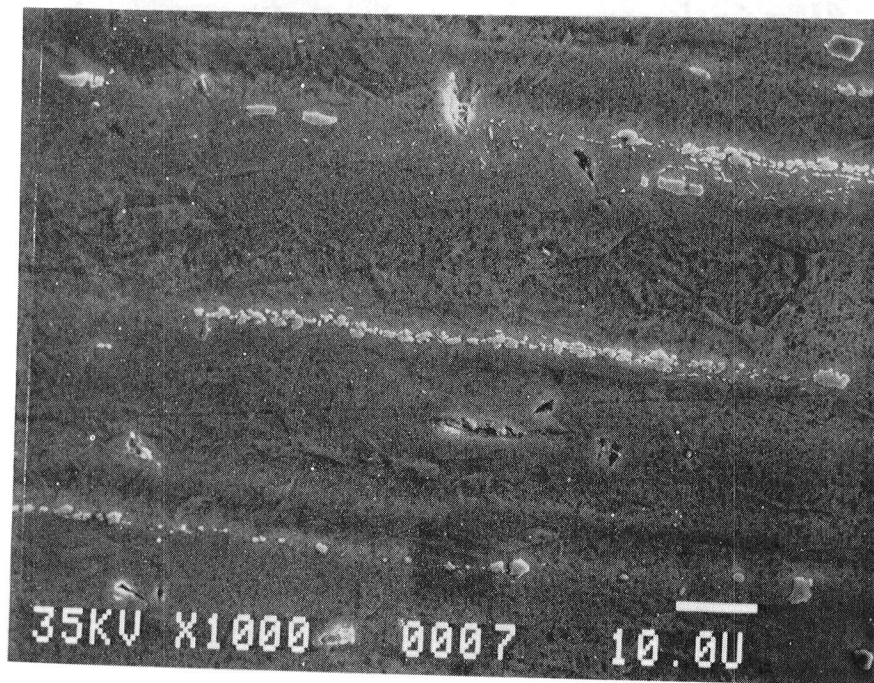
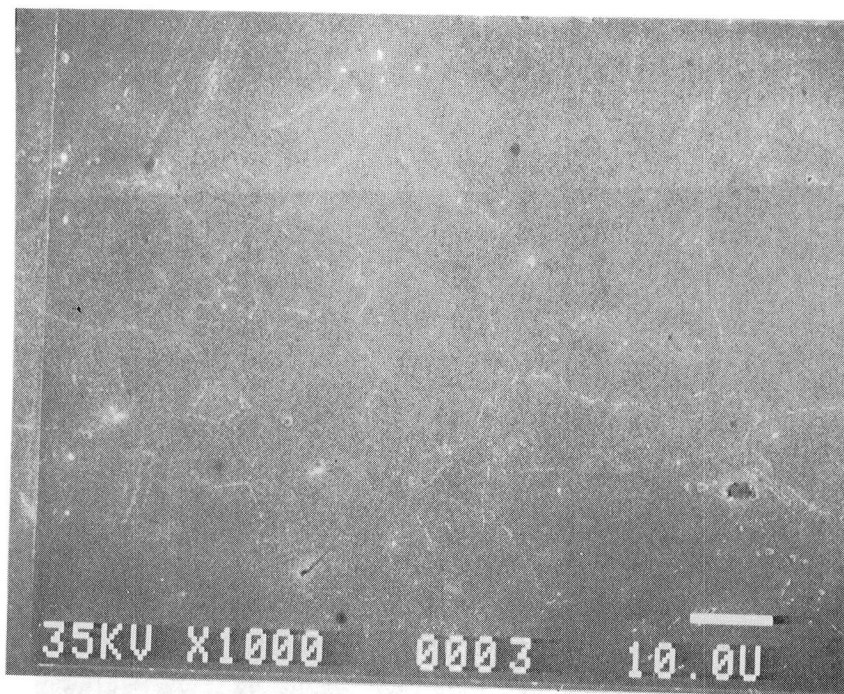


FIGURE 37: REPROCESSED ALLOY 2a AND b; BEFORE AGE HEAT TREATMENT, a) ALLOY 2a; b) ALLOY 2b

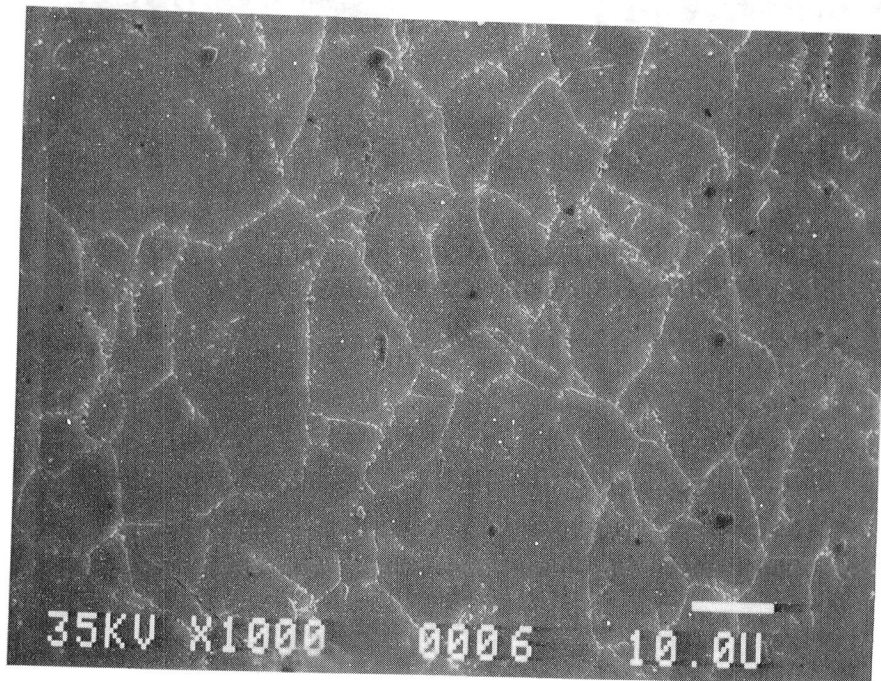
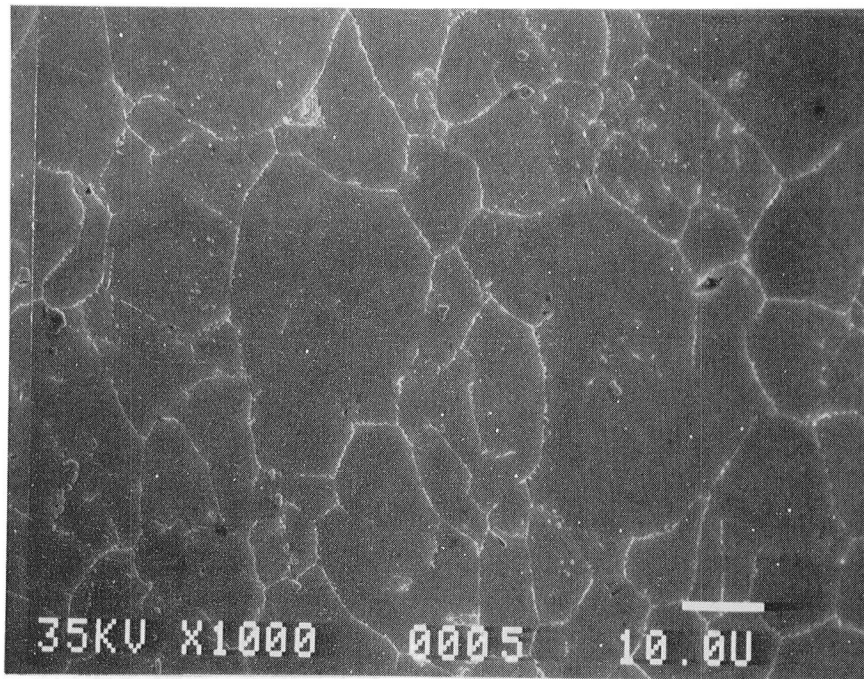


FIGURE 38: REPROCESSED ALLOY 2e AND f; BEFORE AGE HEAT TREATMENT, a) ALLOY 2e; b) ALLOY 2f

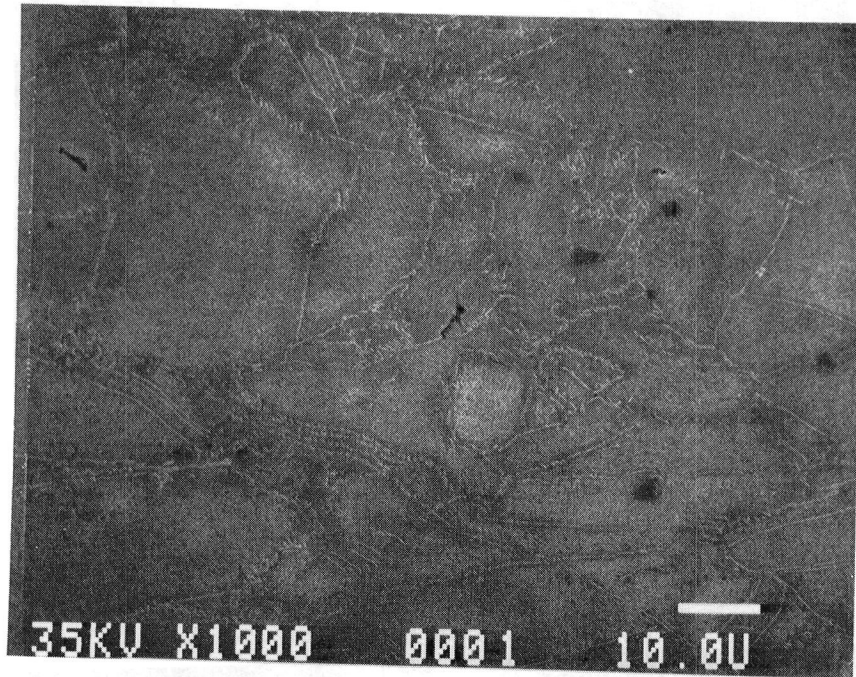


FIGURE 39: DIRECT AGE ALLOY 1a. AGE: 730°C,  
8 HOURS F.C., 620°C, 8 HOURS, A.C.

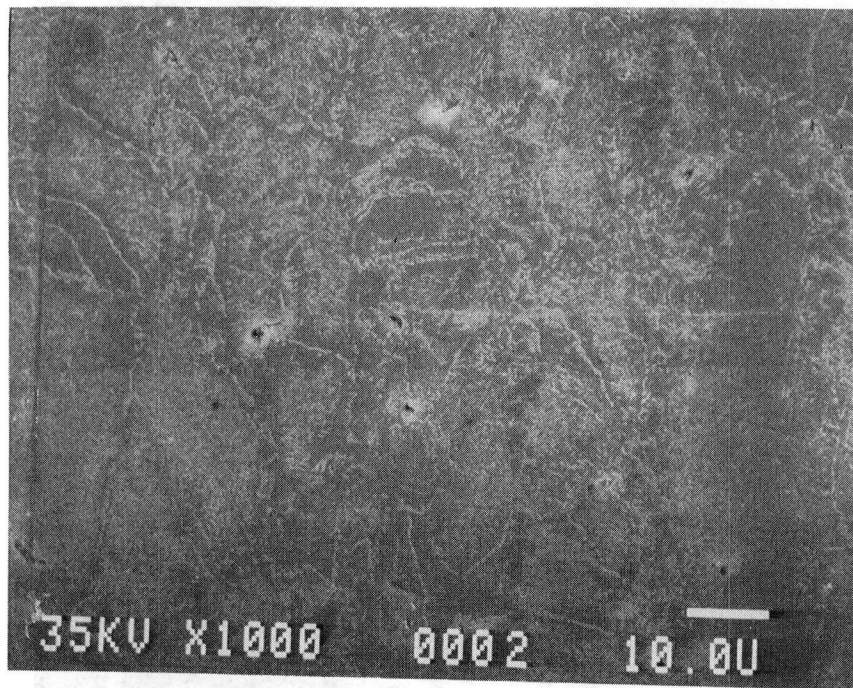


FIGURE 40: DIRECT AGE ALLOY 1b. AGE: 730°C,  
8 HOURS F.C., 620°C, 8 HOURS, A.C.

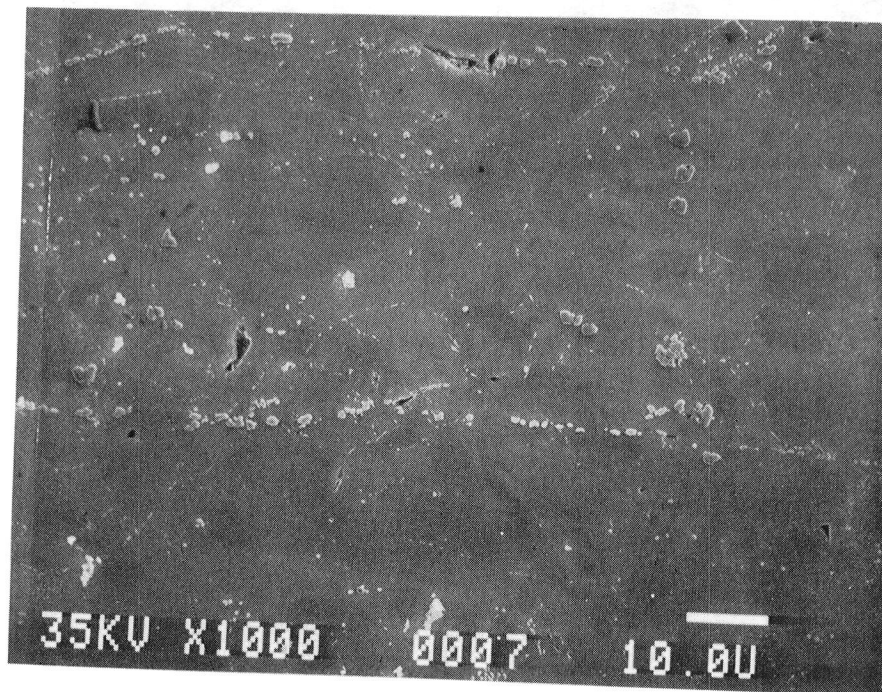
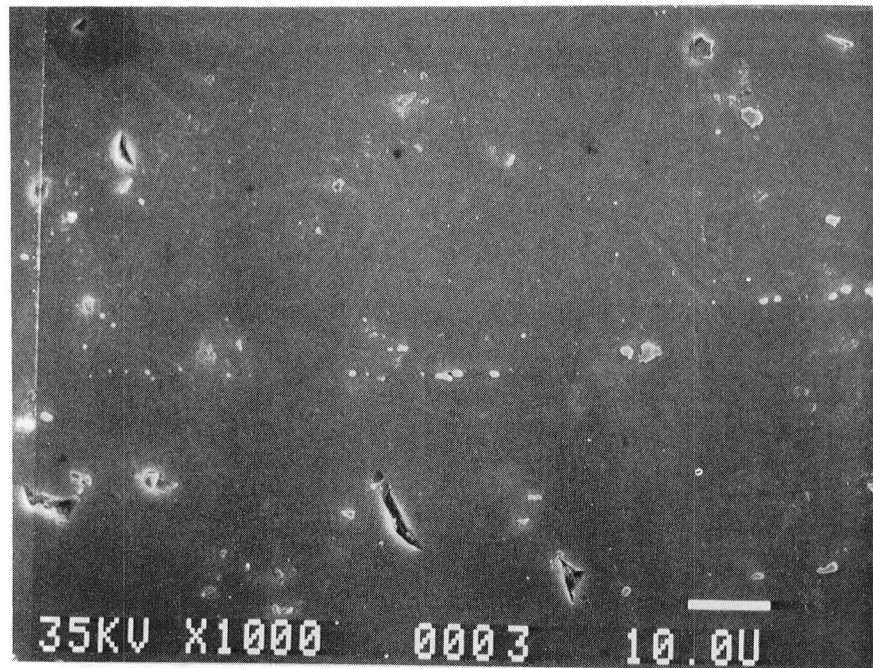


FIGURE 41: DIRECT AGE ALLOY 2a AND b. AGE: 730°C, 8 HOURS, F.C., 620°C, 8 HOURS, A.C. a) ALLOY 2a, b) ALLOY 2b.

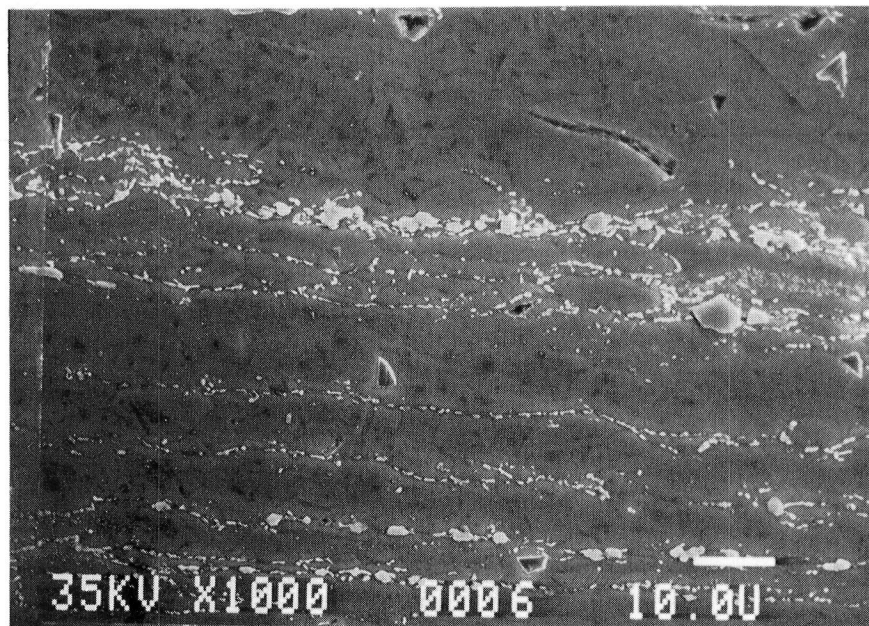
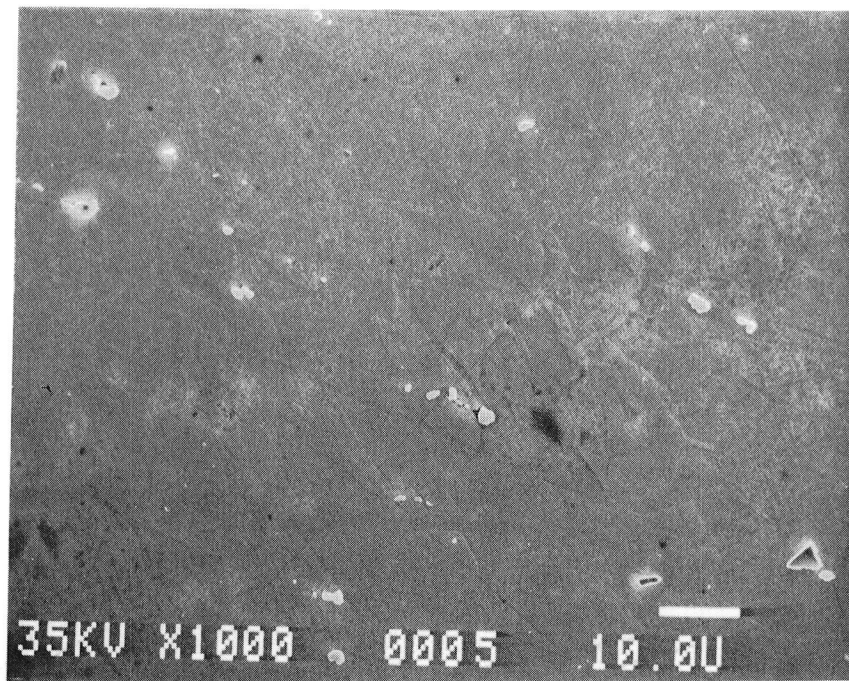


FIGURE 42: DIRECT AGE ALLOY 2e AND f. AGE: 730°C, 8 HOURS, F.C., 620°C, 8 HOURS A.C. a) ALLOY 2e, b) ALLOY 2f.

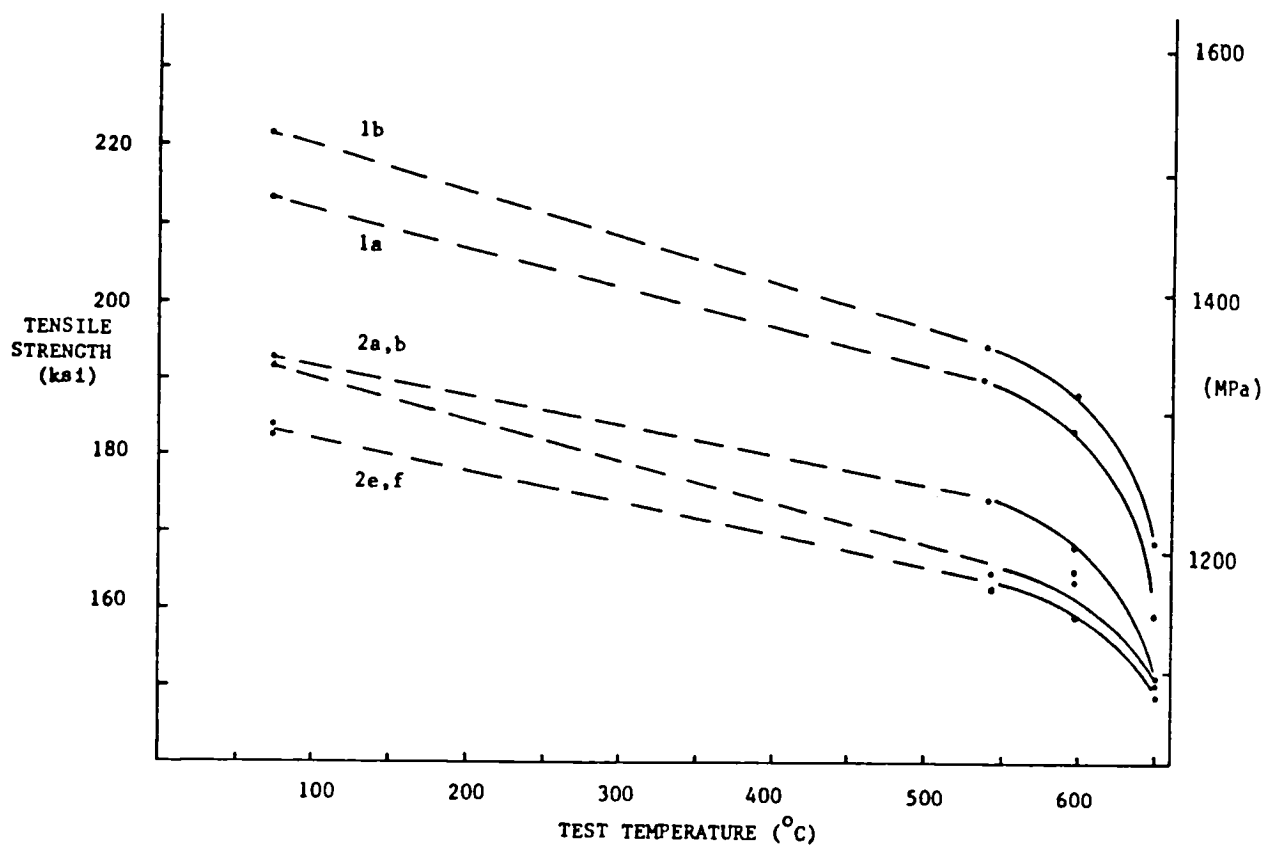


FIGURE 43: TENSILE STRENGTH OF DIRECT AGE ALLOYS AS A FUNCTION OF TEST TEMPERATURE.

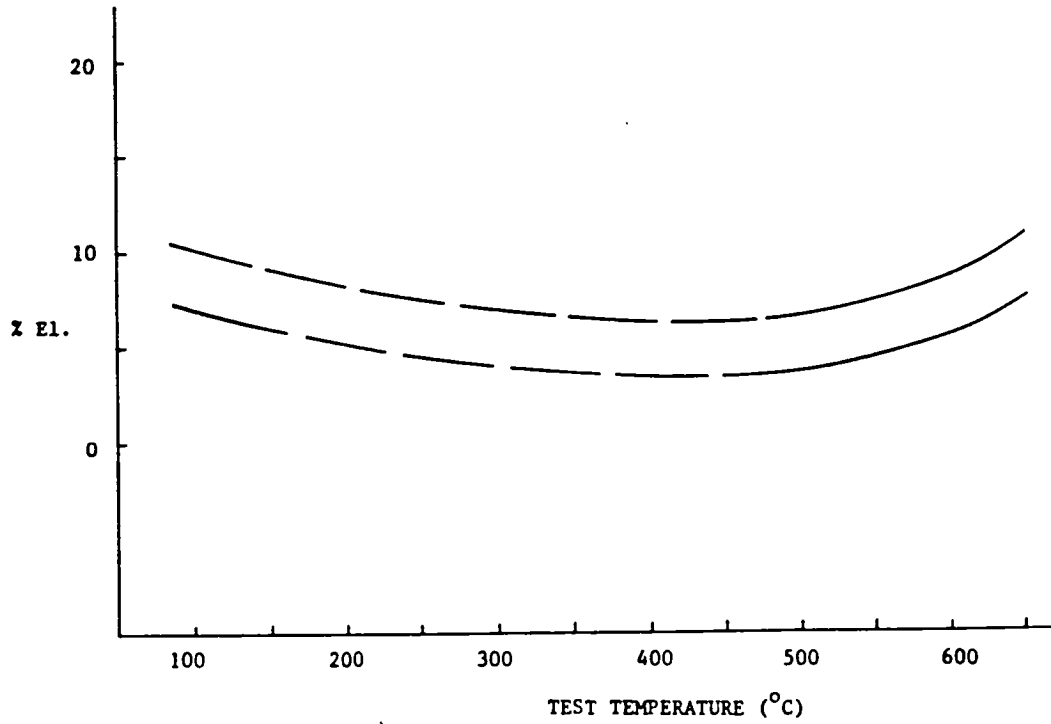


FIGURE 44: TENSILE DUCTILITY OF DIRECT AGE ALLOYS AS A FUNCTION OF TEST TEMPERATURE. THIS IS A RANGE FOR ALLOYS 1a, b AND 2a, b, e, f.

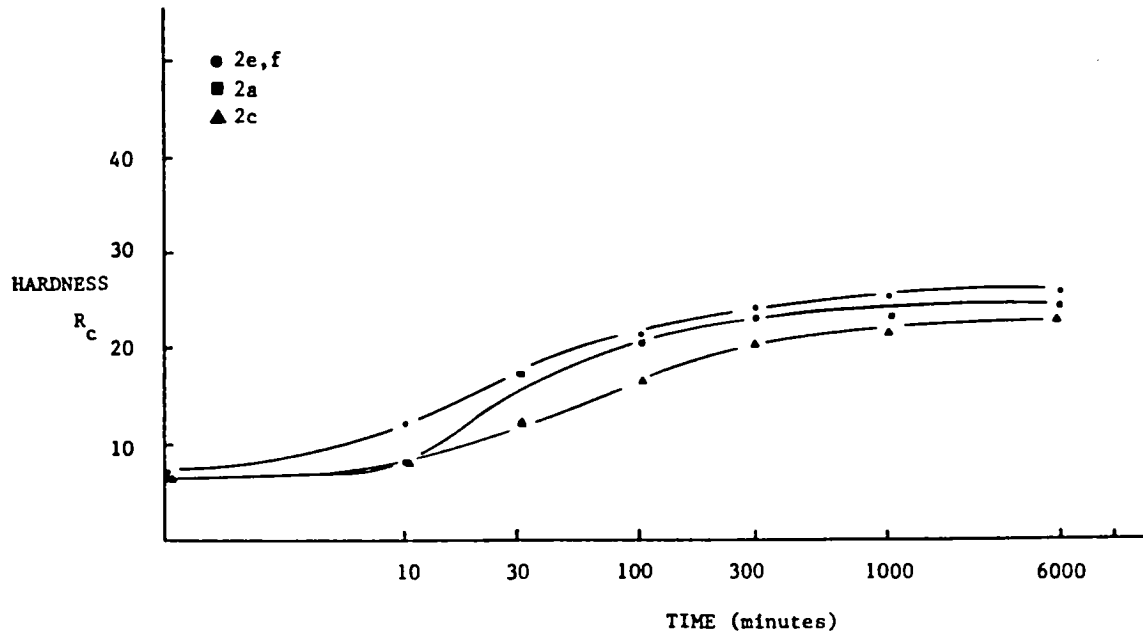


FIGURE 45: HARDNESS OF ALLOYS 2a, c, e, f AS A FUNCTION of 705°C (1300°F) AGE TIME. ALL ALLOYS SOLUTIONED AT 1040°C (1900°F).

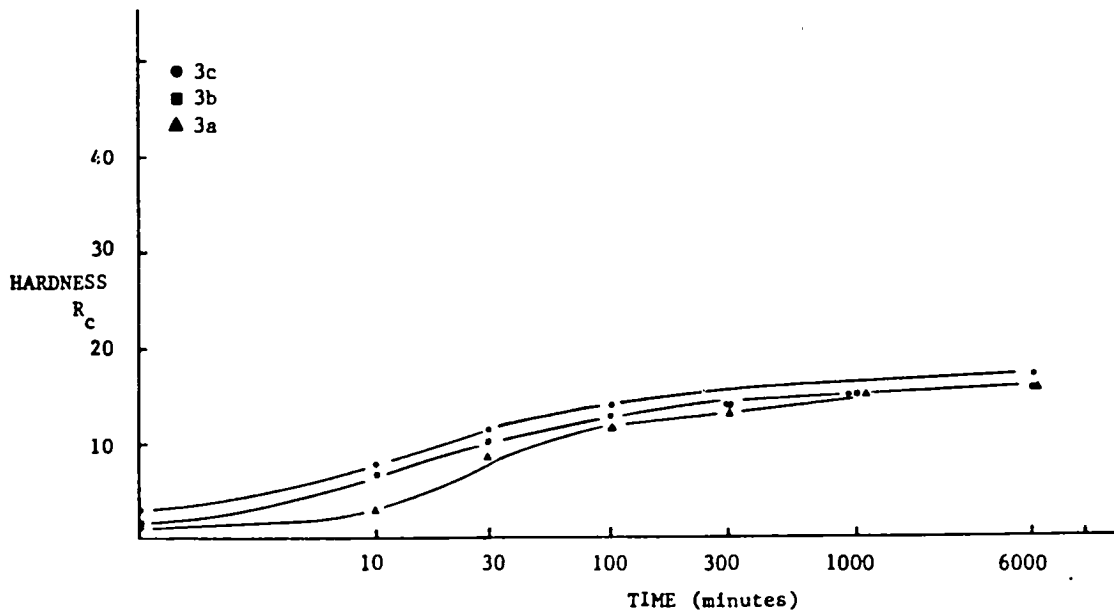


FIGURE 46: HARDNESS OF ALLOYS 3a, b, c, AS A FUNCTION of 705°C (1300°F) AGE TIME. ALL ALLOYS SOLUTIONED AT 1040°C (1900°F).

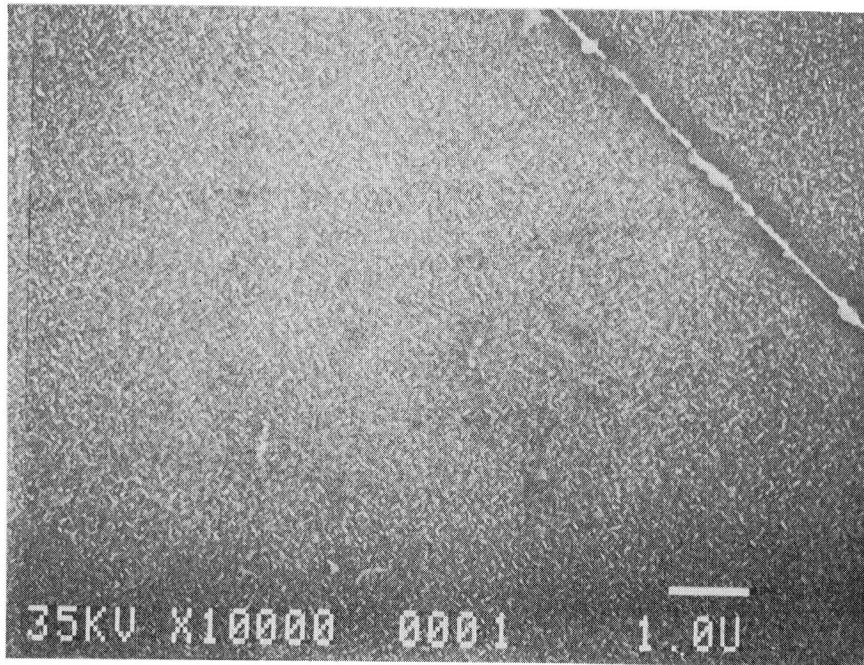


FIGURE 47: SOLUTION AND AGE ALLOY 1a;  
(Al+Ti)/Cb = 0.655 PREDOMINANTLY  $\gamma'$  PRECIPITATION.

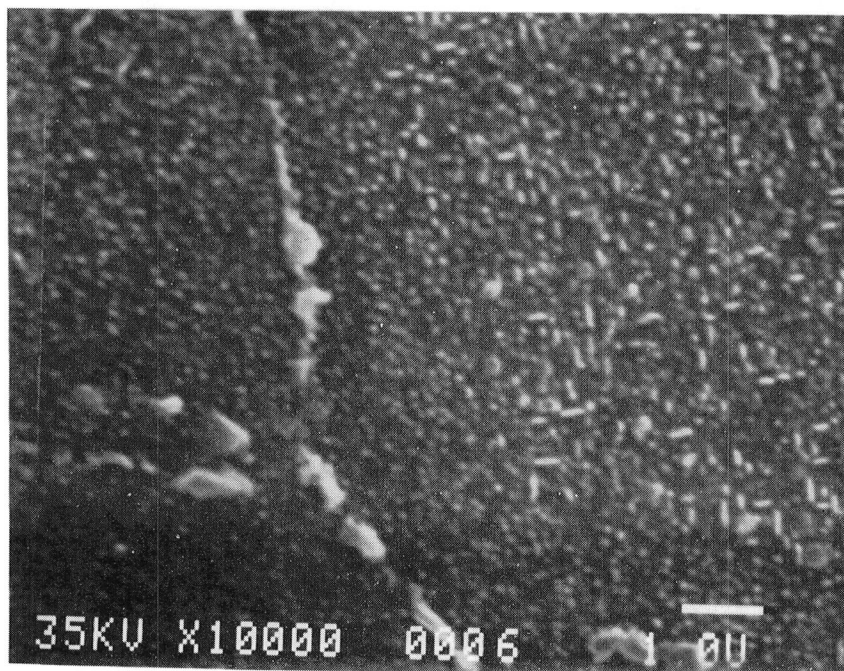
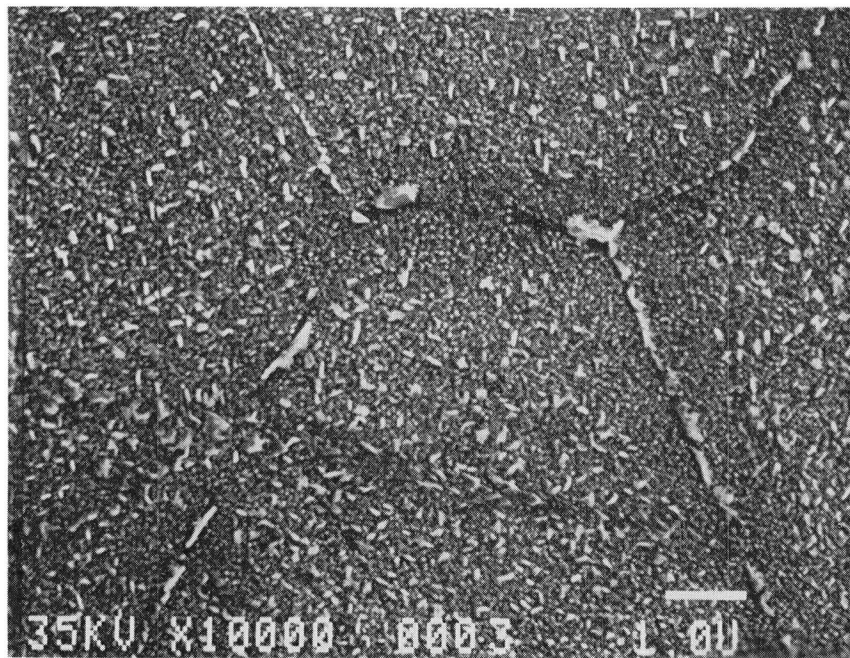


FIGURE 48: SOLUTION AND AGE ALLOY 2a;  
 $(Al+Ti)/Cb = 1.135$  BALANCED  $\gamma'$  AND  $\gamma''$  PRECIPITATION,  
 a) ALLOY 2a; b) ALLOY 2f.

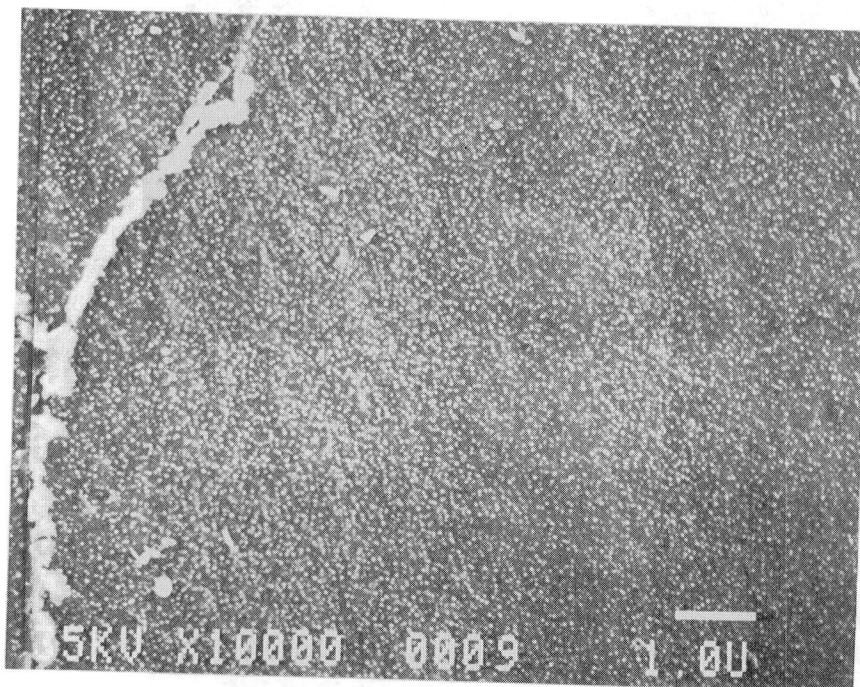


FIGURE 49: SOLUTION AND AGE ALLOY 3a;  
 $(Al+Ti)/Cb = 3.357$  PREDOMINANTLY  $\gamma''$  PRECIPITATION

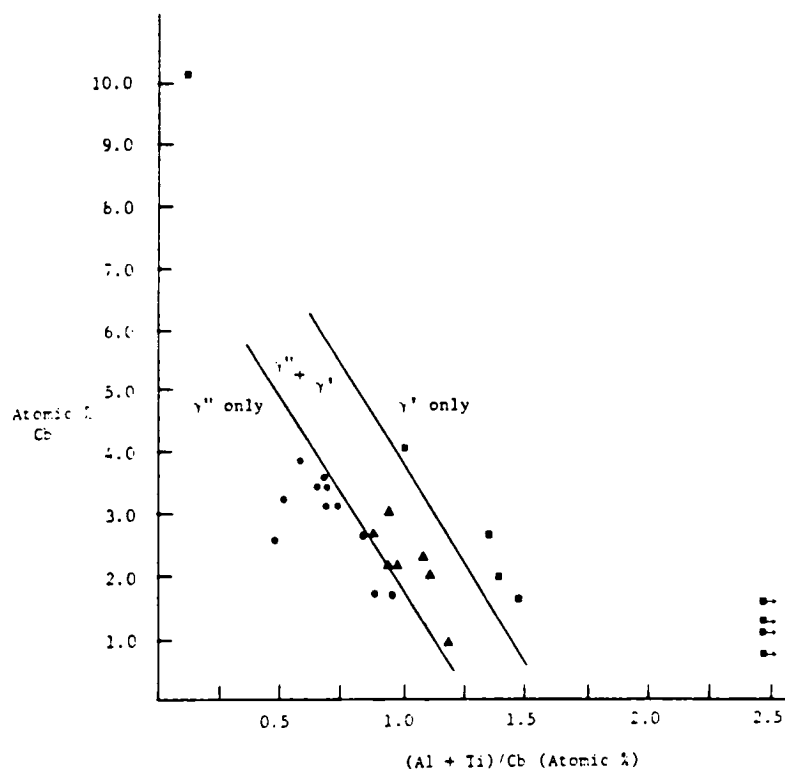


FIGURE 50: TYPE OF STRENGTHENING PRECIPITATES IN ALLOY 718 AS FUNCTION OF (Al + Ti) AND Cb.

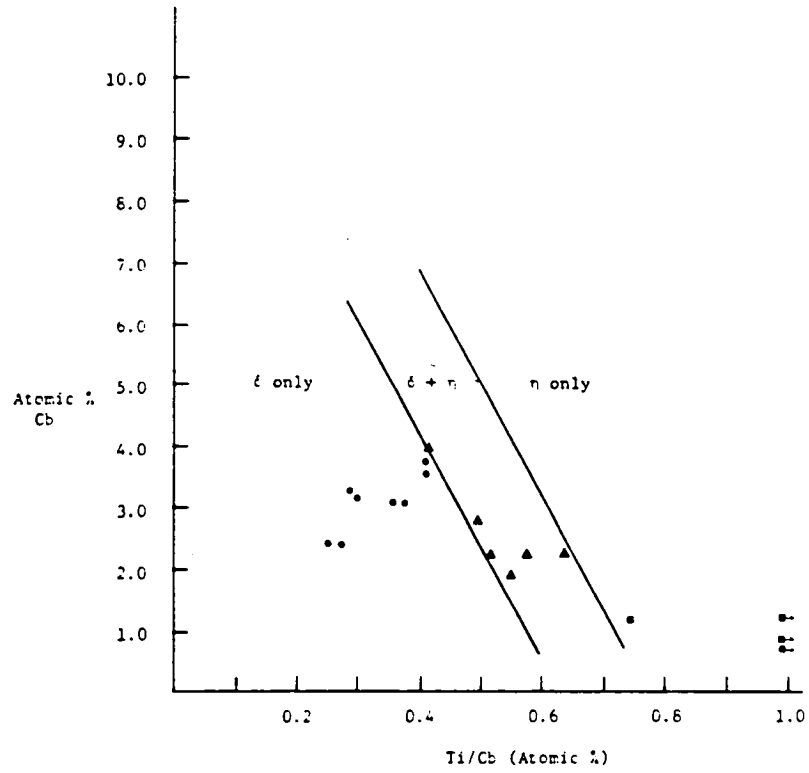


FIGURE 51: TYPE OF STABLE (OVERAGED) PHASE PRECIPITATED IN ALLOY 718 AS A FUNCTION OF Ti AND Cb.

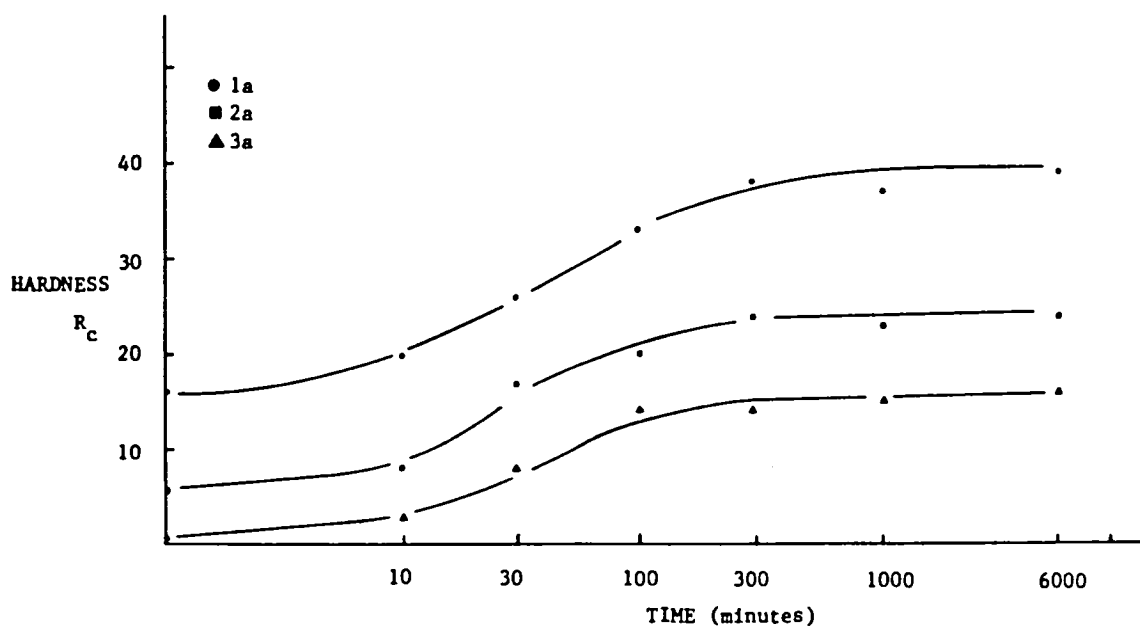


FIGURE 52: HARDNESS OF ALLOYS 1a, 2a, 3a AS A FUNCTION OF 705°C (1300°F) AGE TIME. ALL ALLOYS SOLUTIONED AT 1040°C (1900°F).

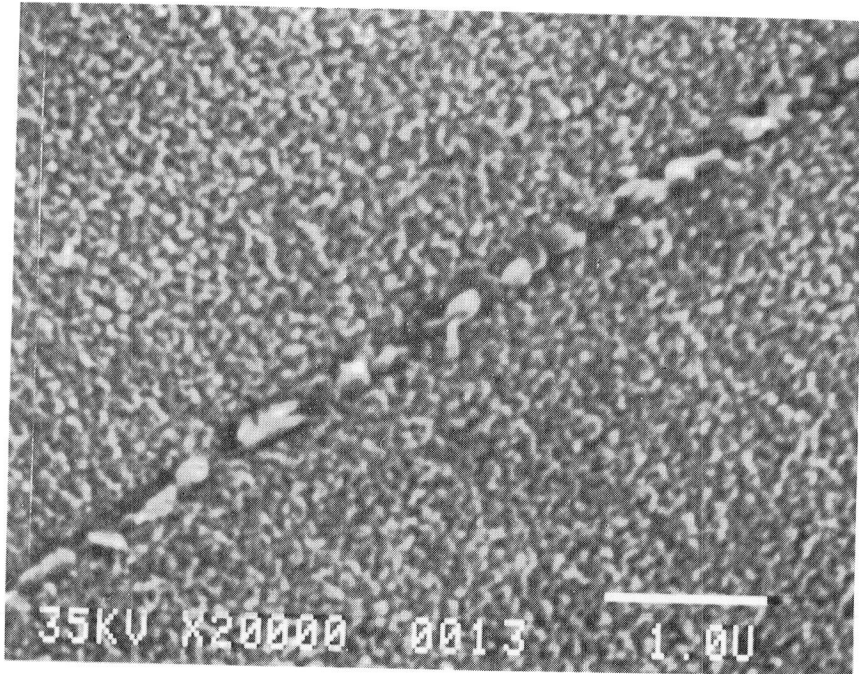


FIGURE 53: SOLUTION AND AGE ALLOY 4.  
DETAIL OF GRAIN BOUNDARY

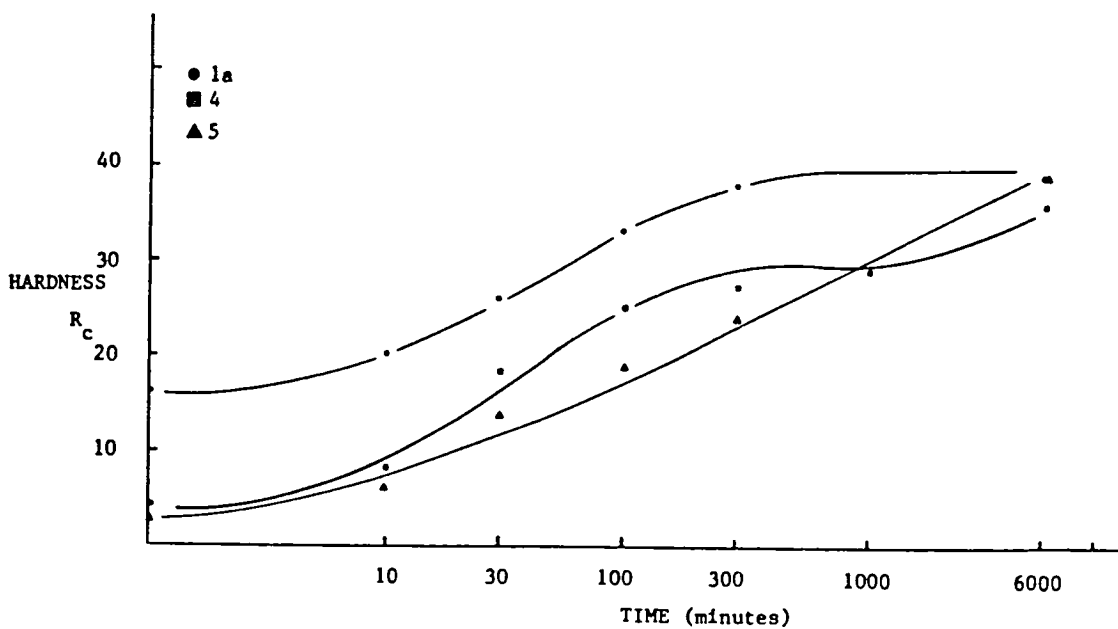


FIGURE 54: HARDNESS OF ALLOYS 1a 4, 5 AS A FUNCTION OF 705°C (1300°F) AGE TIME. ALL ALLOYS SOLUTIONED AT 1040°C (1900°F).

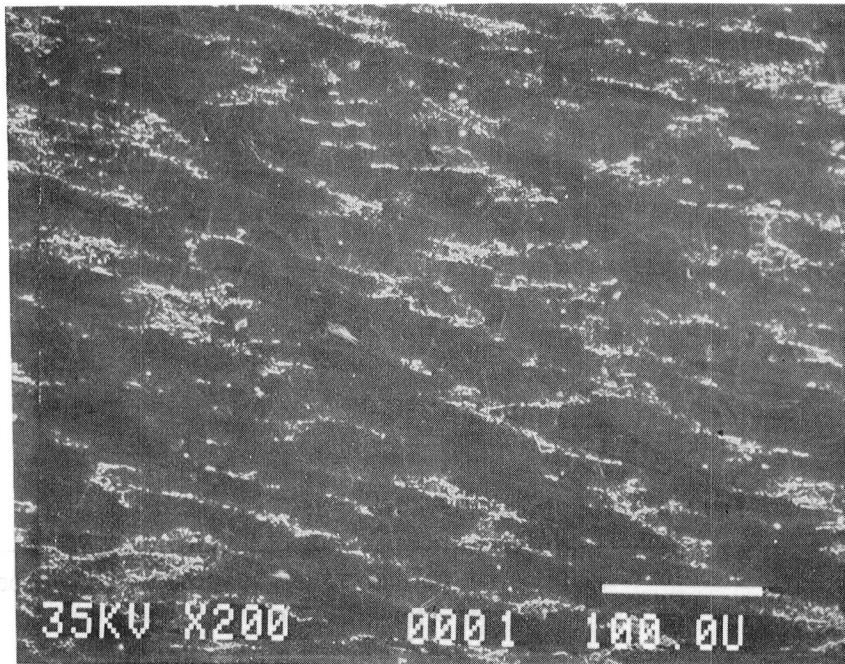


FIGURE 55: ORIGINAL DIRECT AGE ALLOY 1a,  
BEFORE AGE HEAT TREATMENT.



FIGURE 56: ORIGINAL DIRECT AGE ALLOY 2a,  
BEFORE AGE HEAT TREATMENT.

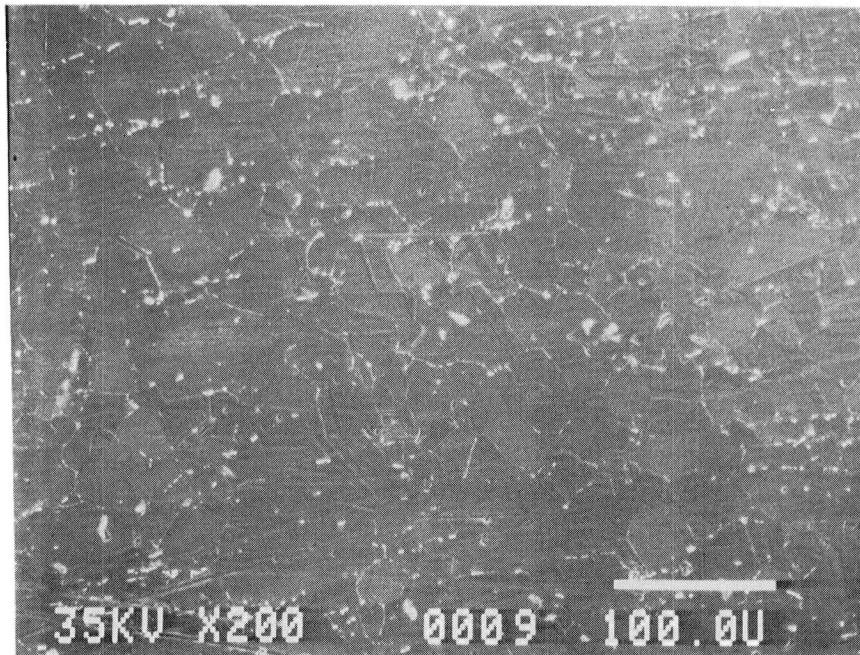


FIGURE 57: ORIGINAL DIRECT AGE ALLOY 3a,  
BEFORE AGE HEAT TREATMENT.



1. Report No. NASA CR-174841		2. Government Accession No.		3. Recipient's Catalog No.	
4. Title and Subtitle  Effect of Reduction of Strategic Columbium Addition in 718 Alloy on the Structure and Properties				5. Report Date  January 1985	
				6. Performing Organization Code	
7. Author(s)  Karl R. Ziegler and John F. Wallace				8. Performing Organization Report No.  None	
				10. Work Unit No.	
9. Performing Organization Name and Address  Case Western Reserve University 10900 Euclid Avenue Cleveland, Ohio 44106				11. Contract or Grant No.  NAG 3-268	
				13. Type of Report and Period Covered  Contractor Report	
12. Sponsoring Agency Name and Address  National Aeronautics and Space Administration Washington, D.C. 20546				14. Sponsoring Agency Code  505-33-62	
15. Supplementary Notes  Final report. Project Manager, Robert L. Dreshfield, Materials Division, NASA Lewis Research Center, Cleveland, Ohio 44135.					
16. Abstract  Inconel Alloy 718 is a Nickel-Iron-base superalloy strengthened by the precipitation of the metastable $Ni_3Cb-\gamma''$ phase. Large coherency strains between $\gamma''$ and the matrix result in a slow precipitation rate and an intermediate maximum use temperature. The combination of slow precipitation rate and the relative formability and machinability of Alloy 718 make it a popular material for the fabrication of superalloy components. The dependence on foreign sources of Cb has pointed out the desirability of reducing the Cb content of Alloy 718 while maintaining the tensile and stress-rupture properties of the original alloy. The purpose of this investigation was to determine the effects of reduced Cb, and substitutions for Cb, on the properties of Alloy 718. A series of alloys was developed having a base composition similar to Alloy 718, with reduced Cb levels of 3.00 and 1.10 wt% Cb. Substitutions of 3.0% W, 3.0W + 0.9V or Mo increased from 3.0 to 5.8% were made for the Cb in these alloys. Two additional alloys, one containing 3.49% Cb and 1.10% Ti and another containing 3.89% Cb and 1.29% Ti were also studied. Solution and age heat treatments were optimized for each alloy to develop a proper microstructure. Some alloys were also processed by direct aging for substitution in the high strength applications of standard alloy. Tensile properties at room and elevated temperatures, stress-rupture tests and an analysis of extracted phases were carried out for each of the alloys. The reduction in Cb content required the substitution of other elements to maintain the properties of the original alloy. Additions of solid solution elements to a reduced Cb alloy had no significant effect on the properties of the alloys under either process condition. The solution and age alloys with substitutions of 1.27% Ti at 3.89% Cb had tensile properties similar to those of the original alloy and stress-rupture properties superior to the original alloy. The improved stress-rupture properties were the result of significant precipitation of $Ni_3Ti-\gamma'$ in the alloy, which is more stable than $\gamma''$ at the elevated temperatures. At lower temperatures the new alloy benefits from $\gamma''$ strengthening. With more precise control and proper processing, the reduced Cb direct-age alloy could substitute for Alloy 718 in high strength applications.					
17. Key Words (Suggested by Author(s))  Nickel alloys Columbium Superalloys			18. Distribution Statement  Unclassified - unlimited STAR Category 26		
19. Security Classif. (of this report)  Unclassified		20. Security Classif. (of this page)  Unclassified		21. No. of pages  178	
				22. Price*  A09	



National Aeronautics and  
Space Administration

Washington, D.C.  
20546

Official Business  
Penalty for Private Use, \$300



IL



Postage and Fees Paid  
National Aeronautics and  
Space Administration  
NASA-451

**NASA**

POSTMASTER: If Undeliverable (Section 158  
Postal Manual) Do Not Return

---